TÉCNICO LISBOA

Impact of Alternative Fuels on the Operational and Environmental Performance of Commercial Aircraft

Ricardo Manuel Pereira Gaspar

Thesis to obtain the Master of Science Degree in

Aerospace Engineering

Supervisor: Prof. João Manuel Melo de Sousa

Examination Committee

Chairperson: Prof. Filipe Szonolky Ramos Pinto Cunha
Supervisor: Prof. João Manuel Melo de Sousa
Member of the Committee: Prof. Fernando José Parracho Lau

July 2016

”All we have to decide is what to do
with the time that is given us.”
J.R.R. Tolkien,
The Fellowship of the Ring.

Acknowledgments

The present thesis represents the culmination of my academic career. I would like, then, to extend my sincere thanks to all the people that supported and helped me throughout this journey.

I would like to express my deepest gratitude to my family. Each one of them helped me be the person that I am today. I thank my father Alberto, mother Maria de Fátima, brother Paulo, sister Cristina and beloved girlfriend Daniela for all the love, support and care.

To my colleagues and friends that helped me in this journey, I am thankful for all the friendship and mutual support.

I would like to thank Prof. Dr. João Manuel Melo de Sousa for encouraging the present study, which has been an interest of mine in recent years. I am thankful for his continuous and invaluable support, assistance and constructive criticism during the last 6 arduous months.

For willingly sharing her knowledge and support, I thank Eng. Mónica Ferreirinho, Supply Coordinator Portugal at BP Portugal.

Most of all, I am grateful to all the people that, in one way or another, shaped my life, leading me to this moment. These last 5 years of my life were a intense, fulfilling and unforgettable phase of my life and will certainly define my future, on a professional and personal level.

Resumo

A produção global de combustíveis alternativos sustentáveis tornou-se um elemento importante para o objectivo da aviação em reduzir os impactos ambientais e a dependência de combustíveis fósseis. O presente trabalho foca-se na viabilidade técnica de um alargado conjunto de combustíveis alternativos, com diferenças de desempenho e emissões resumidas. Os modos de produção alternativos considerados são os seguintes: *Fischer-Tropsch*, *Hydrotreated Esters and Fatty Acids*, *Synthesized Iso-Paraffins*, *Alcohol-to-Jet*, *Catalytic Hydrothermolysis* e *Hydrodeoxygenation*. A análise da queima de diferentes combustíveis será puramente termodinâmica, com a modelação numérica 0-D de um turborreactor de duplo fluxo para análises em condições fora de projeto e em regime transiente, sendo os modelos validados comparando resultados de desempenho obtidos com o que se obteria através do software GasTurb 12, para um combustível convencional. As abordagens seguidas, para obtenção de estimativas de propriedades de combustíveis e temperaturas de chama e implementação de modelos de evaporação e de gás, são apresentadas e validadas. Para diferentes condições de vôo, resultados de desempenho e emissões poluentes para os combustíveis estudados são apresentados, discutidos e comparados com resultados obtidos na literatura. Finalmente, diferentes cenários dinâmicos são simulados e a influência dos combustíveis analisada. Com o presente trabalho, é possível concluir que a maioria dos combustíveis alternativos sustentáveis podem melhorar em termos operacionais e ambientais o desempenho de uma aeronave, quando comparado com combustíveis convencionais, confirmando assim que os mesmos, embora limitados economicamente, representam uma aposta segura para o futuro próximo da aviação.

Palavras-chave: Combustíveis Alternativos, Aviação, Turborreactor de Duplo Fluxo, Desempenho Fora de Condições de Projeto, Resposta Transiente, Emissões Poluentes

Abstract

The wide-scale supply of sustainable alternative fuels has become a major element of the aviation industry's aim of reducing environmental impacts while easing fossil fuels dependence. The present work will address the technical feasibility of a wide range of alternative fuels, with differences in performance and pollutant emissions summarized. The alternative production pathways considered in this study are the following: Fischer-Tropsch, Hydrotreated Esters and Fatty Acids, Synthesized Iso-Paraffins, Alcohol-to-Jet, Catalytic Hydrothermolysis and Hydrodeoxygenation. The analysis of the burning of different fuels will be based purely on a 0-D engine thermodynamic approach, with a numerical modelling of a typical two-spool turbofan for off-design and transient simulations. Through comparison of performance results obtained relative to what would be obtained with GasTurb 12, for a conventional kerosene, the aero-engine numerical model is validated. The approaches followed, for the estimation of required fuel properties and flame temperatures and for the implementation of evaporation and gas models, are presented and validated. For different flight conditions, performance and pollutant emissions outputs for the fuels studied are presented, discussed and compared with results obtained in the literature. Finally, different transient scenarios are simulated and the influence of fuels analysed. With the present work, it is possible to conclude that most sustainable alternative fuels may improve the overall performance and pollutant emissions when compared with a conventional kerosene, which confirms that the supply of alternative fuels, although constrained economically, is a safe route going forward for the aviation industry.

Keywords: Alternative Fuels, Aviation,Turbofan, Off-Design Performance, Transient Response, Pollutant Emissions

Contents

List of Tables

List of Figures

List of Symbols

Greek symbols

α	Thermal expansion coefficient in equation A.4 (ASTM D1250), $^{o}C^{-1}$
β	Auxiliary map coordinate
δ	Nondimensional total pressure
η	Efficiency
γ	Specific heat ratio
λ	Evaporation constant, m^2/s
μ	Dynamic viscosity, $N.s/m^2$
ν	Kinematic viscosity, m^2/s
Ω	Combustion chamber loading, $kg.m^3/s.Pa^{1.8}$
Φ	Equivalence ratio
π	Pressure ratio
Ψ	Specific thrust, m/s
ψ	Hydrogen-to-carbon ratio
ρ	Density, kg/m^3
σ	Surface tension, N/m
τ	Combustion residence time, s
τ_e	Evaporation time, s
θ	Nondimensional total temperature
φ_s	Entropy function, equation 3.14

Roman symbols

ΔH	Net heat of combustion, J/kg

$\dot{m}$	Mass flow rate, kg/s
$\dot{m}_f$	Fuel mass flow rate, kg/s
$\dot{W}$	Power, W
A	Cross section area, m^2
API	API gravity
B	Bypass ratio
C_D	Derivative gain
C_I	Integral gain
C_P	Proportional gain
C_p	Specific heat, J/kg.K
C_{ex}	Thermal expansion coefficient in equation A.6, K^{-1}
D	Drop mean diameter, m
D_0	Initial liquid fuel drop mean diameter, m
e	Polytropic efficiency
EI	Emission index, g / kg of fuel
F	Thrust, N
f	Fuel-air ratio, kg of fuel / kg of air
H	Altitude, m
h	Specific enthalpy, J/kg
$H\%$	Hydrogen content, weight %
I	Polar moment of inertia, $kg.m^2$
k	Conductivity, W/m.K
K_W	Watson K factor
L	Latent heat of vaporization, J/kg
M	Mach number
MW	Molecular weight, kg/kmol
N	Relative spool speed
N_{abs}	Absolute spool speed, RPM

N_x Corrected relative spool speed at component x

P Power setting, %

p Pressure, Pa

Q Transfer number

q Fraction of air

R Gas constant, J/kg.K

RNI Reynolds Number Index

S Soot concentration, mg / kg of exhaust gas

s Specific entropy, J/kg.K

SFC Specific fuel consumption, g/kN.s

SG Specific gravity

T Temperature, K

t Time, s

T_b Boiling temperature, K

T_f Initial liquid fuel temperature, K

V Velocity, m/s

VCF Volume correction factor

x_n Molar ratio

x_v Volume ratio

x_w Weight ratio

Subscripts

∞ Ambient

a Air

b Burner or combustion chamber

c Sonic condition

$comp$ Compressor (or fan)

$corr$ Corrected

cr Critical

d	Diffuser
eff	Effective
F	Liquid fuel
fan	Fan
fn	Bypass (or fan) nozzle
g	Gas
H	High-pressure
HPC	High-pressure compressor
HPT	High-pressure turbine
L	Low-pressure
LPC	Low-pressure compressor
LPT	Low-pressure turbine
m	Mechanical
map	Unscaled parameter value read from component map
mix	Fuel mixture
n	Nozzle
pz	Primary zone
R	Reference (design)
r	Reduced
$read$	Scaled parameter value read from component map
ref	Reference fuel
s	Isentropic or surface (in equations 3.4 and 3.5)
SL	Sea level
st	Stoichiometric
sz	Secondary zone
t	Total or stagnation
$turb$	Turbine

List of Acronyms

0-D	0-Dimensional.
1-D	1-Dimensional.
2-D	2-Dimensional.
3-D	3-Dimensional.
APR	Aqueous Phase Reforming.
ARA	Applied Research Associates, Inc.
ASTM	American Society for Testing and Materials.
ATJ	Alcohol-to-Jet.
BtL	Biomass-to-Liquid.
CAAFI	Commercial Aviation Alternative Fuels Initiative.
CFD	Computational Fluid Dynamics.
CH	Catalytic Hydrothermolysis.
CNG2020	Carbon-Neutral Growth from 2020.
CO_2	Carbon Dioxide.
CO	Carbon Monoxide.
CRC	Coordinating Research and Council.
CtL	Coal-to-Liquid.
DSHC	Direct Sugar to Hydrocarbon.
EIA	Energy Information Administration.
FOG	Fat, Oil, and Grease.
FT	Fischer-Tropsch.
GHG	Greenhouse Gas.
GtL	Gas-to-Liquid.
H_2O	Water Vapour.
H_2	Hydrogen.
HDCJ	Hydrotreated Depolymerized Cellulosic Jet.
HDO	Hydrodeoxygenation.

HEFA Hydrotreated Esters and Fatty Acids.

HPC High-Pressure Compressor.

HPT High-Pressure Turbine.

HP High-Pressure Spool.

HRJ Hydrotreated Renewable Jet.

HVO Hydrotreated Vegetable Oils.

IATA International Air Transport Association.

ICAO International Civil Aviation Organization.

ICV Inter-Component Volume.

LPC Low-Pressure Compressor.

LPT Low-Pressure Turbine.

LP Low-Pressure Spool.

LTO Landing and Take-Off Cycle.

LUC Land-Use Change.

MBMs Market-Based Measures.

MSW Municipal Solid Waste.

N_2 Nitrogen.

NATO North Atlantic Treaty Organization.

NO_2 Nitrous Oxide.

NO_x Oxides of Nitrogen.

NO Nitric Oxide.

O_2 Oxygen.

PID Proportional-Integral-Derivative.

SAF Sustainable Alternative Fuel.

SAK Synthetic Aromatic Kerosene.

SIP Synthesized Iso-Paraffins.

SKA Synthetic Kerosene with Aromatics.

SK Synthesized Kerosene.

SMD Sauter Mean Diameter.

SO_x Oxides of Sulfur.

SPK Synthetic Paraffinic Kerosene.

TF Task Force.

TOC Top of Climb.

TO Take-Off.

U.S. United States of America.

UCO Used Cooking Oil.

UHC Unburned Hydrocarbons.

WtL Waste-to-Liquid.

Chapter 1

Introduction

The aviation industry is the only anthropogenic source of air pollution in the upper troposphere and lower stratosphere. It accounts for about 2% of the global greenhouse gas (GHG) emissions worldwide. While only contributing a small percentage of global GHG emissions, by the year 2030 air traffic is expected to double, with continued growth to 2050. It follows an estimation that aircraft noise and emissions that affect local air quality and global climate will ultimately increase, although at a rate slower than aviation demand [1].

In 2009, International Air Transport Association (IATA) member airlines (covering around 85% of all commercial flight operations) recognized the need to address the global challenge of climate change through the commitment to achieve: improvement in fuel efficiency of 1.5% per annum from 2009 to 2020, carbon-neutral growth from 2020 (CNG2020) and a 50% reduction in CO_2 emissions by 2050, compared to 2005 [2]. This commitment was the world's first sector-specific climate change set of goals. In 2010, at the 37^{th} Session of the International Civil Aviation Organization (ICAO) Assembly, ICAO Member States adopted the following goals for the global aviation industry: global average fuel efficiency of 2% per annum through 2020, aspirational goals for improving fuel efficiency 2% per annum through 2050 and keep CNG2020 target. At the 38^{th} Session of the ICAO Assembly, in 2013, Member States reaffirmed ICAO's collective aspirational goals and agreed on a comprehensive strategy to progress all elements of its "basket of measures", namely: technology, operations, market-based measures (MBMs) and alternative fuels [1].

Technology is the main driver of the aviation industry. With investment in technology, the industry is already delivering on the first target with newer and more efficient aircraft. However, taking into account the constant growth of the aviation industry, with a forecast that passenger demand will increase globally by approximately 5% per annum in the medium term, the industry must adopt measures towards a sustainable growth. In this regard, Sustainable Alternative Fuels (SAF) are accepted as a key component for future aviation sustainable growth and overall carbon emissions reductions [2]. In fact, with the associated high volatility of petroleum fuel cost, the depletion of petroleum sources and terrorist activities in the Middle East, various industrialized and developing countries are already developing domestic sustainable sources of fuel and energy [3].

Considering its relevance for the near-term future of the aviation industry, through steady-state (design and off-design) and transient/dynamic aero-engine numerical performance and emissions analyses, the technical feasibility of adopting sustainable alternative fuels will be evaluated, in the present work. With already proven results for selected types of alternative fuels (with several test flights successfully performed), with the model implemented by the author, different types of fuels will be selected and evaluated exclusively on a thermodynamic basis. In this regard, ASTM fuel specifications are neglected during thermodynamic simulations. In order to compare thermodynamic results for burning of different fuels, a conventional jet fuel is defined and the implemented model is validated through comparison with a commercial model, GasTurb [4]. Then, different results based on the burning of the selected fuels are computed and compared. A subsequent comparison with experimental and theoretical results for similar fuels, available in the literature, is performed to assess the validity of results obtained.

1.1 Alternative Fuels Overview

The wide-scale deployment of Sustainable Alternative Fuels (SAF) is regarded as a crucial step towards meeting the aviation industry's carbon emissions reduction milestones. Allied to technological and infrastructural improvements and efficient operations, sustainable alternative fuels will play an important role in de-coupling emissions from the industry's growth, as schematically presented in Figure 1.1.

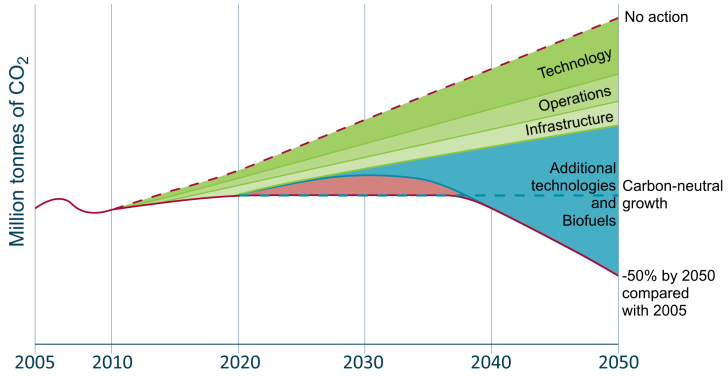

Figure 1.1: Indicative scheme of aviation industry's plan to address the global challenge of climate change ([5], adapted).

The adoption of new alternative fuels in a global scale, besides presenting possible advantages on an environmental basis, is also accepted as the best near-term route to ease aviation dependence on petroleum products (which is depleting), with electric power not expected on commercial aircraft before 2040 [6]. The fossil fuel dependence increased awareness was boosted in 2008, when a record peak of crude oil prices was verified. Additionally, its global implementation may provide new sources of employment as well as facilitate economic development in non-traditional fuel producing regions of the world [1].

Since aircraft and airport fuel storage and delivery systems are designed to last for decades, alternative fuels must be considered as "drop-in" fuels, that is, fuels must not require any modifications in infrastructures, aircraft and operations. Additionally, in order to have a sustainable alternative fuel option,

the feedstock must not compete with food production (non-edible feedstock) and the production must not be associated with land-use change impacts, such as deforestation [7, 8].

In short, the future of the wide-scale development of Sustainable Alternative Fuels is dependent on several key factors, such as, right fuel properties and handling for the engines (”drop-in”), the environmental impact, including CO_2 life cycle analysis, competition with food, water and land, and the economics of return on investment, production and sustainability [3].

Since 2009, five alternative production pathways were approved: FT-SPK and FT-SKA (Fischer-Tropsch process), HEFA-SPK (Hydrotreated Esters and Fatty Acids), SIP (Synthesized Iso-Paraffins) and ATJ-SPK (Alcohol-to-Jet); with SPK and SKA defined as Synthetic Paraffinic Kerosene and Synthetic Paraffinic Kerosene with Aromatics, respectively. Given the rate of production pathways approved (five production pathways approved in about 7 years, and three of them in the last 3 years), with ATJ-SPK not yet approved in the beginning of the writing of this thesis, and taking into account additional production pathways awaiting approval or still under initial development, the relevance and support towards alternative fuel implementation is on the rise. In Figure 1.2, adapted from [9], most relevant production pathways approved or being developed are summarized.

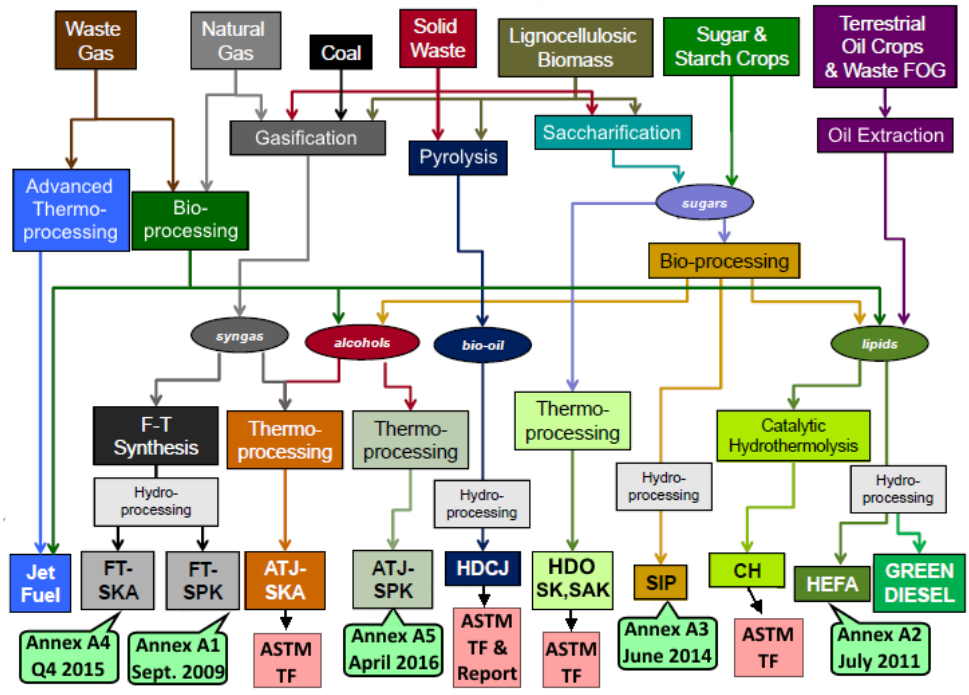

Figure 1.2: Summary of alternative jet fuel pathways and status ([9], adapted).

While technical feasibility was already proven for selected fuels, with several test flights performed since 2008 and over 1700 commercial airline flights (blends up to 50%), commercial deployment of sustainable alternative fuels is dependent on inherent costs for airlines and highly influenced by the competitive structure of the aviation industry. The challenge remains to produce large quantities of sustainably produced alternative fuels at a commercially competitive cost to airlines [2]. Sustainable alternative fuel demand shall be encouraged and supported by governments and policymakers, in the same way as it has been done for road transportation, preserving fair competition.

Continuous effort has been made in this regard with multi-stakeholder groups (airlines, airports, aircraft manufacturers, governments, biomass and biofuel producers and suppliers) working together on initiatives for the deployment of alternative jet fuels, with the highest number of initiatives occurring in 2015 (22 initiatives). In the same manner, several agreements were achieved between airlines and fuel producers, with about 29 agreements reported between 2009 and 2015 [2], being several of them long-term agreements (up to 10 years). With new production pathways being continuously developed, operational and environmental viability of wide range of different fuels must be verified so that the best drop-in solutions may be properly defined and the risk associated with the transition from conventional jet fuel to alternative fuels lowered.

1.2 Fuel Properties and Effects on Combustion Performance and Emissions

1.2.1 Fuel Composition Overview

Conventional and synthetic aviation fuels are mainly composed of different types of hydrocarbons. It is usual to classify the hydrocarbons present in a petroleum fuel into four main groups: paraffinic, olefinic, naphthenic and aromatic. Aviation jet fuels are mostly composed by paraffins (approx. 60%), naphthenes, or cycloparaffins (approx. 20 %), and aromatics (approx. 20%). Sulfur compounds, which are highly corrosive, may also be found (typically around 500 ppm) in jet fuels and olefins are generally only present in trace amounts [3, 10].

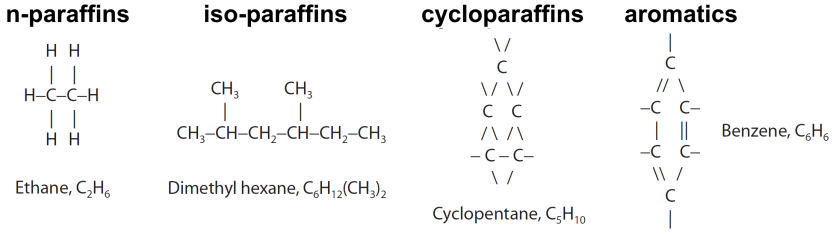

Figure 1.3: Examples of hydrocarbon compound types structures ([3], adapted).

Paraffins are one of the major components of aviation fuels. Paraffins consist of single bonded carbon chains in which each carbon atom is fully saturated with hydrogen. They may be straight chain ('normal') or branched chain (iso-paraffin) molecules, resulting in a very stable structure with high heat release per unit weight [10].

Cycloparaffins (or naphthenes) have a saturated ring structure that decreases the hydrogen-to-carbon ratio and lowers the heat release per unit weight, while increasing their density. Their freezing points are lower than comparable normal paraffins with the same number of carbon atoms [10].

Aromatics (or naphthalenes), in turn, are unsaturated cyclic hydrocarbons, containing one or more carbon rings, each with six carbon atoms. Although similar in structure to the cycloparaffins, they contain less hydrogen and, in consequence, their heat release per unit weight is appreciably lower. In turbine fu-

els, aromatics tend to form smoke (soot) when burned and to form coke deposits on combustor surfaces. On the other hand, low aromatic composition may cause seal swell problems (leaks) [3, 10].

In Figure 1.3, examples of hydrocarbon compound types are presented [3].

1.2.2 Liquid Fuel Combustion Overview

According to Lefebvre [3, 11] and Odgers [12], the main influences of fuel properties in gas turbine combustion, and relevant for the present work, are: atomization quality, evaporation rate, combustion efficiency and exhaust pollutants. Additionally, mention should be made to fuel influences on ignition, flame extinction and liner-wall temperature, although not analysed in the present thesis.

In this regard, to evaluate the influence of a given fuel on combustion, relevant physical properties must be known, such as: liquid density, viscosity, surface tension, distillation range and hydrogen-to-carbon ratio (hydrogen content). Additionally, the knowledge of fuel critical properties (critical temperature and pressure), molecular mass, vapour pressure, specific heat, latent heat of vaporization or thermal conductivity will enable more accurate estimations of a given fuel burning behaviour.

Fuel properties such as the flash and freezing point give relevant information about the viability of adoption of a given fuel for flight and storage purposes. While the flash point is defined as the lowest temperature at which a fuel gives off sufficient vapour to form a flammable mixture with air (a measure of its flammability and useful from the viewpoint of fire risk), the freezing point is defined as the temperature at which a fuel first shows the presence of solid particles or wax crystals, which is relevant given typical flight high altitudes and colder regions on the planet [3].

Combustion Process Overview

In an aero-engine combustor, the chemical energy of the fuel injected is converted into thermal energy [13]. For all gas turbine components, the combustor may be considered as the most complex to analyse theoretically. Much of the combustion design process still relies upon empirically derived design rules [14].

The combustor may be in general divided into 3 main zones: primary, secondary (or intermediate) and dilution zones (Figure 1.4). In the primary zone, combustion conditions are provided and flame is stabilized. Within the primary zone, a recirculation zone is usually defined, where a portion of the hot combustion gases are recirculated to provide continuous ignition. In the primary zone, temperatures above 2000 K are usually verified, at which dissociation may occur with resulting significant concentrations of carbon monoxide (CO) and hydrogen (H_2) in the efflux gases [3].

In the secondary zone, conditions for combustion completion are provided (when necessary). For this reason, in general, the combustor combustion volume accounts for both the primary and secondary zone volumes. Finally, the main function of the dilution zone is to reduce the hot gases temperature to a lower temperature, suitable for turbine operation. Additionally, it may act as an extension of the secondary zone (if required) [3, 13].

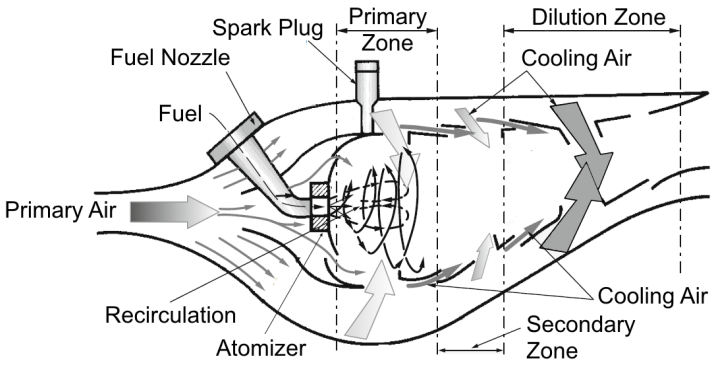

Figure 1.4: Schematic representation of conventional combustion chamber and air distribution ([15], adapted).

Atomization Quality

In an aircraft engine combustion chamber (and most gas turbines), fuel drops (droplets) are injected using an atomizer. The atomization quality of a given fuel is typically measured through the size of the droplets, usually defined as the Sauter Mean Diameter, SMD (in the present work, simply referred as D). According to Lefebvre [3], the atomization quality is dependent on the type of atomizer and, in general, mainly dependent on fuel viscosity, surface tension and density.

Viscosity measures the internal resistance to motion caused by cohesive forces among the fluid molecules and the surface tension quantifies the specific free energy of a liquid surface at interface with another fluid. The fuel liquid density is the mass per unit volume relationship of the fluid, relevant in defining energy content in the fuel tank. With increase in fuel viscosity and surface tension comes, typically, a deterioration of fuel atomization. High values of liquid viscosity are also prejudicial in terms of fuel injection, requiring higher values of injection differential pressure [3, 12].

Evaporation Rate

With liquid fuel properly injected, in the form of droplets, the combustion process may take place. According to Odgers [12] and Lefebvre [3], the overall time of combustion is given by the sum of the evaporation, reaction (chemical) and diffusion time. Typically, the worst it is the atomization quality, the more the combustion becomes evaporation-controlled. The evaporation process may be summarized, in most cases, through the establishment of a steady-state evaporation rate.

According to the work of Chin and Lefebvre [16], when a fuel liquid drop is immersed in a hot quiescent gas, its temperature will rise from its core to its surface. This temperature rise will, eventually, cause an increase of partial pressure and concentration of fuel vapour at its surface and a stage is reached where all of the heat transferred to the droplet is used as heat of vaporization and the droplet temperature stabilizes at a "steady-state" (or wet-bulb) value. In this regard, it is assumed as well, with good accuracy, that eventually the droplet diameter (squared) will decrease linearly with time ($D^2 - Law$). In Figure 1.5 this assumption is verified for two different fuels and heat-up periods.

For given ambient conditions (pressure and temperature), the normal boiling point may be regarded as the most relevant fuel property to estimate fuel evaporation behaviour, since it is directly related to

fuel volatility and vapour pressure. In general, the lower it is the fuel normal boiling point, the higher it is the evaporation rate, that is, the faster it is the evaporation process. To account for the fuel boiling point, its distillation range must be defined. Since aviation fuels are a mixture of many compounds, each having its own boiling point, these fuels have no single boiling point, but rather a distillation range defined by the temperature as a function of the percentage fuel evaporated (or recovered) [3].

The study of evaporation rates is, mainly, considered relevant in cases where different fuels with different volatilities are injected for combustion, which is the case of the study of alternative fuels [16].

Combustion Efficiency

The fuel effects on atomization and evaporation rate will ultimately have an impact on combustion efficiency. In modern aircraft, low levels of combustion efficiency are considered as unacceptable due to the inherent decrease in fuel efficiency and the increase in pollutant emissions (mainly UHC and CO). Therefore, values in the order of 99% of combustion efficiency are usually verified [3]. Although its actual calculation is highly complex, through comparisons of atomization and evaporation qualities, different combustion efficiencies with burning of different fuels can be compared with good accuracy assuming evaporation-rate controlled combustion [3, 11], as in Figure 1.6.

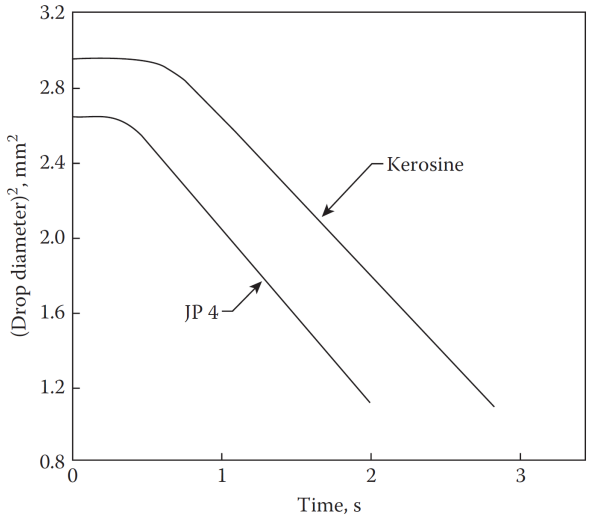

Figure 1.5: Evaporation rate curves for kerosene and JP-4 [3].

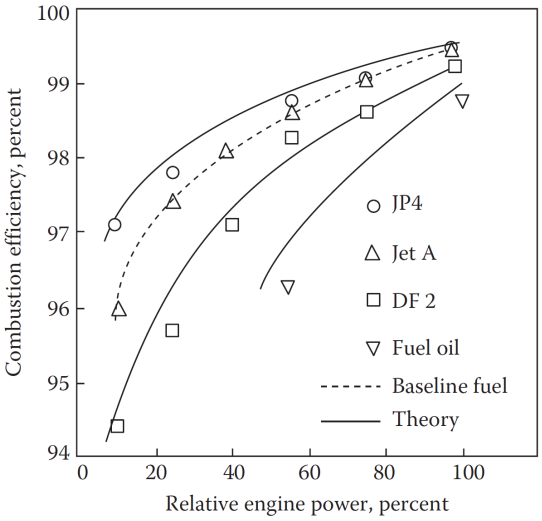

Figure 1.6: Influence of fuel type on combustion efficiency. Theoretical results based on evaporation-controlled combustion assumptions [3].

Although fuel consumption may be highly dependent on combustion efficiency, it will always be dependent as well on the fuel heating value (in this work referred typically as net heat of combustion). The heating value is a relevant combustion property of a fuel, which quantifies the heat liberated when the fuel is burned to completion. Its value is mostly dependent on its composition, such as the hydrogen-to-carbon ratio, with some correlation between relative density and heating value also typically valid (the higher the density the lower the heating value) [3]. In this regard, alternative fuels should maintain or increase the heating value in comparison with conventional kerosene (around 43.2 MJ/kg [10]).

Pollutant Emissions

With complete combustion, carbon dioxide, CO_2, and water, H_2O, in vapour form, are the ideal products present in the exhaust gases. Emission of both substances is associated with enhanced greenhouse effects, with water vapour having an increased relevance in aircraft engines emissions with the resulting formation of contrails (condensation trails). However, the actual combustion when incomplete and due to high temperatures result in emissions of undesired substances: oxides of nitrogen, NO_x, carbon monoxide, CO, unburned hydrocarbons, UHC, soot (or smoke) and oxides of sulfur, SO_x [13].

While NO_x and soot pollutant emissions concentrations increase with engine power setting, UHC and CO have the opposite behaviour (Figure 1.7). Therefore, maximum NO_x and soot production occurs at take-off and UHC and CO at idle conditions. Currently, pollutant emissions of such species, are regulated based on emissions standards set by the ICAO, for a reference Landing and Take-Off (LTO) cycle [13, 17].

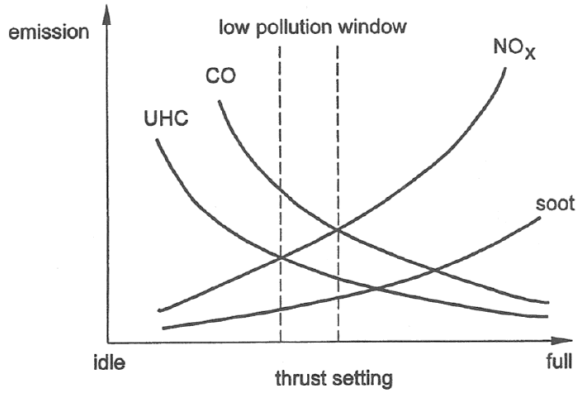

Figure 1.7: Typical influence of thrust setting on NO_x, CO, UHC and soot pollutant emissions [13].

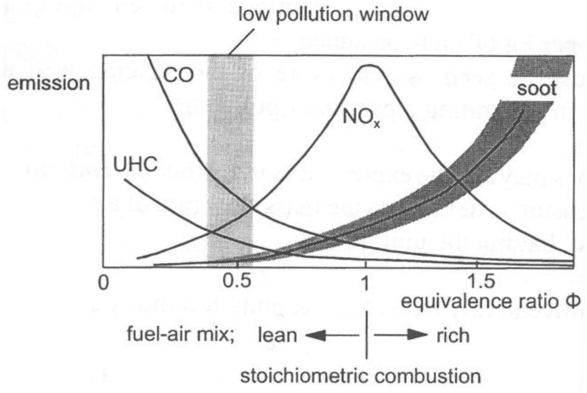

Figure 1.8: Typical influence of fuel-air mixing on NO_x, CO, UHC and soot pollutant emissions [13].

To quantify pollutant emissions of a given substance (subscript i), it is calculated the emission index parameter, EI_i. The emission index of a certain combustion product enables the comparison between the amount of fuel burned and the amount of pollutant emitted [13]. Typically, and true throughout the present thesis, this index comes in g_i / kg of fuel. For the case of soot pollutant emissions, its concentration, S, is typically given in mg of soot with kg of exhaust gas [18].

The most undesired pollutant emissions are NO_x emissions (typically 90% NO and 10 % NO_2). The major concerns associated with NO_x emissions are the production of photochemical smog at ground level, but also the damage caused to plant life and acid rain added problem. For subsonic aircraft its effect is mainly visible through ozone formation in the troposphere (up to 12 km of altitude), which may be associated with respiratory illnesses, impaired vision, headaches, and allergies [3, 13].

The most relevant NO_x formation mechanism is the thermal-NO_x process. In short, due to high flame temperatures and, as consequence, with occurrence of thermal dissociation of oxygen (O_2=2O) and water vapour, H_2O, with increase in hot gases residence time, there is an increase in NO production. Fuel-air ratio also plays an important role in NO_x formation with highest concentration levels occurring near stoichiometric conditions, as in Figure 1.8. NO_x formation (mainly NO) may be summarized with

the following chemical reactions [13]:

$$N_2 + O \leftrightarrow NO + N$$

$$N + O_2 \leftrightarrow NO + O$$

$$N + OH \leftrightarrow NO + H$$

The presence of CO and UHC species in the exhaust gases is a manifestation of incomplete combustion. In the case of CO emissions, inadequate burning rates, due to low fuel-air ratio or insufficient residence time, or inadequate mixing of fuel and air, are the main reasons associated with the pollutant formation. In turn, unburned hydrocarbons, UHC, include fuel that emerges from the combustor in the form of drops or vapour, as well as products with lower molecular weight such as methane, normally associated with poor atomization and inadequate burning rates. Both species are considered as toxic [3, 11].

Soot formation (or smoke), although highly complex, is mainly associated with fuel atomization and fuel-air mixing. It consists almost entirely of carbon (black) particles and creates problems of exhaust visibility and soiling of the atmosphere [3, 13]. From the referred undesired pollutant emissions, smoke emissions are usually regarded as the most influenced by the fuel composition; example being the fact that with increase in aromatic content an increase in soot formation is associated [3]. Smoke emissions are regulated through the definition of a Smoke Number, SN, as in [17].

According to reference [3], for aircraft equipped with modern engines, NO_x emissions predominate both in the vicinity of the airport (LTO cycle) and during altitude cruise, with a larger fraction of the total emissions mass occurring during cruise.

1.3 Aero-Engine Thermodynamic Modelling, 0-D

To take into account sustainable alternative fuels effects on overall aircraft engines performance and influence on undesired pollutant emissions, a generic two-spool turbofan (Figure 1.9) will be thermodynamically modelled in the present work. A 0-D engine model approach was selected to fulfil this essay's objectives. With this engine model, all components are defined by fluid inlet and outlet conditions without requiring detailed component geometric information.

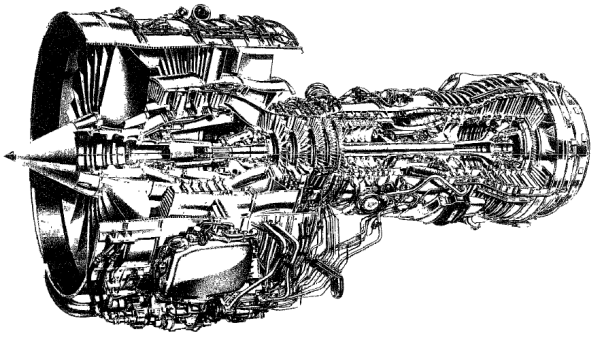

Figure 1.9: Example of a twin-spool turbofan engine (cutaway view) [19].

Over the course of years, advances in computer technology have led to the increasingly widespread use of CFD for engine analysis and design purposes. Given the high complexity associated with combustor simulation, CFD calculation of flow fields throughout a combustor are widely performed [3]. However, given the scope of the present work, it is considered that, fuel effects on an aircraft performance should be analysed considering different flight and engine operating conditions. Doing so, a more accurate and useful preview of real fuel effects may be estimated.

Due to its simplicity, when compared with 1-D, 2-D or 3-D models, and accurate results obtained, a 0-D model will be followed for all thermodynamic analyses: design point, off-design and transient analyses. They can be run on all computer types, which is an extremely helpful feature due to the wide range of people who may need to run engine performance models [20].

For the numerical programming, MATLAB® language will be used. Being a high-level language and interactive environment for numerical computation, visualization, and programming, with more than a million engineers and scientists in industry and academia using MATLAB [21], it is considered as an adequate programming language for the scope of this thesis.

1.3.1 Design Point Modelling

The performance of a certain engine at a various number of flight conditions is dependent on its design point performance. Therefore, design point performance is central to the engine concept design process. The resulting overall performance of the designed engine will be crucial to its commercial success or otherwise [14].

The design point is usually defined based on the operating condition where the engine spends the most time or based on a high-power condition. In the present work, high-power condition was selected as the engine design point, through the definition of Top of Climb, TOC (or maximum climb) [22].

The off-design and transient simulations will require detailed knowledge of several design point parameters of the chosen engine cycle. The design performance thermodynamic cycle calculation follow the widely used procedure described by several authors, such as in [14, 15, 19, 20, 23]. In short, a straightforward thermodynamic cycle calculation is performed, based on turbofan spool work balances, polytropic compression and expansion processes and separate nozzles exhaust gases conditions [22]. For increased accuracy of the results obtained, a variable specific heat gas model is considered throughout the modelling of the design point, off-design and transient models.

In the present work, it was not the aim of the study to precisely simulate a particular engine. However, for consistency in calculations and results, parameter selection was based on reasonable assumptions enabling a comparison of different fuels burning effects on a ”generic” commercial turbofan. Most of the assumptions (component efficiencies and pressure losses, for example) were based on the work of Mattingly [23]. This topic is discussed in detail in chapter 3 (section 3.7).

1.3.2 Off-Design Modelling

Being the engine properly defined, through design point performance calculation, an off-design performance analysis may be performed. While design point performance analysis is of a parametric nature, the off-design performance calculation is based on a previously defined engine.

With the engine geometry fixed by the design point calculation, the performance at other key operating conditions can be evaluated. It follows that, parameters such as the total thrust, specific fuel consumption, bypass ratio or inlet air mass flow may be computed with variations in altitude, flight Mach number, spools speeds and/or the high-pressure turbine inlet temperature. In this regard, operating conditions like the take-off, the ground and flight idle and cruise flight, may be simulated [13, 14].

In the off-design performance calculation procedure, there are mainly two approaches usually followed. In a simplified approach, assumption of constant component efficiencies and constant total pressure losses is performed with reasonable results. For more accurate results, information about each compressor and turbine characteristics is used through the reading of component maps. In short, for a given inlet mass flow rate and relative spool speed (corrected values), a correspondent pressure ratio across the component and adiabatic isentropic efficiency are readily obtained, as presented in Figure 1.10. These component maps are usually constructed based on theoretical aerodynamic models and rig testing [20]. Off-design performance thermodynamic cycle calculations are widely described in the literature, such as in [4, 14, 15, 19, 20, 23].

In the present work, the off-design performance calculation procedure will follow the latter approach referred, based on known component characteristics through component map reading. This approach is considered due to its inherent increase in accuracy, with actual effects of spool speeds verified, but also due the intended additional study of transient simulations.

This approach is followed by Kurzke, a gas turbine performance specialist who has worked since the 1970's in the field of gas turbine simulation and development, author of the commercial gas turbine software, GasTurb. This software enables to evaluate the design and off-design performance of the most common types of gas turbines [4]. This fact was considered as highly important for model validation, which, in this work, is performed for a given fuel through comparison with performance results obtained with the referred software.

It is an highly multi-variable iterative process, with the widely used Newton-Raphson method being followed in the present work. Details on the implementation are displayed in chapter 3 (section 3.8).

1.3.3 Transient Response Modelling

The engine performance behaviour (through burning of different fuels) will be completed with a simplified 0-D aero-engine transient analysis. Transient performance deals with the operating regime where engine performance parameters are changing with time [14].

With implementation of a transient engine model, engine operation during manoeuvres (often referred to as handling) such as slam accelerations or decelerations may be evaluated. This implementation will ultimately be associated with the control system employed to account for schedules of fuel mass

flow [14].

Engine transient behaviour is mainly a result of differences in compression power required and turbine power generated, induced by a certain change in engine operation, mainly through fuel mass flow rate schedules. This will result in either a spool deceleration (Figure 1.11) or acceleration.

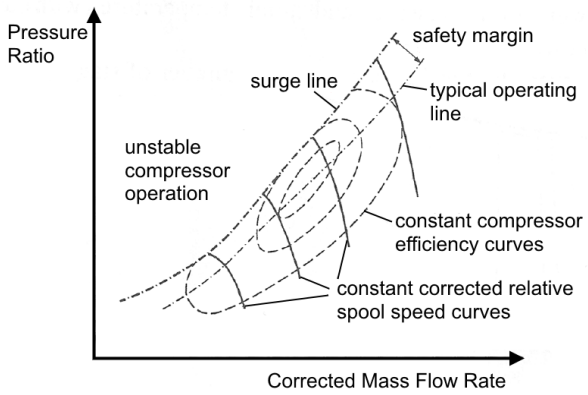

Figure 1.10: Typical compressor map ([13], adapted).

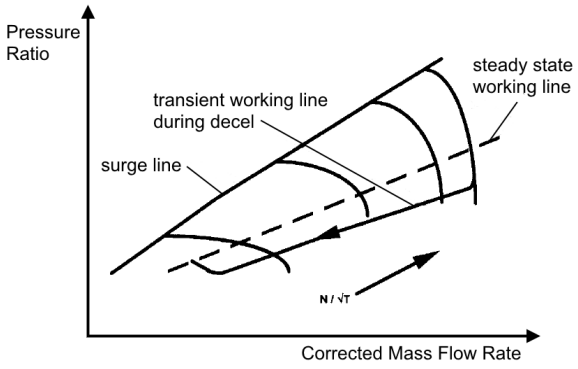

Figure 1.11: Typical transient deceleration behaviour on a compressor map ([14], adapted).

Traditionally, two transient methods are used for transient simulations. In the inter-component volume method (ICV), mass flow imbalances, in a given component volume, are accounted for [24]. On a different approach, transient calculations may be performed through a constraint satisfying iterative method, where a similar iterative method to that of off-design calculation is performed for each time step. Although the ICV is preferred in terms of computation time, it is less accurate when compared with the latter approach [25]. Aero-engine thermodynamic transient simulations, based on referred numerical methods, are described in the literature [4, 14, 19, 20].

In the present work, the transient iterative method will be assumed since, given the main aim of the study, it is considered of higher importance the accuracy of calculations when compared with computational consumption. Following the same procedure as for off-design calculations, a Newton-Raphson method will be used and results validated through comparison with GasTurb 12 [4] results. The implementation of the transient model is properly detailed in chapter 3 (section 3.9).

1.3.4 Pollutant Emissions Prediction Models

As previously stated, along with engine performance calculations at different flight operating conditions, it is of interest to evaluate the influence of the burning of different fuels on pollutant emissions. Several empirical and semi-empirical emissions models have been proposed in the literature to provide estimates of the exhaust emissions of NO_x, CO, UHC, and soot. Due to the higher complexity involved in the prediction of UHC and soot emissions, the majority of empirical and semi-empirical emission models account for NO_x and CO emissions [18].

The calculation procedures in most of these models are based on the concept that the concentrations of various species are governed by reaction rate, mean residence time, and the mixing process. It is recognized that factors inhibiting the formation of one pollutant may enhance the formation of the others

[18]. Due to the inherent simplicity of implementation, these models enable a good overall pollutant emissions prediction for different flight conditions without compromising their integration in the overall engine model. In fact, for better understanding of pollutant emissions and for design purposes, CFD analysis should be performed, which may be infeasible due to both computing power limitations and economic reasons [26].

Empirical models can be highly important in the design and development of low-emissions combustors, reducing the complex problems associated with emissions to forms that are more meaningful and tractable to the combustion engineer [3]. In fact, this approach is widely used for low-emissions turbofan analyses, as in reference [26] where an early-stage design optimization of a low NO_x emissions turbofan is performed at off-design operating conditions.

Most of NO_x prediction methods available in the literature are based on the works of Lipfert, Lefebvre, Odgers and Kretschemer, Lewis or Rizk and Mongia, with respective models summarized in references [3, 27]. Similar correlations have been developed for CO prediction, with one important difference being the fact that the formation of CO in the combustion zone takes more time. Most relevant correlations for CO emissions estimation are detailed in the work of Lefebvre [3] and Rizk and Mongia [18]. Fewer accurate models for soot and UHC are available in the literature. There are, however, reasonable correlations for both species in the work of Rizk and Mongia [18].

For consistency, and since the work of Rizk and Mongia acknowledges the importance of fuel evaporation, in the present work, prediction models based on [18] will be followed for all species emissions predictions. Details on the correlations and implementation are present in chapter 3 (section 3.10).

1.3.5 Numerical Iterative Method

For a certain system of equations, the Newton-Raphson iterative method only requires initial solution guesses and the calculation of the Jacobian matrix of the system, $[J]$, at each iteration. The iteration process may be summarized with the following equation:

$$x_{k+1} = x_k - \frac{f(x_k)}{[J]}, \tag{1.1}$$

where x represent the unknown variables, f the system solutions and the subscript k defines the iteration at which the unknown or solution is defined. In the present work, besides one-variable calculations due to variable specific heat gas model followed (as explained in chapter 3), off-design and transient calculations take advantage of this iterative procedure through mass, fixed-geometry and work (only in off-design) compatibility errors calculations.

The main disadvantage of the present method has to do with the fact that the Jacobian matrix must be calculated in each iteration. In turn, convergence is obtained for most cases (damping may be required), even if poor initial guesses are made. The Newton-Raphson iterative method will be followed throughout the present work, either through multi-variable or single-variable implementation. Additional details about the Newton-Raphson iterative method are detailed in [4, 20].

1.4 Objectives

In the present work, the main goal is to analyse the impact of burning of different fuels in the performance and pollutant emissions of a typical turbofan, through a numerical analysis.

In order to do so, fuels of interest must be properly studied. In this regard, it will be considered of great relevance the study of feasible Sustainable Alternative Fuels, so that conclusions can be achieved about the possibility of transitioning from crude dependent jet fuel production to a greener alternative route in the near-term.

A thermodynamic aero-engine model will be implemented by the author, with MATLAB as the programming language used. Then, a model enabling steady-state, for design and off-design conditions, and transient thermodynamic calculations, will be the basis of all the results that are to be obtained (performance and pollutant emissions), resulting in the need to properly validate computed results by comparison with results obtained in the literature and with a scientifically accepted commercial software.

With the goal of implementing a numerical aero-engine model for steady-state and transient calculations properly achieved, integration of fuel effects on combustion for different operating conditions must also be achieved. This part of implementation will ultimately allow the comparison of burning of different fuels in an operational and environmental perspective.

Although, in the present thesis, simplified approaches such as the implementation of a 0-D aero-engine model, the adoption of empirical pollutant emissions models or the implementation of a (quasi) steady-state evaporation model are followed, the results here obtained may contribute to a better understanding of the actual technical feasibility of a worldwide use of a wide range of alternative fuels by the aviation industry, towards becoming independent of conventional petroleum-based kerosene.

1.5 Thesis Outline

In the next chapter (chapter 2), a general understanding of the types of fuels to be analysed (conventional and sustainable alternative fuels) is performed. Then, the implementation of steady-state and transient aero-engine models as well as the modelling of fuel effects on pollutant emissions are detailed in chapter 3.

Being the numerical model properly detailed, results of the burning of alternative fuels and a conventional fuel (from crude oil) are presented, discussed and validated on the following chapters. While in chapter 4 and chapter 5, off-design and transient performance results are presented, respectively, in chapter 6 steady-state pollutant emissions results are presented.

In the last chapter (chapter 7), the conclusions arrived at, with the development of the present thesis, are presented. It should also be highlighted additional work details and results that are presented in the Appendix. In fact, fuel properties estimations, the fuel blending model and an overall summary of the fuels of interest properties are presented in Appendix A, supplementary data in Appendix B and details concerning the gas model implemented in Appendix C.

Chapter 2

Sustainable Alternative Fuels

The main aim of the present work is to compare the technical feasibility of a wide range of alternative jet fuels. In this chapter, the alternative jet fuels to be analysed and respective production pathways are briefly summarized, for a better understanding of each alternative route.

The types of alternative production pathways to be considered are: Fischer-Tropsch (FT), Hydrotreated Esters and Fatty Acids (HEFA), Alcohol-to-Jet (ATJ), Synthesized Iso-Paraffins (SIP), Catalytic Hydrothermolysis (CH) and Hydrodeoxygenation (HDO).

The selection of the alternative fuels to be studied was based on the most relevant production pathways described at the time of the writing of the thesis and, ultimately, based on the availability of fuel properties information in the literature. In fact, additional fuels from production pathways such as HDCJ or FT-SKA, that would be eligible for the present study, are not considered due to lack of relevant fuel properties information available in the literature, at the time of writing of the thesis.

In the present chapter, the conventional jet fuel properties and standard specifications limits are briefly summarized. Then, the FT, HEFA, ATJ, SIP, CH and HDO production pathways are detailed, with brief references to the certification status, the feedstock required and production process. It follows a brief summary of alternative fuels selected for the present study and fuel properties and composition comparison. Finally, environmental and economical impacts of alternative fuels implementation are summarized as well.

2.1 Conventional Kerosene

As previously reported, the major goal of the present thesis is to compare turbofan engine performance and emissions results obtained considering alternative fuels opposed to what would be obtained conventionally. In order to accomplish that, the first step is to define the reference fuel.

In the United States of America, civil aviation turbine fuels requirements are defined by the international standard ASTM D1655 and the most common grades are designated as Jet A and Jet A-1 (JP-8 is the equivalent military grade). Both grades present the same specifications limits, except for the freezing point, where Jet A-1 has a lower maximum limit [10]. To account for alternative jet fuels certification, the

specification ASTM D7566 was created. In Europe, the standard DefStan 91-91 mirrors the U.S. ASTM certification for alternative fuels [28].

Since jet fuel properties may vary according to the quality of crude oil and refinement process, the quantity produced or even the accuracy of measurements, properties are not fixed and for the present work typical values must be assigned. With that goal, the collecting of conventional kerosene properties data was based mainly on *CRC's Handbook of Aviation Fuel Properties* [10]. A typical value for hydrogen content (in weight percentage) was obtained from reference [29]. The conventional kerosene grade selected for this purpose was Jet A-1. The most relevant properties of the Jet A-1 along with ASTM D1655 specification limits are presented in the Appendix A, Table A.1.

2.2 Alternative Production Pathways

2.2.1 Fischer-Tropsch, FT

Overview

In 2009, the first pathway for synthetic kerosene production was approved by the ASTM. This production pathway is designated by the Fischer-Tropsch (FT) process [28]. The aviation fuel produced from such a process is known as Fischer-Tropsch Synthetic Paraffinic Kerosene, or FT-SPK. Currently, commercial scale fuel production from the FT process is only performed from coal (Sasol) or natural gas (Shell and Syntroleum) [30].

Certification

The approval by the ASTM of the FT production pathway limits a maximum blend ratio of 50% with a conventional jet fuel, under ASTM D1655 specifications (Annex A1). The minimum aromatic content of 8% for jet fuels has motivated a growing interest in synthetic kerosene aromatics (SKA) [31]. Fischer-Tropsch Synthetic Kerosene with Aromatics (FT-SKA) is viewed as a good candidate to achieve neat synthetic kerosene (100% blend). According to CAAFI [32], this route was approved as a blend (maximum blend ratio of 50%) by the ASTM in the fourth quarter (Q4) of 2015 (Annex A4 to ASTM D7566).

Feedstocks

The FT process can be defined considering the feedstock: from Coal (Coal-to-Liquid, CtL), from Natural Gas (GtL), from Biomass (BtL) or from wastes, like municipal solid wastes, MSW, (WtL) [33]. For sustainable jet fuel, the feedstock should be biomass or wastes [30]. Lignocellulosic biomass such as woody energy crops, agricultural and forestry residues, algal biomass and municipal solid wastes are suitable for the production of jet-fuels via the Fischer-Tropsch process [2, 34].

Production

This production pathway consists of four main steps. In the first step, the feedstock is converted into syngas (a mixture of CO and H_2) with the gasification process. The syngas is then treated and further processed into hydrocarbon chains of varying length, through the proper Fischer-Tropsch synthesis process by feeding pure syngas at controlled pressure and temperature, over a catalyst that assists in the formation of the desired hydrocarbon molecules. The product must then be refined through hydrocracking and isomerization. In the final step, the raw product is distilled and separated into individual products, such as jet fuel, diesel and lubricants. If the feedstock is biomass or wastes, an additional initial step of pretreatment is required to reduce particle sizes [28, 30, 35, 36].

2.2.2 Hydrotreated Esters and Fatty Acids, HEFA

Overview

In July 2011, another production pathway was approved, as Annex A2 to ASTM D7566, designated by HEFA (Hydrotreated Esters and Fatty Acids). Until ASTM certification, this pathway was usually referred to as HVO, for Hydrotreated Vegetable Oils, but, as ASTM aims for a generic specification and some feedstocks are solid fats rather than oils, a new acronym was introduced [28]. The aviation fuel produced from such a process is designated by HEFA-SPK (or HRJ-SPK). One of the main advantages of this technology pathway is the possibility to integrate this process into an old oil refinery (with an additional step) [2].

Certification

Like the FT-SPK fuel, it does not contain aromatic compounds, and is only certified for use as a blend with a 50% maximum blend ratio. Approval is currently pursued for a process exclusively yielding aromatics, and such aromatics could be used in conjunction with HEFA kerosene. Based on the HEFA production pathway, Boeing proposed a ”green diesel” (or renewable diesel) approach to be considered as aviation drop-in for low blending. Although a flight test with 15% of green diesel was successfully completed in December 2014, the proposal is still at a fairly early stage [2, 28].

Feedstocks

The production of HEFA fuels requires triglycerides such as vegetable oils or waste FOG (fats, oils and grease) as feedstock [9]. The most promising candidates for the production of jet fuel are inedible oils such as those produced by crops (e.g. camelina or pennycress) or shrubs or trees (e.g. castor or jatropha). Some yeasts, fungi, and certain algae (and microalgae) are also capable of fermenting sugars into lipids. However, as of now, algae oils are still in early stages of development. On the category of wastes, UCO (used cooking oil) or Tallow (animal fat) are examples of possible HEFA feedstocks [2, 34].

Production

The process to convert oils into fuel, HEFA-SPK, is performed in a similar way to that of crude oil refinement [2]. The first stage of production corresponds to the pretreatment and preparation of the biomaterial. Then, the feedstock (oil) is hydrotreated. This phase corresponds to a reaction of the feedstock with hydrogen to remove the oxygen and convert the triglyceride into hydrocarbons. These hydrocarbons are then cracked and isomerized to the desired chain lengths, to yield a mixture of n-alkanes and isoalkanes, in order to fit the target specifications (e.g. cold flow properties). The product is then distilled and separated into individual products, such as green (or renewable) diesel and jet fuel. In fact, HEFA production mostly generates green diesel and an additional cracking stage may be necessary to achieve 50-70% jet fuel [28, 30].

2.2.3 Synthesized Iso-Paraffins, SIP

Overview

SIP stands for Synthesized Iso-Paraffins produced from Hydroprocessed Fermented Sugars. SIP is the acronym under which this fuel has been certified by ASTM in 2014 [28]. Over the literature (mainly prior to its certification under SIP) this production pathway may be referred to as DSHC (Direct Sugar to Hydrocarbons). Currently, the main provider is Amyris, which already proved the possibility of SIP production on a commercial scale [30].

Certification

In June 2014, SIP was approved by ASTM as Annex A3 of ASTM D7566. However, compared to HEFA-SPK and FT-SPK, its approval only enables blends up to 10%. Because this jet component, mainly farnesane, is not a mixture of different hydrocarbons, it does not meet some of the jet fuel specifications as stand-alone molecule (e.g. boiling range, viscosity and density). Although being limited to 10% volume blending ratios, tests were also performed at 20% blending ratios, showing no significant deviation as compared to conventional jet fuel [28, 30].

Feedstocks

The production of SIP requires sugars as feedstock. Although SIP fuel is currently produced using sugar from sugarcane as a feedstock, as it is the focus of Amyris, it can potentially be produced from all kinds of plant sugars, including cellulosic sugars. It is therefore conceptually possible to eventually produce SIP fuel from woody biomass and avoid conflict with food use [28, 30].

Production

In the SIP pathway, a biological platform (microbes or yeast) are fed sugars (starch, sucrose or cellulosics) and the organism produces straight hydrocarbons. The main objective is to produce farnesene, which is a branched C15 alkene with four double bonds (with no oxygen). In the next step, farnesene is

converted into the respective alkane, a molecule with no double bonds, by reacting hydrogen with farnesene through a catalytic bed. The resulting product is a saturated alkane, which in the next step is then purified by distillation to produce an aviation grade. The final resulting SIP fuel ideally consists purely of farnesane, although, in practice, traces of remaining farnesene and olefins (partially hydrogenated farnesene) may be present in the final product as well as some other trace by-products [28, 30].

2.2.4 Alcohol-to-Jet, ATJ

Overview

As of the time of writing of the present thesis, the last production pathway approved by ASTM is the Alcohol-to-Jet pathway, ATJ. As the designation of the pathway points out, this pathway starts with the production of an alcohol. The aviation fuel produced from this process is designated by ATJ-SPK. One significant advantage of ATJ over other processes is that it can tap into U.S. supplies of corn [7].

Certification

In April 2016, ASTM International has published the revision of ASTM D7566 and Gevo's renewable alcohol-to-jet fuel (ATJ) became eligible to be used as a blending component in standard Jet A-1 for commercial airline use (Annex A5). Gevo's ATJ is eligible to be used for up to a 30% blend with conventional jet fuel for commercial flights [37]. As for FT-SPK and HEFA-SPK fuels, ATJ-SPK's aromatic content is negligible, and a different production pathway is still pursuing approval by the ASTM, ATJ-SKA. With this alternative route, 100% blend is expected to be possible. Certification work has been mainly performed by Swedish Biofuels and Byogy [28].

Feedstocks

With this production pathway, a wide range of alcohols may be used, such as, ethanol, isobutanol, propanol, methanol and long-chain fatty alcohols [30, 35]. From these, ethanol and isobutanol are the most promising, with ethanol readily available and isobutanol being the first alcohol approved for the production of ATJ. These alcohols can be produced from a wide variety of biomass (or even inorganic substances) feedstocks and technological pathways . Raw material types to produce alcohols in such a pathway consist mainly in sugars and starches (e.g corn and sugarcane), with an alternative route of lignocellulosic biomass or wastes also possible [34].

Production

As stated before, the first step in producing ATJ fuel corresponds to the production of alcohols from their raw materials. For sugars and starches, a fermentation stage is required to produce alcohols, with starches requiring to be hydrolyzed first. For example, Gevo's process begins with the production of isobutanol from corn. Then, the alcohol is first dehydrated (-OH removal) into an olefinic gas. The resulting gas is oligomerized into higher molecular weight unsaturated compounds. Unsaturated oligomers,

that have molecular weight approximately consistent with jet fuel, are separated and further processed in the third major step: hydrogenation over a solid-phase catalyst with hydrogen gas. Finally, the hydrogenated product is distilled and jet fuel is produced with diesel generated as by-product, typically [28, 30, 34].

For the ATJ-SKA alternative route, an additional aromatization step is required. This step is dependent of the provider's technological capabilities, but can be performed as an integrated stream in the overall production process [28].

2.2.5 Catalytic Hydrothermolysis, CH

Overview

CH stands for Catalytic Hydrothermolysis. This designation is a result of a novel process that has been developed and patented by Applied Research Associates Inc., ARA, for producing renewable drop-in fuels (with aromatics). This production pathway may also be designated by Hydrothermal Liquefaction. A jet fuel produced by this method (ARA's process) is commonly referred to as ReadiJet (or ReadiDiesel, for diesel by-products) [28, 35]. The designation "CH" only refers to the process stage that is proprietary to ARA (additional steps are required to achieve the final product). In some cases, this process may be referred to as BIC (Biofuels ISOCONVERSION) or HEFA-SKA (although fairly different) [28].

Certification

Although certification work is being performed by ARA and tests have already been conducted (e.g. test flight in 2012), approval by the ASTM is still pursued. According to ARA, its approval is expected soon and neat (100%) blends are a real possibility and a major milestone. However, current tendency of ASTM has been (so far) to permit a maximum of 50% blend, which can become an obstacle to achieve, in the near future, a neat biofuel certification for commercial flight usage. The expectation that a neat CH fuel may become a fully drop-in biofuel, that could substitute conventional jet fuel, comes from the fact that its composition and properties are very similar to crude kerosene [28].

Feedstocks

The feedstocks for CH jet fuel production are similar to those required for HEFA-SPK's production. In fact, CH jet fuel may be obtained from plant, algae oils, fatty acids and animal fats. Research has already proven the suitability of a variety of triglyceride-based feedstock like soybean, jatropha, camelina, tung and carinata oil. The main focus of ARA has been carinata, a non-edible oil (2^{nd} generation biofuel) [28, 35].

Production

Jet fuel as a result of the CH process starts with a Catalytic Hydrothermolysis, which, as stated above, names the overall pathway. In this stage, the oil (triglycerides, other esters or fatty acids) is converted

into n-paraffins, iso-paraffins, cycloparaffins and aromatic compounds. In the next step, the material requires hydrotreatment to saturate residual olefins and remove oxygen. In a similar manner to what happens with previously discussed pathways, the hydrotreated material is distilled and fractioned into the final products (e.g. jet fuel, diesel and naphtha) [28].

2.2.6 Hydrodeoxygenation, HDO

Overview

Based on Virent's (U.S. company) designation of a jet fuel produced by a trademarked process designated by BioForming, HDO-SK stands for Hydrodeoxygenated Synthesized Kerosene. In a similar way, HDO-SAK (Hydrodeoxygenated Synthesized Aromatic Kerosene), containing high aromatic content, is another pathway being developed to produce alternative jet fuel [28]. As concluded in [28], HDO-SK are intended to be blended with a fuel with low cycloparaffins content and HDO-SAK to provide aromatic content. These are usually referred to as simply SK and SAK.

Certification

HDO-SK is currently a Virent specific process and is still pursuing ASTM approval. If approved, its goal is to achieve blends in up to 50%, since, due to its composition (about 80% cycloparaffins), as stated above, it would be useful as a blend with a fuel requiring a higher proportion of cycloparaffins in its composition. Certification work and tests are being performed (with cooperation of Shell) and certification isn't expected to be approved soon. Similarly, HDO-SAK is also pursuing ASTM approval with no success expected for the near-future [28].

Feedstocks

With this pathway, fuel can be produced from a broad variety of cellulosic biomaterial, such as, wood or straw, starchs and sugars. Actual production by Virent has corn syrup as main feedstock focus [28, 38].

Production

In the first step of the HDO-SK production pathway, the feedstock is catalytically hydrodeoxygenated (HDO), producing alcohols, ketones and other oxygenates. This step can be achieved with an aqueous phase reforming, APR ($in-situ$ hydrogen production), or with steam reforming ($ex-situ$ hydrogen production) [38]. Then, the referred intermediate products are dehydrated, oligomerised and hydrogenated to produce a mixture of normal paraffins, iso-paraffins, cycloparaffins and aromatics. The last stage mixture is hydrotreated and distilled and fractioned to the final product; one of which is jet fuel. The HDO-SAK production process is similar to HDO-SK's, with the main difference arising from the fact that aromatics, resembling those of conventional jet fuel, are obtained catalytically [28].

2.3 Fuels of Interest

In this study, along with the analysis of a conventional kerosene (Jet A-1), properties of 10 different types of alternative fuels, obtained in the literature, are considered. As is summarized in Table 2.1, this study will focus on two types of FT-SPK (from coal and natural gas) and HEFA-SPK fuels (from mixed fats and camelina), and a type of ATJ-SPK, ATJ-SKA, SIP, CH, HDO-SK and Green Diesel fuels.

Designation	Feedstock	Pathway
CTL	Coal	FT-SPK
GTL	Natural Gas	
HEFA R-8	Mixed Fats	HEFA-SPK
HEFA Camelina/C.	Camelina Oil	
CH	Carinata Oil	CH
ATJ-SPK	Corn	ATJ-SPK
ATJ-SKA	Biomass	ATJ-SKA
SIP	Sugars	SIP
HDO-SK	Biomass	HDO-SK
Green Diesel	Vegetable Oil	HEFA

Table 2.1: Alternative fuels of interest.

The fuels selected for analysis shall be viewed as representative of the respective production pathways approaches, although due to the type of feedstock or quantity produced some differences in fuel properties may arise. All relevant properties of the referred alternative fuels are presented in the Appendix A, in Table A.1, along with the identification of the sources. It is worth mentioning that in cases where all relevant properties gathering was not successfully obtained from a single source, additional data was obtained from alternative sources (for the fuel in question).

It should also be noted that, although FT-SPK fuels from natural gas and coal are not sustainable alternative fuels, their analysis is important given the lack of relevant properties for FT-SPK from biomass or wastes and common assumption of similar fuel properties, due to same refining process.

2.4 Fuel Properties and Composition Analysis

A fuel that complies with ASTM D7566 meets the ASTM D1655 conventional jet fuel specification automatically [28]. Therefore, selected properties of the alternative fuels in question will be evaluated according to ASTM D1655 to check what property(ies) may constraint the neat fuel employment. In Table A.1, in the Appendix, one can analyse all fuel properties useful for the MATLAB model implemented (which will be described in the next section), as well as additional relevant ASTM specifications limits and properties like smoke point, freezing point, flash point, lubricity and aromatic content (in volume %). Other properties like sulphur content, naphthalene content or conductivity, for example, are not presented in the present thesis.

Conventional jet fuels are composed mainly by n-paraffins, iso-paraffins, cycloparaffins and aromatics. By comparing the composition of each type of fuel, one can preview whether or not the fuel in

question may present itself as a neat substitute of conventional fuels. Based on the analysis presented in reference [39] and brief information of HDO-SK's composition in reference [40], it is possible to analyse the main compositional differences presented in Figure 2.1.

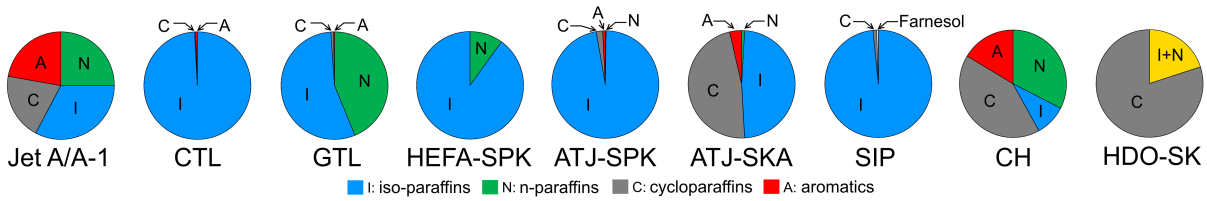

Figure 2.1: Typical jet fuel paraffin-based and aromatic composition [39, 40].

With a simple analysis of the figure, it is possible to conclude that a jet fuel produced from the CH pathway followed by a ATJ-SKA fuel would present similar properties to those of kerosene and therefore can be viewed as potential neat substitutes.

The analysis of fuel properties (Table A.1) may lead to several additional conclusions. It follows that, fuel density limits may constrain blending proportions of GTL, CTL, HEFA R-8 and HEFA Camelina. Cold flow viscosity may slightly constrain ATJ-SPK and highly constrain SIP and Green Diesel blending proportions. In terms of distillation range, blending of SIP and Green Diesel may be constrained as well. Although, a maximum of 25% in aromatic content (in volume) is not violated, a minimum of 8% [10] is only verified for CH and ATJ-SKA. It should also be highlighted that, blending of fuels such as CTL and HEFA R-8 may also be constrained by the lubricity. This simple analysis confirms that CH and ATJ-SKA would be the only fuels, from the ones studied, where, ideally, "100% blend" could be achieved.

2.5 Life Cycle Emissions Comparison

In order to assess the sustainability of a certain fuel production pathway, it is required that the greenhouse gases (GHG) life cycle emissions balance is better compared with the conventional route. According to IATA [2], when producing jet fuel from renewable sources, not all types of biomass considered as feedstock are eligible to improve the life cycle emissions. Based on the type of biomass considered, effects of Land-Use Change (LUC), use of fertilizers and energetic needs for production and transportation must be accounted for.

When indirect effects of Land-Use Change are considered, some possible biomass feedstocks become highly undesirable [2]. In this regard, sustainable fuels produced from wastes (tallow and UCO, for example) or from woody biomass or agricultural residues present better life cycle emissions when compared with production based on oil crops. Fuels produced from algae may even reach carbon neutral or reduce GHG emissions through the absorption of CO_2.

Nevertheless, as summarized in reference [35], all production pathways studied in the present work showcase great possibilities of decreasing the life cycle emissions GHG of jet fuel production when compared with the conventional route (from crude oil). This capability is presented in Figure 2.2, where results based on several researches available in the literature were summarized.

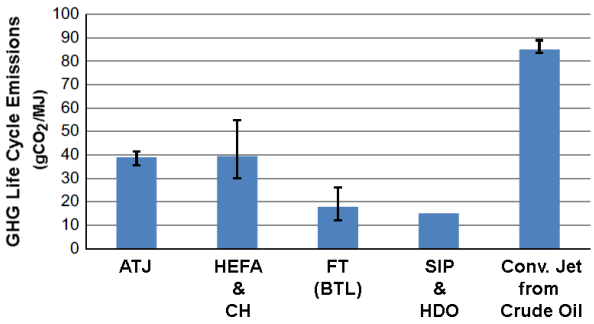

Figure 2.2: Life cycle emissions for different production pathways ([35], adapted).

The presented summary of results may be considered as a guide, showcasing that research has already proven the possibility of decreasing life cycle GHG emissions with new production pathways of sustainable alternative fuels (with feasible minimum decreases in the order of 50%, compared with the conventional route). Ultimately, these excellent results will be dependent on the quality of implementation of the production pathway.

2.6 Economical Comparison

Detailed information regarding fuel prices for alternative production pathways is still scarce. The worldwide commercial adoption of sustainable alternative jet fuels is highly dependent on the cost of jet fuel produced from crude oil. In fact, the increase in agreements between airliners and alternative fuel producers, verified in 2008 [8], coincided with the high price of crude oil barrel verified in that year. In Figure 2.3, spot prices, in dollars, per gallon of petroleum-based kerosene are presented from April of 1990 (0.540 $/gallon) to May of 2016 (1.299 $/gallon) [41]. Despite its high volatility, it is widely accepted [8], that conventional jet fuel price is expected to increase, due to increased crude global demand, with a EIA's high price scenario projection of 5$/gallon in 2040 (in 2012 dollars).

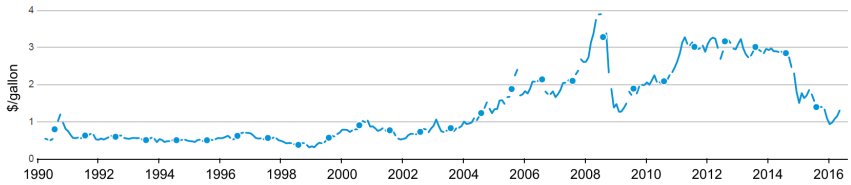

Figure 2.3: Spot prices for U.S. Gulf Coast jet fuel cost in $/gallon, from April 1990 to May 2016 (EIA [41]).

Based on a 2014 report from IATA [8], average selling prices of 38.26 $/gallon, 3.76 $/gallon, 59 $/gallon and 25.73 $/gallon were registered (from 2007 to 2012) for purchases of HEFA-SPK, FT (GTL and CTL), ATJ-SPK and SIP, respectively. Additionally, theoretical minimum selling prices estimates are also presented in 2014 IATA's report (excluding transport, taxes and retail markup). Based on this theoretical estimation, with an expected increase in petroleum fuel prices and maturity of alternative fuels production pathways, aviation biofuels may have the potential to become cost competitive with conventional jet fuel in the near future [8].

Chapter 3

Turbofan Model: Design, Off-Design, Transient and Pollutant Emissions

In the present chapter, the modelling of a turbofan engine thermodynamic cycle (design, off-design and transient) is presented. Along with the conventional modelling of a turbofan engine, a summary of the definitions and approximations used to define fuel properties (that have an impact on combustion), the adiabatic flame temperature estimation, the drop evaporation and the gas model, assumed in all engine performance models, are presented. Finally, the pollutant emissions model considered is also detailed.

It should be noted that, due to the scope of the thesis and for concision, proper detailing of the flame temperature and evaporation models considered is not given in this work. Additionally, the present pollutant emissions model will be incorporated with the design and off-design model and for transient calculations only steady-state conditions, reached during transient simulations, are analysed.

3.1 Fuel Properties

One of the most important components of the modelling in this work is the estimation of unknown fuel properties. Given the nature of the thesis, where different fuels are to be used in a numerical implementation of a turbofan engine and results compared to those obtained for a conventional fuel (Jet A-1), the accuracy of fuel properties estimates is significant. Typically, for the fuels that are to be analysed (presented in chapter 2), most fuel properties were successfully obtained in the literature. However, for cases where no data was obtained concerning a specific fuel property or for temperature dependence, estimations must be performed.

Fuel properties estimations for the alternative fuels considered followed a main assumption, that is to use same correlations and estimation methods described for pure hydrocarbons and petroleum fractions [42, 43]. With no exception, the net heat of combustion, ΔH, of every fuel was successfully obtained in the literature. In Appendix A, the remaining relevant properties and all required fuel properties estimations are presented and validated. It includes detailing of fuel density, ρ_F, average boiling point, T_b, surface tension, σ_F, kinematic and dynamic viscosities, ν_F and μ_F, respectively, hydrogen-to-carbon ra-

tio, ψ, hydrogen content (in weight %), $H\%$, critical temperature and pressure, T_{cr} and p_{cr}, respectively, and molecular weight, MW_F.

3.2 Flame Temperature Estimation

Although alternative fuels eligible to be blended with conventional kerosene present, in general, similar properties, the adiabatic flame temperature rise estimation due to fuel burning is significant for temperature-dependent pollutant emissions. So that influences in fuel properties are accounted for, in the present work, the work of Gülder [44] will be followed. With this approach, the flame temperature will be given based on the fuel-air ratio, f, inlet combustion chamber temperature, T_{t3} and pressure, p_{t3}, the hydrogen-to-carbon ratio, ψ, the initial temperature of the fuel in liquid form, T_f, the liquid fuel density as a function of temperature, ρ_F, and the normal boiling temperature, T_b.

To include the effects of the presence of the fuel in liquid form and in a different temperature compared to the inlet gas, estimations of the latent heat of vaporization, L [16], and the specific heat, c_{p_F} [44], of the fuel are required. For more information regarding the formulation of flame temperature calculation, a detailed description of the process can be reviewed in [44].

For 2 MPa of inlet pressure and the direct implementation of the flame temperature model, results computed are compared with adiabatic flame temperature rise results given in [3]. With properties of JP-5 based on [3, 16], for 300 K, 500 K, 750 K and 1000 K of inlet temperature, good agreement was verified, with average errors of 2.1%, 3.2%, 3.4% and 2.5%, respectively, obtained (results presented in the Appendix B, in Figure B.1).

3.3 Evaporation Model

The study of evaporation rates in a turbofan engine at different operating conditions for each fuel considered, in this thesis, will follow the work of Chin and Lefebvre [16]. In this approach, (quasi) steady-state evaporation is assumed. It follows that, as previously stated, the variation of a drop diameter, D, with time, t, is defined, with good accuracy, by the "D^2-*Law*", as

$$D(t)^2 = D_0^2 - \lambda.t, \tag{3.1}$$

where D_0 is the initial drop diameter and λ the evaporation constant. The estimation of evaporation time, τ_e, of a certain drop may be obtained with equation 3.1 for $D(\tau_e) = 0$, neglecting the heat-up period. For the assumption of steady-state evaporation, the evaporation constant, λ in m^2/s, may be defined as

$$\lambda = \frac{8\ln(1+Q)}{\rho_F(c_p/k)_g}. \tag{3.2}$$

In equation 3.2, ρ_F is the fuel liquid density in kg/m^3, c_{p_g} the gas specific heat in J/kg.K, k_g the gas thermal conductivity in W/m.K and Q the transfer number (usually designated by B, in the literature).

In the evaporation process of a liquid droplet, an accurate calculation of the transfer number is required, although not as important as proper c_{p_g} and k_g estimations [16]. According to [12], the transfer number, which represents the driving force for the evaporation process, may be as a first approximation (errors up to 20% may be involved) estimated by

$$Q = \frac{1575 - 0.5T_b}{T_b - 118}, \tag{3.3}$$

with the boiling point, T_b, given in K. In a more accurate approach [16], this parameter may be defined in two ways: "mass transfer number", Q_M (equation 3.4), if evaporation rates are controlled by mass diffusion processes, or "heat transfer number", Q_T (equation 3.5), where heat transfer rates control the evaporation. For the present case, "steady-state", it is assumed that: $Q = Q_M = Q_T$.

$$Q_M = \frac{Y_{F_s} - Y_{F_\infty}}{1 - Y_{F_s}} = \frac{Y_{F_s}}{1 - Y_{F_s}}. \tag{3.4}$$

$$Q_T = \frac{c_{p_g}(T_\infty - T_s)}{L}. \tag{3.5}$$

where Y_{F_s} is the mass fraction of fuel vapour at the droplet's surface, T_∞ is the surrounding temperature in K (assumed as the flame temperature [45]), T_s the droplet surface temperature in K and L the latent heat of fuel vaporization in J/kg.

Then, strictly following the method properly detailed in reference [16], the evaporation constant , λ, will be calculated with an iterative process where the steady-state assumption of $Q_T = Q_M$ is to be achieved as a function of the droplet surface temperature, T_s. For the present case, a simple Newton-Raphson iterative procedure is followed.

It should be highlighted that, the required estimation of air thermal conductivity, k_a, is obtained using the relations presented in [46] with good results, compared with plotted results presented in [16] (average relative error of 0.61%). The calculation of fuel saturation pressure will be based on the knowledge of the normal boiling point, T_b, and the calculated fuel critical properties (p_{cr} and T_{cr}).

Taking advantage of the present model and properties estimations, as described in Appendix A, for an ambient temperature of 2000 K and a range of pressures from 100 kPa to 2000 kPa, calculated values of evaporation constant, λ, for JP-5, JP-4 and DF-2 (diesel grade) showcase an average relative error of 1.7%, 1.0% and 3.4%, respectively, when compared with [16] results. In Figure B.2 (in Appendix B), results for JP-5 (a) and JP-4 (b) are plotted. Additionally, at 1 atm and 2000 K ambient pressure and temperature, with experimental values [16] of evaporation constants for DF-2 and n-heptane of 0.79 and 0.97 mm^2/s, respectively, calculated results of 0.807 and 0.999 mm^2/s, respectively, represent a relative error of 2.15% and 2.99% respectively, which evidences an overall good agreement.

It should be highlighted however that the present model is not accurate for all ambient conditions. Defining reduced pressures and temperatures as $p_r = p_\infty / p_{cr}$ and $T_r = T_\infty / T_{cr}$, respectively, based on the work of Givler and Abraham [47], for $T_r > 2$ and $p_r > 1$ or $p_r > 2$ and $T_r > 1$, with good approximation, steady-state evaporation is not valid and the evaporation is entirely transient. In this regard, as detailed in [48], it is concluded that a maximum evaporation constant is obtained for an ambient pressure in the vicinity of the fuel critical pressure, p_{cr} (for the range of temperatures considered in this study). Then, in the present model, if the range of ambient pressures and temperatures for fuel evaporation is not valid, a value for critical ambient pressure is assumed.

3.4 Gas Model

Since, in the present thesis, different fuels will be analysed and their impact on the engine overall performance compared, all cycle calculations will be based on variable air specific heat, $C_p(T)$ in J/kg.K. On an academic approach, constant specific heat is typically assumed, inducing errors of up to 5% in leading performance parameters [14]. For the present study, it was considered incorrect to analyse fuel effects on an engine cycle considering such approximation, due to reduced accuracy and since the combustion gases properties may differ (even if slightly).

According to [15], the combustion gases specific heat (or dry air, for no fuel-air ratio, i.e. $f = 0$) may be defined as a polynomial, as a function of temperature, T, in K:

$$C_p(T) = A + B.T + C.T^2 + D.T^3 + E.T^4, \tag{3.6}$$

where, A, B, C, D and E (in equation 3.6) are the polynomial coefficients of the gas specific heat.

The gas model implemented will enable the calculation of the gas constant, R in J/kg.K (equation 3.7), dependent of the gas molecular weight, MW_g in kg/kmol, as well as the calculation of the specific ratio, γ (equation 3.8).

$$R = \frac{8314.472}{MW_g} \,. \tag{3.7}$$

$$\gamma = \frac{C_p}{C_p - R} \,. \tag{3.8}$$

For presentation simplicity and concision, the gas specific heat will only by referenced to as a function of temperature, although its calculation is also based on the fuel-air and hydrogen-to-carbon ratios. Further details concerning the implementation of the gas model are presented in Appendix C.

3.5 Notation and Assumptions

Based on [23], the two-spool turbofan station numbering, presented in Figure 3.1, is in accordance with the Aerospace Recommended Practice 755A. The type of turbofan to be studied in this thesis operates with two separate exhausts and two spools, designated according to the pressure level in each zone: the low-pressure spool (LP) and the high-pressure spool (HP). The low-pressure turbine, LPT, drives the low-pressure compressor, LPC, and the fan through the low-pressure spool, whereas the high-pressure turbine, HPT, drives the high-pressure compressor, HPC, through the high-pressure spool.

The turbofan model will be simplified under assumptions of no leakage (from and to bypass stream), no air bleeding (e.g. handling and overboard bleed) and no turbine cooling. For the exhausts modelling, convergent nozzles (bypass and core nozzle) will be assumed. All engine components, except the combustion chamber, will be modelled assuming adiabatic behaviour. For simplicity, in all cases, engine inlet air mass flow does not take into account relative humidity effects (dry air).

Throughout the modelling of the turbofan, total temperatures and pressures will be commonly computed. In this thesis, a total (or stagnation) property will be identified with subscript t, preceding the number of the station, i. Therefore, the total pressure and total temperature of a given station, i, will be referenced as p_{ti} and T_{ti}, respectively. For the same station, static pressure and temperature is

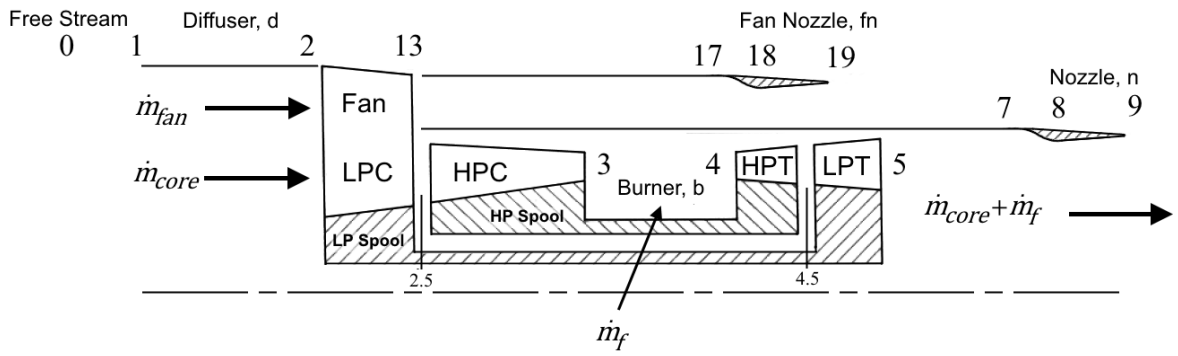

Figure 3.1: Two-spool turbofan station numbering ([19], adapted).

simply referred to as p_i and T_i, respectively. A total temperature, T_{ti}, represents the temperature that a gas stream with static temperature T_i and velocity V_i would possess if brought to rest adiabatically and without work transfer [19]. In the present model, this relationship will be based on enthalpy, h (J/kg), calculations. The relationship between total enthalpy and static enthalpy is given by

$$h_{ti} = h_i + \frac{{V_i}^2}{2}, \tag{3.9}$$

where gas velocity V_i comes in m/s. The difference between enthalpies of different states, j and i, corresponding to temperatures T_j and T_i, $\Delta h = h(T_j) - h(T_i)$, is calculated based on the specific heat of the gas, $C_p(T)$ (given in equation 3.6), in the following way:

$$\Delta h = \int_{T_i}^{T_j} C_p(T).dT. \tag{3.10}$$

The total pressure and static pressure relationship is based on the same principle of conservation of energy with the assumption of isentropic behaviour (a reversible process). A process is isentropic when the entropy difference, Δs, between the final and initial conditions, is equal to zero. The differential entropy equation for a perfect gas (based on Gibbs equation) is given by [23]

$$ds = \frac{dh}{T} - R\frac{dp}{p}. \tag{3.11}$$

Then, by integrating the previous equation, the entropy difference Δs between a state j (T_j and p_j) and a state i (T_i and p_i) is computed with equation 3.12.

$$\Delta s = \int_{T_i}^{T_j} \frac{c_p(T).dT}{T} - R.\ln\frac{p_j}{p_i}. \tag{3.12}$$

For an isentropic and adiabatic process ($\Delta s = 0$), pressures and temperatures of certain states (j and i) relate in the following way:

$$\ln\frac{p_j}{p_i} = \varphi_s(T_j, T_i), \tag{3.13}$$

where φ_s will be referred to as *entropy function*, and given by

$$\varphi_s = \frac{1}{R}\int_{T_i}^{T_j} \frac{c_p(T).dT}{T}. \tag{3.14}$$

It should be noted that, although enthalpy and entropy differences between generic states j and i (equations 3.10 and 3.12, respectively) were defined for generic static properties (T_j, p_j, T_i and p_i), the same procedures are used for total (stagnation) properties (T_{tj}, p_{tj}, T_{ti} and p_{ti}).

When referring to pressure ratios in an engine component, such as the fan, a compressor (LPC or HPC), a turbine (HPT and LPT) and nozzles, the notation will be: π_x. It follows that

$$\pi_x = \frac{\text{pressure at the outlet of component } x}{\text{pressure at the inlet of component } x}. \tag{3.15}$$

In the present work, all mass flow rates come in kg/s. The total mass flow rate at the diffuser, $\dot{m}$, is divided into two separate flows: a core mass flow, $\dot{m}_{core}$, and a bypass mass flow, $\dot{m}_{fan}$, as presented in Figure 3.1. To relate the two mass flow rates, the definition of the bypass ratio, B, is used:

$$B = \frac{\dot{m}_{fan}}{\dot{m}_{core}}. \tag{3.16}$$

Therefore, for a given inlet mass flow rate, $\dot{m}$, $\dot{m}_{core}$ and $\dot{m}_{fan}$ are readily computed:

$$\dot{m}_{core} = \frac{\dot{m}}{1+B}, \tag{3.17}$$

$$\dot{m}_{fan} = \frac{B.\dot{m}}{1+B}. \tag{3.18}$$

In the combustor (burner), fuel is injected with a given mass flow rate, $\dot{m}_f$. Through the turbines (HPT and LPT) and core nozzle, the mass flow will be the sum of $\dot{m}_{core}$ and $\dot{m}_f$. The fuel mass flow rate is related with the core mass flow rate through the fuel-air ratio, f, with

$$f = \frac{\dot{m}_f}{\dot{m}_{core}}. \tag{3.19}$$

In the present work, for a given station i, the following nondimensional total temperature, θ_i, and pressure, δ_i, shall be defined as [4]

$$\theta_i = \frac{T_{ti}.R_i}{T_{SL}.R_{SL}}, \tag{3.20}$$

$$\delta_i = \frac{p_{ti}}{p_{SL}}, \tag{3.21}$$

with T_{SL} and p_{SL}, the temperature and pressure at sea level International Standard Atmosphere (ISA) conditions, respectively, with correspondent values of 288.15 K and 101325 Pa, respectively. Based on the gas model implemented (section 3.4), dry air R_{SL} is assumed with a value of 287.05 J/kg.K.

3.6 Engine Components

To accurately model the thermodynamic cycle of a turbofan engine, its components must be analysed individually. The main components of the engine detailed next are the engine diffuser, the fan and compressors (LPC and HPC), the combustor (burner), the turbines (HPT and LPT) and the nozzles (bypass and core). For each component, relations between inlet and outlet properties are detailed.

3.6.1 Diffuser

The diffuser is the component modelled between stations 1 and 2. It will be assumed that the diffuser is adiabatic ($T_{t2} = T_{t1}$). To compute the pressure loss across the diffuser, an intake map relating the flight Mach number, M_0, and the relative corrected LPC spool speed, N_{LPC}, will be used. In the design point, the relative corrected speed is considered unitary. In the present work, the intake map used was obtained from [4] and its graphical representation, obtained in the present work, is presented in Appendix B, in Figure B.3. The map will enable the calculation of $\pi_d = p_{t2}/p_{t1}$.

3.6.2 Compressors and Fan

The fan and compressors, LPC and HPC, will be defined by their polytropic (or small-stage) efficiency, e_{fan}, e_{LPC} and e_{HPC}, respectively. The polytropic efficiency of a fan or compressor, is the ratio of the ideal work of compression over the real work of compression for a differential pressure change. Based on [23] comes the generic calculation, e_{comp}, for a compressor or fan:

$$e_{comp} = \frac{dh_{t,s}}{dh_t}, \tag{3.22}$$

where $dh_{t,s}$ represents the ideal (isentropic) enthalpy differential of the component. Combining equation 3.22, equation 3.11 and equation 3.13, for inlet state i and outlet state j, we have

$$\ln \frac{p_{tj}}{p_{ti}} = e_{comp}.\varphi_s(T_{tj}, T_{ti}). \tag{3.23}$$

To fully define the component behaviour, the pressure ratio ($\pi_{comp} = p_{tj}/p_{ti}$) must be defined. For design point calculations this pressure ratio is a design input for the fan, LPC and HPC.

With the relation between temperatures and pressures obtained, it is possible to define the isentropic efficiency for a generic compressor or fan, η_{comp}. An isentropic efficiency relates the ideal over the real work of compression for a given overall pressure ratio and is given by

$$\eta_{comp} = \frac{h_{tj,s} - h_{ti}}{h_{tj} - h_{ti}}. \tag{3.24}$$

This calculation requires the knowledge of the ideal temperature at the outlet $T_{tj,s}$ which is obtained with equation 3.13, solving for given T_{ti} and pressure ratio π_{comp}.

3.6.3 Combustion Chamber

To characterize the degree to which the chemical reactions have gone to completion, combustion efficiency is defined, η_b. According to [23], for ΔH given in J/kg, the combustion efficiency is given by

$$\eta_b = \frac{(1+f).h_{t4} - h_{t3}}{f.\Delta H}. \tag{3.25}$$

Assuming an evaporation rate-controlled system [11], where mixing and reaction rates are fast enough for fuel evaporation to be the rate-controlling step, the combustion efficiencies obtained for a given fuel, η_b, and obtained for a reference fuel, $\eta_{b,ref}$, are related in the following way (high efficiencies, >90%):

$$\frac{1-\eta_b}{1-\eta_{b,ref}} = \left(\frac{\lambda_{eff,ref}}{\lambda_{eff}}\right) \cdot \left(\frac{D_0}{D_{0,ref}}\right)^2 . \tag{3.26}$$

λ_{eff} is the effective evaporation constant (accounting for Reynolds effects). Considering a pressure-swirl atomizer and low Reynolds at the combustion chamber [3, 11], that is $\lambda_{eff} = \lambda$ (equation 3.2), the initial drop diameters ratio, $D_0/D_{0,ref}$, is dependent on the fuel liquid surface tension, σ_F, and dynamic viscosity, μ_F:

$$\frac{D_0}{D_{0,ref}} = \left(\frac{\sigma_F}{\sigma_{F,ref}}\right)^{0.25} \cdot \left(\frac{\mu_F}{\mu_{F,ref}}\right)^{0.25} . \tag{3.27}$$

In a combustion chamber, according to [23], viscous losses and the fact that combustion takes place at a finite Mach number, result in an overall pressure loss across the chamber. This pressure loss will be quantified by defining the pressure ratio $\pi_b = p_{t4}/p_{t3}$.

3.6.4 Turbines

The polytropic efficiencies of turbines (HPT and LPT), e_{HPT} and e_{LPT}, respectively, are defined as the actual turbine work over the ideal turbine work for a differential pressure change [23]. Therefore, a generic turbine polytropic efficiency, e_{turb}, relation is given by

$$e_{turb} = \frac{dh_t}{dh_{t,s}}. \tag{3.28}$$

In a similar way to the procedure for compressors and fans, the relationship between total pressures and temperatures at the inlet and outlet (states i and j, respectively) is given by

$$\ln \frac{p_{tj}}{p_{ti}} = \frac{1}{e_{turb}} . \varphi_s(T_{tj}, T_{ti}). \tag{3.29}$$

In analogy to compressors and fans, to measure the turbine's performance, the isentropic efficiency, η_{turb}, can be defined as well. In this case, it relates the actual turbine work over the ideal turbine work for a given overall pressure ratio across the turbine, with

$$\eta_{turb} = \frac{h_{ti} - h_{tj}}{h_{ti} - h_{tj,s}}. \tag{3.30}$$

3.6.5 Nozzles

As assumed for the diffuser, nozzles will be considered as adiabatic, which means: $T_{t9} = T_{t5}$ and $T_{t19} = T_{t13}$. Therefore, the exhaust core nozzle and bypass nozzle (or fan nozzle) will be defined by their respective pressure ratios $\pi_n = \pi_{t9}/\pi_{t5}$ and $\pi_{fn} = \pi_{t19}/\pi_{t13}$. These pressure ratios account for the pressure loss verified mainly due to under or overexpansion and due to losses in the transition between the turbine and the core nozzle [23].

3.7 Design Point Model

The design point model, although useful on its own (for engine parametric analysis), is of great relevance for off-design and transient aero-engine simulations. Based on the engine design point, the engine becomes thermodynamically defined and results in different operating conditions are eligible to be obtained.

In this section, the turbofan design point model will be detailed. First, the design point inputs must be defined (summary in Table 3.1). The MATLAB implementation of the design point model of a typical turbofan is, then, summarized through the detailing of equations and assumptions used. The design point implementation follows the conventional approach studied in Aerospace Engineering, thoroughly detailed in the literature [14, 19, 23].

3.7.1 Design Point Model Inputs

Fuel Selection

For the present model, the user has to define (as an input) which fuel is desired to be analysed. The MATLAB code is implemented in such a way that for a type of fuel selection input variable, with user selection of fuel type, a fuel database is read (an editable spreadsheet) and properties of the fuel selected are saved for calculations. In comparison calculations to the reference value, properties of the reference fuel, Jet A-1, are automatically read.

Ambient Conditions

The performance of an engine is highly dependent on the ambient conditions, at free stream (the first stage of the thermodynamic model). Ambient conditions are defined with a flight Mach number, M_0, and altitude, H (m). The altitude will have an impact on the values for free stream static temperature, T_0 (K), and pressure, p_0 (Pa). In accordance with the International Standard Atmosphere (ISA) (as in [4])

$$T_0 = \begin{cases} 288.15 - 0.0065.H \\ 216.65 \end{cases} \quad \text{and} \quad p_0 = \begin{cases} 101325\left(1 - \frac{0.0065H}{288.15}\right)^{5.25588}, & \text{if } H \leq 11000 \text{ m} \\ 22632e^{-0.000157688(H-11000)}, & \text{if } H > 11000 \text{ m} \end{cases} \tag{3.31}$$

Based on the calculated free stream static temperature, T_0, and flight Mach number, M_0, the flight velocity, V_0 in m/s, is computed:

$$V_0 = M_0\sqrt{\gamma_0 R_0 T_0}. \tag{3.32}$$

Level of Technology Inputs

Polytropic efficiencies, combustion efficiency for reference fuel, combustion overall pressure ratio, nozzle pressure ratios and shaft mechanical efficiencies ($\eta_{m,L}$ and $\eta_{m,H}$) will be based on the definition of Level of Technology. The Level of Technology takes into account the period when the engine was produced. For more information, see reference [23] (Table 6.2, page 373).

Engine Design Parameters

So that the model is fully defined and the thermodynamic cycle can be computed, several parameters need to be selected. These can be grouped as "engine design parameters". These include pressure ratios across the compressors (LPC and HPC) and the fan, the bypass ratio, B_R, and the high-pressure turbine inlet temperature, $T_{t4,R}$. In the present work, although typically not mandatory, the inlet air mass flow rate, $\dot{m}_R$, will be a design parameter, mainly relevant for off-design and transient calculations.

Although not required for design point computations, values of low-pressure and high-pressure spools speeds, respectively $N_{L,R,abs}$ and $N_{H,R,abs}$, in RPM, must be defined for off-design and transient implementations. Design combustion chamber parameters such as the fraction of air employed in the primary and secondary zones, q_{pz} and q_{sz}, respectively, must be defined as well. Additionally, an initial liquid fuel temperature (before injection on the combustion chamber), T_f, must be selected.

Ambient and Flight Data	**Pressure Losses**	**Engine Design Parameters**
$M_{0,R}$, H_R	$\pi_{b,R}$	$\dot{m}_R$
Component Efficiencies	$\pi_{n,R}$, $\pi_{fn,R}$	B_R
e_{fan}, e_{LPC}, e_{HPC}, e_{HPT}, e_{LPT}	**Combustion Chamber Design**	$T_{t4,R}$
$\eta_{b,R,ref}$	T_f	$\pi_{fan,R}$, $\pi_{LPC,R}$, $\pi_{HPC,R}$
$\eta_{m,L}$, $\eta_{m,H}$	q_{pz}, q_{sz}	$N_{L,R,abs}$, $N_{H,R,abs}$

Table 3.1: Design point inputs.

3.7.2 Design Point Numerical Modelling

Assuming that all design inputs are selected and defined in the model, the numerical design point calculation may take place. As previously stated, it starts with the fuel selection and free stream data processing.

Fuel Selection

For a given user input, a fuel is selected and its properties, presented on Table A.1, are read. In order to compute the combustion efficiency for a given fuel, in all design point calculations, properties of Jet A-1 are also read for comparison.

Free Stream

For a given flight altitude, the ambient static pressure, p_0, and temperature, T_0 are calculated in accordance with ISA standards (equation 3.31). From the knowledge of T_0 and the air gas constant R_0, $c_{p,0}$ and γ_0 are calculated with equations 3.6 and 3.8, respectively. Flight velocity, V_0, may then be computed with equation 3.32.

The total free stream temperature, T_{t0}, is obtained taking advantage of the polynomial result of an enthalpy difference, as a function of temperature. With simple algebraic manipulations and taking advantage of MATLAB's function "roots", T_{t0} is obtained from equation 3.9. Then, knowing total and

static free stream temperatures and static pressure, from equation 3.13 and recurring to an iterative Newton-Raphson scheme (with known derivatives), the free stream total pressure, p_{t0}, is calculated. It is assumed that total conditions are constant between free stream and station 1, i.e. $p_{t1} = p_{t0}$ and $T_{t1} = T_{t0}$.

Diffuser

As previously stated, the diffuser is modelled with a component map. For the design flight Mach number defined and the corrected low-pressure compressor relative spool speed, N_{LPC}, equal to 1 (design point), π_d is interpolated from the map and p_{t2} readily computed, with calculated p_{t1}. Assuming adiabatic behaviour, $T_{t2} = T_{t1}$. At this station, the design mass flow rate defined as an input is $\dot{m}_R$.

Fan

With design input of the fan pressure ratio, $\pi_{fan,R}$, p_{t13} is calculated, based on previously calculated p_{t2}. Then, for a given fan polytopic efficiency, e_{fan}, T_{t13} is calculated with equation 3.23, for inlet state 2 and outlet state 13. In a similar manner, the ideal (isentropic) outlet temperature, $T_{t13,s}$, is calculated with equation 3.13. Both calculations are performed with the Newton-Raphson iterative method.

At this point it is possible to calculate the fan isentropic efficiency, $\eta_{fan,R}$, with equation 3.24. The bypass (fan) air mass flow rate, $\dot{m}_{fan}$ or $\dot{m}_{13}$, is calculated with equation 3.18.

Low-Pressure Compressor, LPC

The total properties at the outlet of the low-pressure compressor, LPC, are obtained in the same manner as detailed for the fan. Differences arising from different pressure ratio considered, $\pi_{LPC,R}$, and polytropic efficiency, e_{LPC}. Then, with inlet properties T_{t2} and p_{t2}, one can calculate $T_{t2.5}$, $T_{t2.5,s}$ and $p_{t2.5}$.

The low-pressure compressor isentropic efficiency, $\eta_{LPC,R}$, is calculated, as before, with equation 3.24. The core air mass flow rate, $\dot{m}_{core}$, is calculated with equation 3.17 at this stage.

High-Pressure Compressor, HPC

The total properties at the outlet of the low-pressure compressor, HPC, are obtained in the same manner as detailed for the fan and the LPC. Differences arising from different pressure ratio considered, $\pi_{HPC,R}$, and polytropic efficiency, e_{HPC}. Then, with inlet properties $T_{t2.5}$ and $p_{t2.5}$, one can calculate T_{t3}, $T_{t3,s}$ and p_{t3}.

The high-pressure compressor isentropic efficiency, $\eta_{HPC,R}$, is calculated, as before, with equation 3.24. From the low-pressure compressor to the high-pressure compressor, there is mass flow continuity and therefore: $\dot{m}_3 = \dot{m}_{2.5} = \dot{m}_{core}$.

Combustion Chamber

This is the first stage where fuel is injected, and therefore, from this point, changes in performance may arise due to the injection of different fuels. As previously stated, the combustion chamber modelling starts with the estimation of the design combustion efficiency for a given fuel, $\eta_{b,R}$, compared to a reference design input for a conventional jet fuel, Jet A-1, $\eta_{b,R,ref}$.

A initial result, based on equations 3.26 and 3.27 and on approximations given in [3, 11, 12] is approximated with

$$\eta_{b,R} = 1 - (1 - \eta_{b,R,ref}).\left[\frac{\ln(1+Q_{ref})}{\ln(1+Q)}\right].\left[\frac{\rho_F(T_b)}{\rho_F(T_{b,ref})}\right].\left(\frac{\sigma_F}{\sigma_{F,ref}}\right)^{0.5}.\left(\frac{\mu_F}{\mu_{F,ref}}\right)^{0.5}, \tag{3.33}$$

where

$$\frac{\lambda_{eff,ref}}{\lambda_{eff}} = \frac{\ln(1+Q_{ref})}{\ln(1+Q)}.\frac{\rho_F(T_b)}{\rho_F(T_{b,ref})}, \tag{3.34}$$

with transfer numbers for each fuel (Q and Q_{ref}) given by equation 3.3 and liquid densities at normal boiling points calculated with equation A.6.

For the calculated combustion efficiency, the fuel-air ratio, f, is computed with algebraic manipulation of equation 3.25. Since at station 4, specific heat is dependent on the fuel-air ratio, the actual computation of fuel-air ratio requires additional algebraic manipulations to the polynomial specific heat equation defined in section 3.4, so that it is defined as function of f and T. It is, then, possible to directly compute the fuel-air ratio. It should be highlighted that, based on reference [19], $h_t(T_{t4})$ and $h_t(T_{t3})$ are calculated compared to a reference value at 298.15 K, i.e. $h_t(T_{t4}) \Rightarrow h_t(T_{t4}) - h_t(298.15)$ and $h_t(T_{t3}) \Rightarrow h_t(T_{t3}) - h_t(298.15)$.

Based on the calculated f and calculating a more accurate ratio of evaporation constants, based on the evaporation model described in section 3.3, design combustion efficiency, $\eta_{b,R}$ (with equation 3.26), and fuel-air ratio (with rearranged equation 3.25) are recalculated. In an iterative approach, if the difference between the latest fuel-air ratio calculated and the previous calculation is below a certain tolerance level, combustion efficiency, $\eta_{b,R}$, and fuel-air ratio, f, calculation is completed.

The actual fuel mass flow rate, $\dot{m}_f$, may then be computed as

$$\dot{m}_f = f.\dot{m}_3. \tag{3.35}$$

At the outlet of the combustion chamber, p_{t4} is obtained with design input of combustion chamber pressure loss, $\pi_{b,R}$, and the mass flow rate is no longer assumed as dry air, but the sum of the core air mass flow and fuel mass flow and therefore: $\dot{m}_4 = \dot{m}_3.(1+f)$.

High-Pressure Turbine, HPT

To obtain gas properties at the outlet of the high-pressure turbine, HPT, work compatibility is considered. The following equations, detail the computation of the high-pressure compressor required power, $\dot{W}_{HPC}$,

and the produced high-pressure turbine power, $\dot{W}_{HPT}$:

$$\dot{W}_{HPC} = \dot{m}_3.\left[h_t(T_{t3}) - h_t(T_{t2.5})\right], \quad (3.36) \qquad \dot{W}_{HPT} = \eta_{m,H}.\dot{m}_4.[h_t(T_{t4}) - h_t(T_{t4.5})]. \quad (3.37)$$

Considering work compatibility, $\dot{W}_{HPT} = \dot{W}_{HPC}$, from equations 3.36 and 3.37, the outlet temperature, $T_{t4.5}$, is calculated through polynomial roots calculation, based on

$$\dot{m}_3.[h_t(T_{t3}) - h_t(T_{t2.5})] = \eta_{m,H}.\dot{m}_4.[h_t(T_{t4}) - h_t(T_{t4.5})]. \quad (3.38)$$

The design pressure ratio across the high-pressure turbine, $\pi_{HPT,R}$ ($p_{t4.5} = \pi_{HPT,R}.p_{t4}$), is calculated with the polytropic efficiency, e_{HPT}, and equation 3.29. Then, as with compressors and fan, $T_{4.5,s}$ is calculated with equation 3.13 and the isentropic efficiency, $\eta_{HPT,R}$, readily computed with equation 3.30. The mass flow at the outlet of the high-pressure turbine results of flow compatibility $\dot{m}_{4.5} = \dot{m}_4$.

Low-Pressure Turbine, LPT

The power produced by the low-pressure turbine, $\dot{W}_{LPT}$, and the combined required power for air compression, for the low-pressure compressor, $\dot{W}_{LPC}$, and the fan, $\dot{W}_{fan}$, are given by

$$\dot{W}_{LPC} = \dot{m}_{2.5}.[h_t(T_{t2.5}) - h_t(T_{t2})], \quad (3.39) \qquad \dot{W}_{fan} = \dot{m}_{13}.[h_t(T_{t13}) - h_t(T_{t2})], \quad (3.40)$$

$$\dot{W}_{LPT} = \eta_{mL}.\dot{m}_{4.5}.[h_t(T_{t4.5}) - h_t(T_{t5})]. \quad (3.41)$$

Considering work compatibility, $\dot{W}_{LPT} = \dot{W}_{fan} + \dot{W}_{LPC}$, from equations 3.39, 3.40 and 3.41, the outlet temperature T_{t5} is calculated through polynomial roots calculation, based on

$$\dot{m}_{13}.[h_t(T_{t13}) - h_t(T_{t2})] + \dot{m}_{2.5}.[h_t(T_{t2.5}) - h_t(T_{t2})] = \eta_{m,L}.\dot{m}_{4.5}.[h_t(T_{t4.5}) - h_t(T_{t5})]. \quad (3.42)$$

The design pressure ratio across the low-pressure turbine, $\pi_{LPT,R}$ ($p_{t5} = \pi_{LPT,R}.p_{t4.5}$), is calculated with the polytropic efficiency, e_{LPT}, and equation 3.29. Then, as with the high-pressure turbine, $T_{t5,s}$ is calculated with equation 3.13 and the isentropic efficiency, $\eta_{LPT,R}$, readily computed with equation 3.30. The mass flow at the outlet of the high-pressure turbine results of flow compatibility $\dot{m}_5 = \dot{m}_{4.5}$.

Nozzles

With the knowledge of the design pressure losses across the nozzles ($\pi_{n,R}$ and $\pi_{fn,R}$), it follows:

$$p_{t9} = p_{t5}.\pi_{n,R}, \quad (3.43) \qquad p_{t19} = p_{t13}.\pi_{fn,R}. \quad (3.44)$$

Then a verification if the nozzle is choked is performed. To do so, sonic conditions are assumed $M_9 = M_{19} = 1$. At sonic conditions, critical static temperatures are defined (subscript c). Given the relation between velocity and Mach number (equation 3.32), the energy conservation equation (equation 3.9) and the dependence on fuel-air ratio for core nozzle calculations, $T_{9,c}$ and $T_{19,c}$ may be computed.

Knowing total and static temperatures and total pressures (core and fan nozzles), it is possible to calculate static sonic nozzle pressures, $p_{9,c}$ and $p_{19,c}$, with the isentropic relation given by equation 3.13.

If $p_{9,c} > p_0$, the core nozzle is choked and $p_9 = p_{9,c}$ and $T_9 = T_{9,c}$. Otherwise, $p_9 = p_0$ and T_9 is calculated with the isentropic relation, for given p_9, p_{t9} and T_{t9} (equation 3.13). In a similar way, if $p_{19,c} > p_0$, the fan nozzle is choked and $p_{19} = p_{19,c}$ and $T_{19} = T_{19,c}$. Otherwise, $p_{19} = p_0$ and T_{19} calculated with the isentropic relation, for given p_{19}, p_{t19} and T_{t19} (equation 3.13).

Nozzle velocities are then computed as follows (based on equation 3.9):

$$V_9 = \sqrt{2.[h_t(T_{t9}) - h(T_9)]}, \qquad (3.45) \qquad V_{19} = \sqrt{2.[h_t(T_{t19}) - h(T_{19})]}. \qquad (3.46)$$

Finally, the core and bypass nozzles design cross section areas, $A_{9,R}$ and $A_{19,R}$ respectively, must be computed for off-design and transient calculations:

$$A_{9,R} = \frac{\dot{m}_5.R_9.T_9}{p_9.V_9}, \qquad (3.47) \qquad A_{19,R} = \frac{\dot{m}_{13}.R_{19}.T_{19}}{p_{19}.V_{19}}. \qquad (3.48)$$

Outputs

In the present work, the main performance results to be considered, with the purpose of comparing different fuels burning during flight, are related with the total thrust available and how much fuel is consumed, in comparison with conventional results. Therefore, the total thrust, F, the specific-thrust, Ψ, and the specific fuel consumption, SFC, will be calculated in order to compare the turbofan performance for different fuels combustion.

The total thrust of a turbofan aero-engine, F, comes from the thrust generated by the bypass (fan), F_{fan}, and the core of the engine, F_{core} [23]:

$$F = F_{fan} + F_{core}, \qquad (3.49)$$

with

$$F_{fan} = \dot{m}_{fan}.(V_{19} - V_0) + A_{19}.(p_{19} - p_0), \qquad (3.50)$$

$$F_{core} = \dot{m}_{core}.((1+f).V_9 - V_0) + A_9.(p_9 - p_0). \qquad (3.51)$$

In turn, the specific thrust, Ψ, which is a valuable design point output, that does not require the actual knowledge of the air mass flows rates inside the engine, is simply given, in m/s, by [23]

$$\Psi = \frac{F}{\dot{m}}. \qquad (3.52)$$

The most relevant performance output, considered in the present work, is the specific fuel consumption, SFC. This statement comes from the fact that it can become a powerful parameter to compare different fuels performance, since it gives how much fuel is spent to generate a given thrust. SFC is calculated as follows [23], in g/kN.s, for $\dot{m}_f$ given in kg/s and F in N:

$$SFC = \frac{\dot{m}_f}{F} \text{ kg/N.s } = \frac{\dot{m}_f}{F}.10^6 \text{ g/kN.s }. \qquad (3.53)$$

3.8 Off-Design Model

For steady-state aero-engine performance simulations, and for different fuel burning analysis, the off-design model is regarded as a powerful tool. With an off-design model, for the same engine (defined with the design point model), it is possible to analyse the engine performance and influence on pollutant emissions for different power settings and flight conditions.

The off-design model implemented in MATLAB, detailed in the present section, is mostly based on the work of Kurzke [4] and implementation of Gaudet [24]. Since one of the author's objectives was to implement a model capable of off-design and transient simulations (with map reading), this approach was considered as the most adequate in a validation perspective, comparing results of GasTurb 12 for the same components maps reading.

3.8.1 Off-Design Inputs

As previously stated, a design point calculation must be performed before any off-design calculation. Therefore, design input parameters as the ones describe in subsection 3.7.1 and summarized in Table 3.1 must be defined. Additionally, new ambient and flight conditions must be defined, i.e. off-design flight altitude, H, and Mach number, M_0. Then, the user has 3 options to modify the engine operating condition: input high-pressure turbine inlet temperature, T_{t4}, the low-pressure relative spool speed, N_L or the high-pressure relative spool speed, N_H.

For each of the user inputs (T_{t4}, N_L or N_H), a different set of iteration variables, used in the numerical model, follows: if the user defines a certain input, the remaining input parameters become iteration variables of the numerical system. For any case, the off-design bypass ratio, B, and rotating components auxiliary map coordinates, designated by β (detailed in subsection 3.8.2), are fixed iteration variables.

The summary of off-design inputs and iteration variables is given in Table 3.2. Additionally, the most relevant required design point inputs and outputs (subscript R), such as, the design spool speeds, component isentropic efficiencies, rotating component pressure ratios, pressure losses, combustion chamber parameters, stations nondimensional temperatures (θ_i), nozzles cross sections and corrected mass flow rates (explained in subsection 3.8.2), are presented in Table 3.3.

User inputs	H, M_0		
	N_L	N_H	T_{t4}
Input-dependent Iteration Variables	T_{t4} N_H	T_{t4} N_L	N_L N_H
Fixed Iteration Variables	β_{LPC} β_{HPC} β_{HPT} β_{LPT} B		

Table 3.2: Off-design user inputs and iteration variables.

Efficiencies and Pressure Ratios: $\eta_{x,R}$ and $\pi_{x,R}$	**Spools Speeds**
	$N_{L,R,abs}$, $N_{H,R,abs}$
x: fan, LPC, HPC, HPT and LPT	**Pressure Losses**
	$\pi_{b,R}$, $\pi_{fn,R}$, $\pi_{fn,R}$
Corrected Mass Flow Rates: $\dot{m}_{i,R,corr}$	**Nozzles Cross Sections**
i: 2, 2.5, 3, 4, 4.5, 5 and 13	$A_{19,R}$, $A_{9,R}$
Combustion Chamber Parameters	**Nondimensional Temperatures:** $\theta_{i,R}$
$\eta_{b,R}$, $p_{t3,R}$, $T_{t3,R}$, $\dot{m}_{3,R}$	i: 2, 2.5, 4 and 4.5

Table 3.3: Reference input parameters for off-design model.

3.8.2 Component Map Reading

In the present work, the off-design calculations will be based on the reading of engine component maps. As simplified in Figure 1.10, a component map relates the corrected inlet mass flow rate, the pressure ratio and the adiabatic isentropic efficiency with the corrected relative spool speed.

For a generic inlet state of a component, designated by i, the corrected mass flow rate is given by

$$\dot{m}_{i,corr} = \dot{m}_i.\sqrt{\theta_i}/\delta_i. \tag{3.54}$$

In turn, the corrected relative spool speed is calculated based on the relative spool speed, which can be the low-pressure or high-pressure relative spool speeds, respectively N_L or N_H. For a given actual low-pressure spool speed, $N_{L,abs}$, and a given design spool speed, $N_{L,R,abs}$, the relative low-pressure spool speed, N_L, will be simply given by their ratio, as

$$N_L = \frac{N_{L,abs}}{N_{L,R,abs}}, \tag{3.55}$$

with the same approach given for the high-pressure relative spool speed, N_H. Then, for the compressors, LPC (and fan) and HPC, and turbines, HPT and LPT, the following definitions of corrected relative spool speeds arise:

$$N_{LPC} = N_L.\sqrt{\frac{\theta_{2,R}}{\theta_2}}, \tag{3.56}$$

$$N_{HPC} = N_H.\sqrt{\frac{\theta_{2.5,R}}{\theta_{2.5}}}, \tag{3.57}$$

$$N_{HPT} = N_H.\sqrt{\frac{\theta_{4,R}}{\theta_4}}, \tag{3.58}$$

$$N_{LPT} = N_L.\sqrt{\frac{\theta_{4.5,R}}{\theta_{4.5}}}. \tag{3.59}$$

To facilitate the reading of a map of component, auxiliary map coordinates, designated by β, are defined between 0 and 1 (surge line). The component maps considered for the present study, obtained from [4], are presented in Appendix B. These component maps are defined in such a way that (in a readable file), for a given combination of relative corrected component spool speed and β, pressure ratios, adiabatic isentropic efficiencies and corrected mass flow rates are linearly interpolated.

However, one has to take into account, when using "generic" maps of components, that the map may not coincide with the engine being modelled. To avoid this problem, the component map must be scaled. The scaling process consists, in short, in defining, in the unscaled map, the point where the design point should be defined. In order to do so, a reference component (defined here with subscript "x") corrected relative spool speed, $N_{x,R}$, and auxiliary map coordinate, $\beta_{x,R}$, must be defined. In the present work, for all components, $N_{x,R} = 1$ and $\beta_{x,R} = 0.5$.

For a given component corrected relative spool speed, N_x, and map coordinate, β_x, scaled values of pressure ratio, π_x, isentropic efficiency, η_x, and corrected mass flow rate, $\dot{m}_{i,corr,read}$, are given by

$$\pi_x = \pi_{x,read} = (\pi_{x,map}-1).\frac{\pi_{x,R}-1}{\pi_{x,R,map}-1}+1, \tag{3.60}$$

$$\eta_x = \eta_{x,read} = \eta_{x,map}.\frac{\eta_{x,R}}{\eta_{x,R,map}}, \tag{3.61}$$

$$\dot{m}_{i,corr,read} = \dot{m}_{i,corr,map}.\frac{\dot{m}_{i,R,corr}}{\dot{m}_{i,R,corr,map}}, \tag{3.62}$$

where $\pi_{x,map}$, $\eta_{x,map}$ and $\dot{m}_{i,corr,map}$ are the overall pressure ratio, the isentropic efficiency and the corrected mass flow rate, respectively, interpolated from the unscaled map for a given component operating condition defined by the corrected relative spool speed, N_x, and auxiliary map coordinate, β_x. Subscript i, as in other sections in the present work, refers to the inlet state of the referred component. On the other hand, $\pi_{x,R,map}$, $\eta_{x,R,map}$ and $\dot{m}_{i,R,corr,map}$ are the overall pressure ratio, the isentropic efficiency and the corrected mass flow rate, respectively, interpolated from the unscaled map for the reference corrected relative spool speed, $N_{x,R} = 1$, and auxiliary map coordinate, $\beta_{x,R} = 0.5$.

It should be noted that, for turbines, pressure ratio map reading and scaling is based on the pressure ratio from its outlet to its inlet, π_x^{-1}, and, for all components, a Reynolds correction is added through the definition of the Reynolds Number Index, RNI:

$$RNI = \frac{p_{ti}}{p_{SL}} . \sqrt{\frac{R_0 . T_{SL}}{R_i . T_{ti}}} . \frac{\mu(T_{SL})}{\mu(T_{ti})}, \tag{3.63}$$

where μ is the air dynamic viscosity, calculated according to reference [14], neglecting fuel-air ratio and pressure effects. For pressure and mass scaling, a Reynolds correction factor is calculated, correlated linearly with the logarithm of RNI (detailed in [4]).

3.8.3 Off-Design Aero-Engine Numerical Model

In the present subsection, the off-design aero-engine numerical model is detailed as it was the case for the design point model in subsection 3.7.2. Since, many assumptions and calculations are performed in the same way, for the present case, for concision, only relevant differences in implementation to the design point model are detailed. It should be noted that, the numerical procedure is described for a given set of user inputs and iteration variables.

Diffuser

The diffuser, in the off-design model, is defined in the same way as in subsection 3.7.2. The only difference being the fact that the off-design corrected relative low-pressure compressor, N_{LPC}, must be calculated with equation 3.56.

Fan

In the present work, a fan map is used to define the fan and the low-pressure compressor. For a given N_{LPC} and β_{LPC}, values of π_{fan}, η_{fan} and $\dot{m}_{2,corr,read}$ are readily interpolated. Given the pressure ratio, π_{fan}, p_{t13} is calculated. With computed $T_{t13,s}$ (isentropic relations) and interpolated η_{fan}, it is possible to obtain the outlet temperature, T_{t13}, rearranging equation 3.24. At this stage, the inlet mass flow, $\dot{m}$, for off-design calculations is obtained by rearranging equation 3.54 as follows:

$$\dot{m} = \dot{m}_2 = \dot{m}_{2,corr,read} . \delta_2 / \sqrt{\theta_2}. \tag{3.64}$$

Then, with given B, the fan/bypass mass flow rate, $\dot{m}_{fan}$ or $\dot{m}_{13}$, is calculated with equation 3.18.

Low-Pressure Compressor, LPC

In the present model, based on the work of Kurzke [4], the low-pressure compressor pressure ratio, π_{LPC}, and isentropic efficiency, η_{LPC}, are given by

$$\pi_{LPC} = 1 + \frac{(\pi_{fan} - 1).(\pi_{LPC,R} - 1)}{(\pi_{fan,R} - 1)}, \quad (3.65) \qquad \eta_{LPC} = \eta_{fan}.\frac{\eta_{LPC,R}}{\eta_{fan,R}}. \quad (3.66)$$

Then, along the lines of the fan's procedure previously explained, $p_{t2.5}$ and $T_{t2.5}$ are calculated. The core mass flow rate, $\dot{m}_{core}$, is calculated as in subsection 3.7.2, with equation 3.17.

High-Pressure Compressor, HPC

For calculated N_{HPC} and given β_{HPC}, values of π_{HPC}, η_{HPC} and $\dot{m}_{2.5,corr,read}$ are readily interpolated. Given the pressure ratio, π_{HPC}, p_{t3} is calculated. With computed $T_{t3,s}$ (isentropic relations) and interpolated η_{HPC}, it is possible to obtain the outlet temperature, T_{t3}, rearranging equation 3.24.

The difference between the interpolated corrected mass flow rate, $\dot{m}_{2.5,corr,read}$, and the corrected mass flow rate that would be obtained with equation 3.54, $\dot{m}_{2.5,corr}$, assuming the core mass flow rate previously calculated, $\dot{m}_{core}$, represents the first iteration mass flow continuity error. In this work it is designated by $Error_2$:

$$Error_2 = \dot{m}_{2.5,corr,read} - \dot{m}_{2.5,corr}. \quad (3.67)$$

Combustion Chamber

In the off-design model, combustion efficiency, η_b, and burner pressure loss, π_b, are computed based on the chamber loading and squared corrected mass flow rates, respectively. In fact, according to [4], the off-design combustion efficiency relates to the design combustion efficiency, $\eta_{b,R}$, with

$$\log(1 - \eta_b) = \log(1 - \eta_{b,R}) + b.\log\left(\frac{\Omega}{\Omega_R}\right), \quad (3.68) \qquad \Omega = \frac{\dot{m}_3}{p_{t3}^{1.8}.e^{T_{t3}/300}} \times \text{Volume}, \quad (3.69)$$

where b represents the "burner part load constant" and is typically given by 1.6 [4] and Ω the combustion chamber loading (combustion chamber volume not actually required). There will also be a variation on pressure loss across the combustion chamber, as a function of the corrected mass flow rates squared:

$$\pi_b = \pi_{b,R}.\left(\frac{\dot{m}_{3,corr}}{\dot{m}_{3,R,corr}}\right)^2. \quad (3.70)$$

The fuel-air ratio, f, is calculated in the same way as in design calculations (equation 3.25). Then, the calculated corrected mass flow rate at station 4, $\dot{m}_{4,corr}$, is calculated with equation 3.54, with $\dot{m}_4 = \dot{m}_{2.5}.(1 + f)$.

High-Pressure Turbine, HPT

For calculated N_{HPT} and given β_{HPT}, values of π_{HPT}, η_{HPT} and $\dot{m}_{4,corr,read}$ are readily interpolated. Given the pressure ratio, π_{HPT}, $p_{t4.5}$ is calculated. With computed $T_{t4.5,s}$ (isentropic relations) and

interpolated η_{HPT}, one can compute the outlet temperature, $T_{t4.5}$ rearranging equation 3.30.

With the interpolated value (read and scaled from HPT map) of $\dot{m}_{4,corr,read}$ and previously calculated value, $\dot{m}_{4,corr}$, an additional mass flow continuity error is computed with equation 3.71.

Additionally, work compatibility must be achieved (steady-state). To guarantee this requirement, another iteration error is calculated, based on actual differences between calculated high-pressure compressor power demand, $\dot{W}_{HPC}$ (equation 3.36), and calculated high-pressure turbine power, $\dot{W}_{HPT}$ (equation 3.37). $Error_4$ is then computed with equation 3.72.

$$Error_3 = \dot{m}_{4,corr,read} - \dot{m}_{4,corr}. \qquad (3.71)$$

$$Error_4 = \dot{W}_{HPT} - \dot{W}_{HPC}. \qquad (3.72)$$

Low-Pressure Turbine, LPT

For calculated N_{LPT} and given β_{LPT}, values of π_{LPT}, η_{LPT} and $\dot{m}_{4.5,corr,read}$ are readily interpolated. Given the pressure ratio, π_{LPT}, p_{t5} is calculated. With computed $T_{t5,s}$ (isentropic relations) and interpolated η_{LPT}, it is possible to obtain the outlet temperature, T_{t5}, rearranging equation 3.30.

With the interpolated value (read and scaled from LPT map) of $\dot{m}_{4.5,corr,read}$ and calculated value, $\dot{m}_{4.5,corr}$ (with equation 3.54), a final mass flow continuity error is computed with equation 3.73.

Additionally, work compatibility must be achieved. To guarantee this requirement, another iteration error is calculated, based on actual differences between calculated low-pressure compressor and fan power demand, respectively $\dot{W}_{LPC}$ (equation 3.39) and $\dot{W}_{fan}$ (equation 3.40), and calculated low-pressure turbine power, $\dot{W}_{LPT}$ (equation 3.41). $Error_6$ is then computed with equation 3.74.

$$Error_5 = \dot{m}_{4.5,corr,read} - \dot{m}_{4.5,corr}. \qquad (3.73)$$

$$Error_6 = \dot{W}_{LPT} - \dot{W}_{LPC} - \dot{W}_{fan}. \qquad (3.74)$$

Nozzles

The nozzles calculations remain the same as defined for design point model, with the main difference being the change of pressure loss across the nozzles with correct mass flows squared (as in the combustion chamber). It follows that:

$$\pi_n = \pi_{n,R}. \left(\frac{\dot{m}_{5,corr}}{\dot{m}_{5,R,corr}} \right)^2, \qquad (3.75)$$

$$\pi_{fn} = \pi_{fn,R}. \left(\frac{\dot{m}_{13,corr}}{\dot{m}_{13,R,corr}} \right)^2. \qquad (3.76)$$

The core and fan nozzles cross section areas, A_9 and A_{19}, respectively, calculated with the off-design model, must be compared with the values computed in design calculations, respectively $A_{9,R}$ and $A_{19,R}$. Assuming fixed-geometry, 2 iteration errors are calculated as follows:

$$Error_1 = A_{19} - A_{19,R}, \qquad (3.77)$$

$$Error_7 = A_9 - A_{9,R}. \qquad (3.78)$$

3.8.4 Off-Design Iterative Scheme

As previously stated, the present off-design model is based on the Newton-Raphson iterative method. In short, for given set of off-design inputs, initial iteration variables and initial variable variations are

assumed. The off-design aero-engine model explained above is computed and errors saved. For each variable variation, errors are computed and the Jacobian matrix of the system is defined. The sum of all 7 iteration errors (in absolute value) is compared to a specified tolerance (assumed as 10^{-6}).

If the sum of iteration errors calculated is higher than the given tolerance, a new set of iteration variables variations are calculated based on the Jacobian matrix, resulting in updated iteration variables. This procedure is repeated until the sum of iteration errors is lower than the defined tolerance. Off-design performance outputs are then properly defined and additional results, such as pollutant emissions, may be obtained. A flowchart scheme of the off-design model is summarized in Figure 3.2.

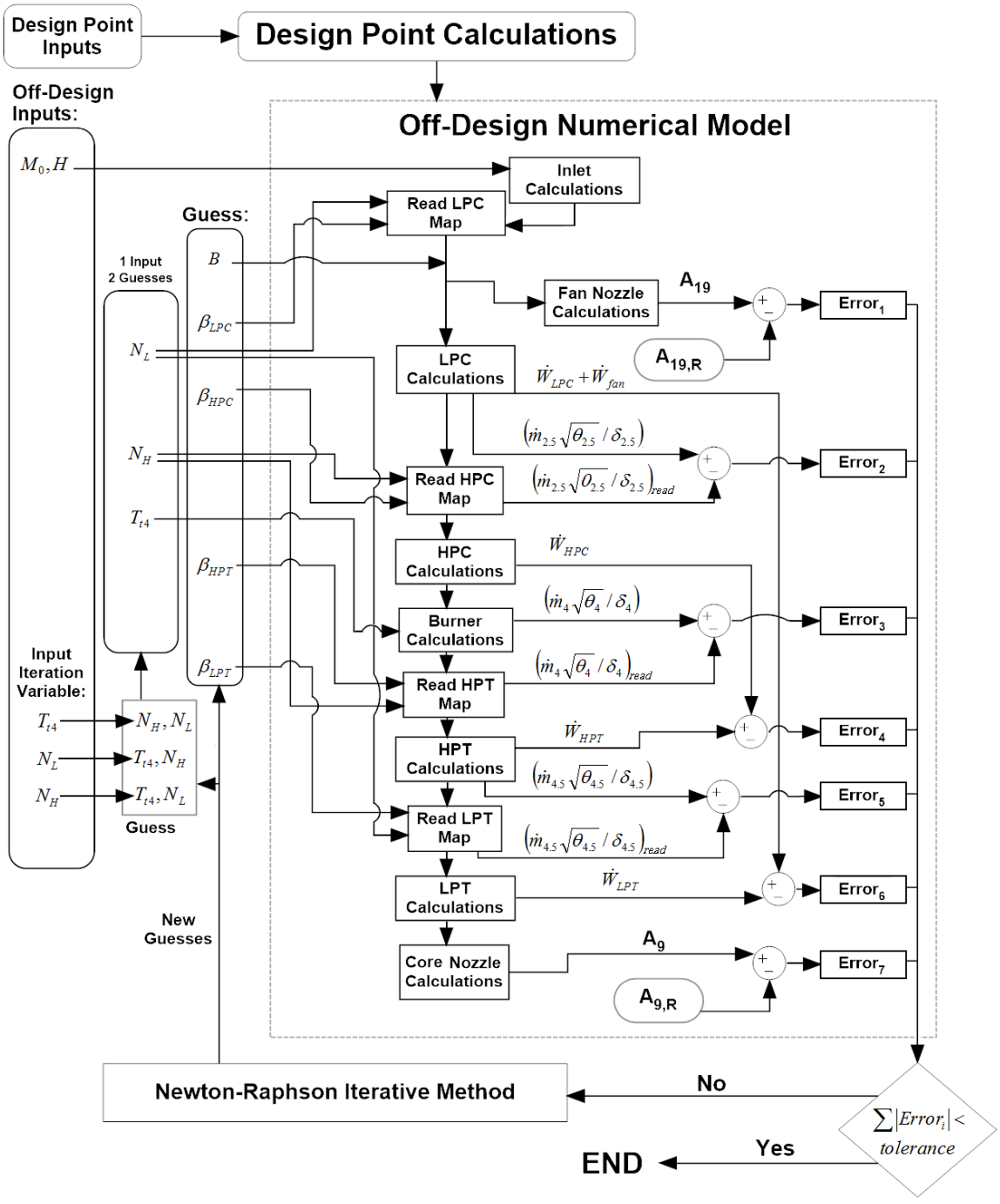

Figure 3.2: Off-design model flowchart scheme.

3.9 Transient Model

Given the scope of the present thesis, so that the technical feasibility of a wide range of alternative fuels is evaluated, transient aero-engine simulations are performed as well. The relevance of transient aero-engine simulations for the burning of different fuels is supported by the fact that an aircraft should be able to safely manoeuvre regardless of the injected fuel.

Then, engine accelerations and decelerations, which typically happen during flight stages such as the take-off or in emergency situations (an unexpected change in flight conditions demanded), are to be analysed so that the influence of the fuel burning in an aero-engine transient response is verified.

In this section, the additional required transient inputs (summary in Table 3.4) and the MATLAB implementation of the aero-engine transient model of a typical turbofan, summarized through the detailing of equations and assumptions used, are detailed. For the same reasons as for the off-design model implementation, the aero-engine transient model, is mostly based on the work of Kurzke [4].

3.9.1 Transient Inputs

In order to simulate any type of aero-engine transient response, a initial flight condition must be defined. This is done with the implemented off-design model, with which the user defines what is the engine operating condition before a transient response is demanded.

In the present model, there are three types of time-dependent, t, user inputs: fuel mass flow rate, $\dot{m}_{f,demand}(t)$, power setting, $P_{demand}(t)$, and thrust demand, $F_{demand}(t)$. Where power setting, P in %, will be directly related with the low-pressure relative spool speed, N_L. This way, when a power setting change is demanded, it will correspond in fact to a different demand of N_L, $N_{L,demand}(t)$. In Table 3.4, transient model inputs and iteration variables are summarized.

User Inputs	
Initial Conditions (Off-Design)	H, M_0 N_L, N_H or T_{t4}
Transient Inputs	$\dot{m}_{f,demand}(t)$ $P_{demand}(t)$ $F_{demand}(t)$
Iteration Variables	
β_{LPC}, β_{HPC}, β_{HPT}, β_{LPT}, B, T_{t4}	

Table 3.4: Transient user inputs and iteration variables.

Whereas for fuel mass flow rate demand, it is assumed for simplicity instantaneous change in actual fuel being injected in the system, with changes in power or thrust demands, a simple PID (proportional-integral-derivative) controller is considered to control the fuel flow rate being injected to achieve demanded conditions. In this regard, proportional, C_P, integral, C_I, and derivative, C_D, gains may be defined. The PID controller implemented is summarized in Figure 3.3.

Transient simulations require the selection of 2 additional engine parameters, i.e. the low and high-pressure spools polar moments of inertia, I_L and I_H, respectively.

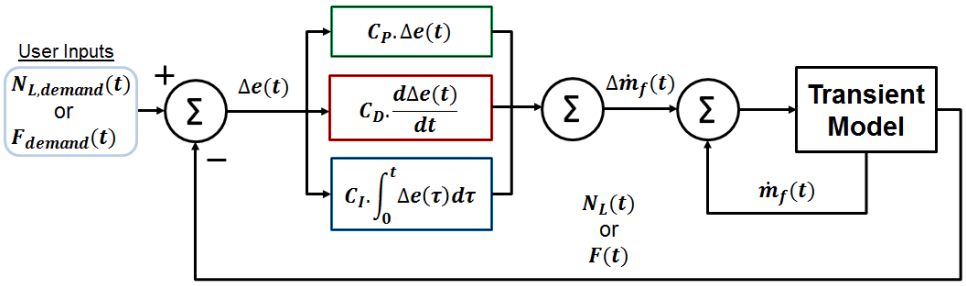

Figure 3.3: Simplified scheme for PID controller implemented for power setting in %, P_{demand} (directly related with $N_{L,demand}$), or total thrust, F_{demand}, time-dependent user input demands.

3.9.2 Transient Aero-Engine Numerical Model

In the following paragraphs, the transient numerical model will be briefly detailed. Since most of assumptions and calculations are identical to the off-design model, it becomes relevant to present the differences in implementation. In fact, in the core, the numerical aero-engine transient model calculations remain the same from free stream conditions until the combustion chamber. It should also be noted that, the procedure here described, is based on a set of iteration variables for a certain simulation time, t.

The transient numerical model system, for a certain simulation time, will be defined by the calculation of 6 iteration errors, $Error_i$, instead of 7 (as in off-design). Work compatibility errors are excluded from the system. In the transient model, numerical errors are now defined as

$$Error_1 = A_{19} - A_{19,R}, \tag{3.79}$$

$$Error_2 = \dot{m}_{2.5,corr,read} - \dot{m}_{2.5,corr}, \tag{3.80}$$

$$Error_4 = \dot{m}_{4,corr,read} - \dot{m}_{4,corr}, \tag{3.81}$$

$$Error_5 = \dot{m}_{4.5,corr,read} - \dot{m}_{4.5,corr}, \tag{3.82}$$

$$Error_6 = A_9 - A_{9,R}. \tag{3.83}$$

A new error, related with fuel mass flow rate, $\dot{m}_f$, is calculated and defined next: $Error_3$.

Combustion Chamber: Fuel Mass Flow Rate Input

For transient calculations, a different iteration error is considered. Taking into account the calculation of the fuel-air ratio (as explained in subsection 3.8.3), f, a calculated value of the fuel mass flow, $\dot{m}_f$, is obtained with equation 3.35. This result is then compared with fuel mass flow required (injected at that time), $\dot{m}_{f,input}$, with a transient iteration error added to the system:

$$Error_3 = \dot{m}_f - \dot{m}_{f,input}. \tag{3.84}$$

High-Pressure Spool Acceleration

Contrary to what is assumed on steady-state calculations, transient calculations are based on the fact that the work required for compression may be different than the work available, at a certain time, t. This energy difference will result in a spool speed acceleration (positive or negative).

At this stage, it is possible to calculate the high-pressure turbine generated power, which compared with the required power for compression gives the high-pressure spool acceleration, dN_H/dt, in RPM/s:

$$\frac{dN_H}{dt} = \frac{\left(\frac{60}{2\pi}\right)^2.(\dot{W}_{HPT} - \dot{W}_{HPC})}{I_H.N_{H,abs}}, \tag{3.85}$$

with $\dot{W}$ given in W and I_H in kg.m^2.

Low-Pressure Spool Acceleration

Based on the same assumptions as before, it is possible to calculate the low-pressure turbine generated power and compare its value with the required power for compression. From that, the low-pressure spool acceleration, dN_L/dt, in RPM/s, is given by

$$\frac{dN_L}{dt} = \frac{\left(\frac{60}{2\pi}\right)^2.(\dot{W}_{LPT} - \dot{W}_{LPC} - \dot{W}_{fan})}{I_L.N_{L,abs}}. \tag{3.86}$$

3.9.3 Transient Iterative Scheme

As a standard in the present work, the iterative method used for transient calculations is the same as for the off-design calculations: the Newton-Raphson method. The main differences being the fact that the fuel mass flow rate becomes an iteration variable and relative spools speeds are now considered as calculated model inputs, since it will be defined at the initial simulation time ($t = 0$ s) with initial off-design conditions and calculated, for each time step, Δt, based on respective accelerations.

In the present transient implementation, for each simulation time, an iterative process, as detailed in the previous subsection, is computed. For a given user input, the transient model computes results for each simulation time and finishes calculations when the total elapsed time reaches the user-defined maximum value. At each time step, with computed spool accelerations (equations 3.85 and 3.86), an explicit integration method is used to compute new values of relative spool speeds. It follows that, for given relative spools speeds, $N_{L,old}$ and $N_{H,old}$, the respective values for the next simulation time, $N_{L,new}$ and $N_{H,new}$, will be based on spool accelerations, $\left(\frac{dN_L}{dt}\right)_{old}$ and $\left(\frac{dN_H}{dt}\right)_{old}$, respectively:

$$N_{L,new} = N_{L,old} + \left(\frac{dN_L}{dt}\right)_{old}.\Delta t, \tag{3.87}$$

$$N_{H,new} = N_{H,old} + \left(\frac{dN_H}{dt}\right)_{old}.\Delta t. \tag{3.88}$$

As previously stated, taking into account the type of transient input, different types of controllers are employed. For the case of power setting, directly related with $N_{L,demand}$, and thrust, F_{demand}, demands, for each simulation time, the demanded parameter is compared with the correspondent numerically computed value, $N_L(t)$ and $F(t)$, respectively. Then, with a PID controller, the difference in demanded and computed results is converted in a variation of fuel mass flow rate, $\dot{m}_f$. If a fuel mass flow rate with time is demanded, an instantaneous change in injection is assumed, that is $\dot{m}_f(t) = \dot{m}_{f,demand}(t)$.

A flowchart scheme of the transient model is summarized next, in Figure 3.4.

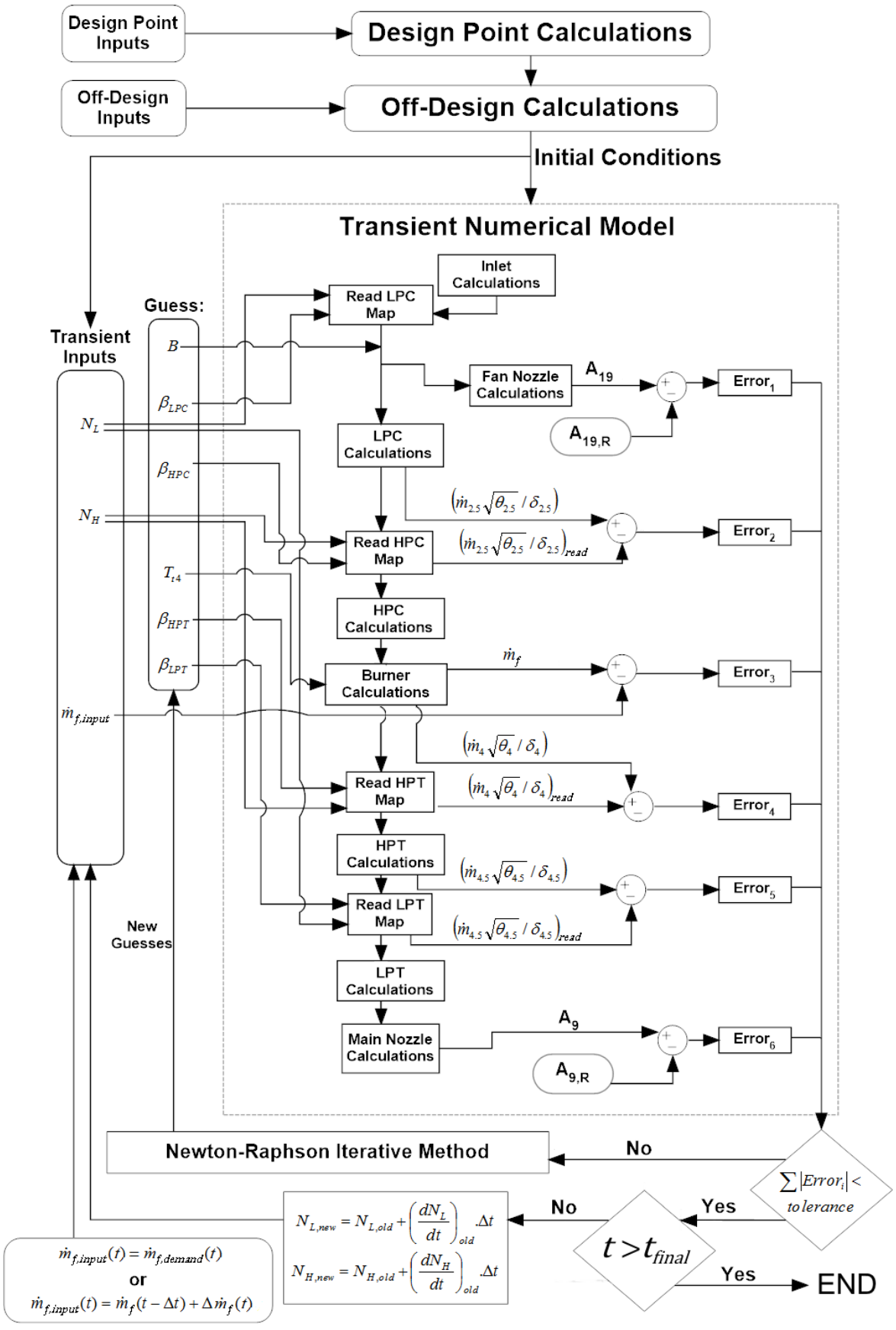

Figure 3.4: Transient model flowchart scheme.

3.10 Pollutant Emissions Model

Along with performance (operational) results, it is of significant importance to estimate pollutant emissions, when studying the viability of different fuels for commercial aviation. The pollutant emissions to be computed will be of undesired substances showing high dependence of temperature: oxides of nitrogen, NO_x, carbon monoxide, CO, unburned hydrocarbons, UHC, and soot (smoke).

The work of Rizk and Mongia [18] was considered in detriment of other correlations mainly due to the fact that all required correlations, for NO_x, CO, UHC and soot pollutant emissions, are properly defined, with included effects of evaporation rates, which may be significant considering different fuel burning.

3.10.1 Oxides of Nitrogen Emissions

The pollutant emissions of oxides of nitrogen are highly influenced by the stoichiometric flame temperature, T_{st}. Considering terms of mixing, evaporation and reaction, NO_x emissions are estimated by

$$EI_{NO_x} = \frac{1.5 \times 10^{15} . \sqrt{\tau - 0.5\tau_e} . e^{\frac{-71000}{T_{st}}}}{p_{t3}^{0.05} . \sqrt{\frac{\Delta p_{t3}}{p_{t3}}}}, \tag{3.89}$$

with τ and τ_e, the combustion residence time and evaporation time, respectively, given in s, T_{st} in K and p_{t3} and $\Delta p_{t3} = p_{t3} - p_{t4}$ given in Pa.

3.10.2 Carbon Monoxide and Unburned Hydrocarbons Emissions

Taking into account the influence of mixing, evaporation and reaction during fuel combustion, the estimation of emitted CO and UHC will be computed with equations 3.90 and 3.91, respectively. In these correlations it is assumed that a significant proportion of the primary zone residence time is required to evaporate the fuel. Considering the primary zone flame temperature, T_{pz}, given in K, it follows:

$$EI_{CO} = \frac{1.8 \times 10^{8} . e^{\frac{7800}{T_{pz}}}}{p_{t3}^{2} . \sqrt{\frac{\Delta p_{t3}}{p_{t3}}} . (\tau - 0.4\tau_e)}, \tag{3.90}$$

$$EI_{UHC} = \frac{7.6 \times 10^{10} . e^{\frac{9756}{T_{pz}}}}{p_{t3}^{2.3} . \left(\frac{\Delta p_{t3}}{p_{t3}}\right)^{0.6} . (\tau - 0.35\tau_e)^{0.1}}. \tag{3.91}$$

It should be highlighted that, the estimation of unburned hydrocarbons is more complex than the estimations of emitted oxides of nitrogen and carbon monoxides. Which is why fewer and less accurate empirical correlations are available in the literature.

3.10.3 Soot Concentration

Soot exhaust emissions estimation is considered as highly complex mainly due to its significant dependence on fuel composition and chemical reactions. However, so that an estimation can be made on this matter, soot concentration, S, given in mg of soot emitted for kg of exhaust gas, based on the fuel hydrogen content (in weight %), $H\%$, primary and secondary zone air fractions, q_{pz} and q_{sz}, respectively,

primary and secondary zone fuel-air ratios, $f_{pz} = f/q_{pz}$ and $f_{sz} = f/q_{sz}$, respectively, and an average secondary zone temperature, T_{sz} in K, will be approximated by [18]

$$S = 0.0145 \times \frac{f_{pz}.\left(\frac{p_{t3}}{1000}\right)^2}{q_{pz}.\dot{m}_3.T_{pz}}.(18 - H\%)^{1.5}.\left(1 - 0.00515\frac{e^{0.001T_{sz}}}{f_{sz}}\right). \tag{3.92}$$

3.10.4 Pollutant Emissions Numerical Model

As easily depicted by analysing equations 3.89, 3.90 and 3.91, the quantification of NO_x, CO and UHC pollutant emissions is highly dependent on accurate estimation of the primary zone residence time and time required for evaporation.

Since, in the present thesis, the main objective is to compare results with change in fuel rather than to accurately quantify results for a specified engine, a value of primary zone residence time for burned Jet A-1, τ_{ref}, will be defined. According to [11], for a given residence time assumed for the burning of Jet A-1, τ_{ref}, for the same combustion volume, the residence time for an alternative fuel, τ, may be approximated by equation 3.93.

Then, the evaporation time required for Jet A-1 evaporation, $\tau_{e,ref}$, will be varied from a minimum value of zero (infinitely fast evaporation) to the residence time. With this range of evaporation times, it is assumed that evaporation is completed within the combustion zone. Each value of reference evaporation time is then compared to what would be obtained for a different fuel with equation 3.94.

$$\tau = \tau_{ref}.\frac{p_{t3}.\dot{m}_{3,ref}.T_{pz,ref}}{p_{t3,ref}.\dot{m}_3.T_{pz}}. \tag{3.93}$$

$$\tau_e = \tau_{e,ref}.\left(\frac{D_0}{D_{0,ref}}\right)^2.\left(\frac{\lambda_{ref}}{\lambda}\right). \tag{3.94}$$

A range of results will be obtained for the condition that both analyses (Jet A-1 and an alternative fuel emissions with evaporation time) are conducted considering complete fuel evaporation in the primary zone for both fuels ($\tau_e < \tau$ and $\tau_{e,ref} < \tau_{ref}$). Computed emissions relative to what would be obtained for Jet A-1 will be given with an average value and maximum and minimum estimations.

According to [11], the primary zone temperature, T_{pz}, is given by

$$T_{pz} = T_{t3} + \Delta T_{pz}, \tag{3.95}$$

with ΔT_{pz} representing the flame adiabatic temperature rise in the primary zone. Then, in the present work, T_{pz} and T_{st} temperatures, are to be calculated with the flame temperature model, described in section 3.2, for primary zone, f_{pz}, and stoichiometric f_{st} (Appendix C, equation C.12), fuel-air ratios, respectively.

It should be highlighted that the soot concentration estimation requires average values of secondary zone temperatures (as well as the air fraction employed). In order to obtain an approximate estimation, in this work, the air fraction on secondary zone, q_{sz}, is assumed based on the selection of the primary zone value, q_{pz}, and the average secondary zone temperature, T_{sz}, approximated as a mean combustor value, weighted by the air fraction as follows:

$$T_{sz} = \left(T_{t4} - \frac{T_{pz} - T_{t4}.q_{pz}}{1 - q_{pz}}\right).q_{sz} + \frac{T_{pz} - T_{t4}.q_{pz}}{1 - q_{pz}}. \tag{3.96}$$

Chapter 4

Design and Off-Design Performance Results

In the present chapter, steady-state performance results (design and off-design) will be presented. The design point selection is briefly summarized first. All results presented in this thesis will be based on the same design point, defined next, except for the design point validation and analysis of an engine with higher overall pressure ratio. Being the design point selected and the model validated, the off-design model performance results are properly validated.

With engine performance results validated, performance results for different alternative fuels and operating conditions are presented and discussed.

4.1 Design Point Selection

For the design point selection, the definition of Level of Technology [23] was used to estimate appropriate values of polytropic efficiencies, the burner combustion efficiency (for burning of Jet A-1), spool mechanical efficiencies and pressure losses. A Level of Technology 3 was considered, which presents reasonable approximations for engines manufactured between 1985 and 2005 [23].

The design point in this thesis, will be defined as a Top of Climb condition (TOC) [22]. The engine design parameters selected will simulate a typical small commercial turbofan engine (similar to ALF502R series), with design parameters based on typical turbofan specifications [15, 49]. The reason for selecting this type of turbofan instead of a turbofan with higher overall pressure ratio, for example, as previously discussed, is due to the fact that the evaporation model defined may fail at higher burner inlet pressures than the critical value for each fuel. The value for reference pressure ratio of the fan is based on a typical maximum of 1.8 [14]. In Table 4.1, the most relevant design point inputs are summarized.

In the present work, additional reference (design) parameters were necessary to be defined and estimated. The considered initial liquid fuel temperature, T_f, is of 25^{o}C, based on the common definition of heating values (net heat of combustion) defined at this temperature [19]. For adiabatic temperature rise calculations, for example, a fraction of air employed in the primary zone must be defined. Based on

Component Efficiencies		Engine Design Parameters		Ambient and Flight Data	
$e_{fan} = 0.86$	$e_{LPT} = 0.89$	$B_R = 5.7$		$M_{0,R} = 0.8$	$H_R = 10668$ m
$e_{LPC} = 0.88$	$\eta_{b,R,ref} = 0.98$	$T_{t4,R} = 1550$ K		**Pressure Losses**	
$e_{HPC} = 0.88$	$\eta_{m,L} = 0.99$	$\dot{m}_R = 100$ kg/s	$\pi_{fan,R} = 1.7$	$\pi_{n,R} = 0.98$	$\pi_{fn,R} = 0.98$
$e_{HPT} = 0.89$	$\eta_{m,H} = 0.99$	$\pi_{LPC,R} = 2$	$\pi_{HPC,R} = 6$	$\pi_{b,R} = 0.94$	

Table 4.1: Design point selection.

typical values presented in [14], it will be considered that for all conditions, 35% of total air is employed in the combustion zone (approximated as the primary zone), i.e. $q_{pz} = 0.35$. The secondary zone fraction of air employed is assumed as of $q_{sz} = 0.6$, based on the selection of q_{pz}.

Design values of low-pressure and high-pressure spools speeds, respectively $N_{L,R,abs}$ and $N_{H,R,abs}$, in RPM, must be defined so that off-design and transient calculations are possible. The values were selected as typical values for each spool and based on reference [50]. This parameters are presented on Table 4.2. It should be highlighted that this nominal values represent the design point values, which, in the present work, refers to Top of Climb condition.

Spools Design Speeds
$N_{L,R,abs} = 10000$ RPM
$N_{H,R,abs} = 13500$ RPM

Table 4.2: Spools design speeds selection.

4.2 Engine Stationary Model Validation

Before computing results for different fuels, it should be verified if for a given fuel (Jet A-1), the performance results obtained are valid. To do so, parametric analyses are performed and compared with the results obtained with the commercial software GasTurb 12 [4].

4.2.1 Design Point Model Validation

To validate the design point model implemented, the specific fuel consumption, SFC, specific thrust, Ψ, and fuel-air ratio, f, results will be evaluated through parametric analysis with the present model and [4] design results. To do so, design parameters such as the high-pressure turbine inlet temperature, the bypass ratio, the high-pressure compressor pressure ratio and the flight Mach number are varied and results obtained presented. Throughout the validation, all design point parameters, except the ones varied during parametric analysis, will remain constant (as in Table 4.1).

In Figures 4.1, 4.2, 4.3 and 4.4, the specific fuel consumption is computed as a function of the flight Mach number, M_0, the high-pressure turbine inlet temperature, T_{t4}, the high-pressure compressor pressure ratio, π_{HPC} and the bypass ratio, B, respectively. With M_0 varying between 0 and 2 (from subsonic to supersonic), T_{t4} between 1200 K and 1800 K, π_{HPC} between 1 and 15 and B between

0 (turbojet) and 10. Relative discrepancies to GasTurb 12 [4] results of 0.12%, 0.151%, 0.067% and 0.064% are obtained respectively for M_0, T_{t4}, π_{HPC} and B parametric analyses.

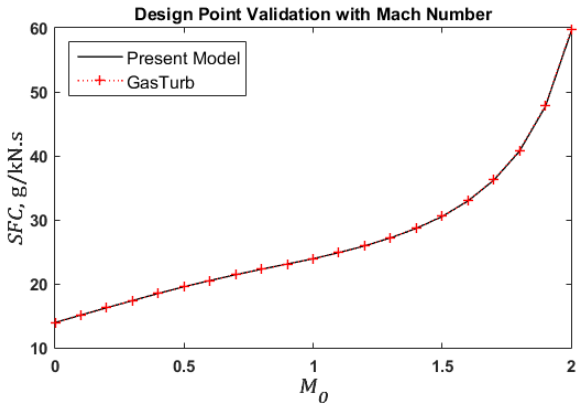

Figure 4.1: Design point validation of specific fuel consumption, SFC, with flight Mach number, M_0.

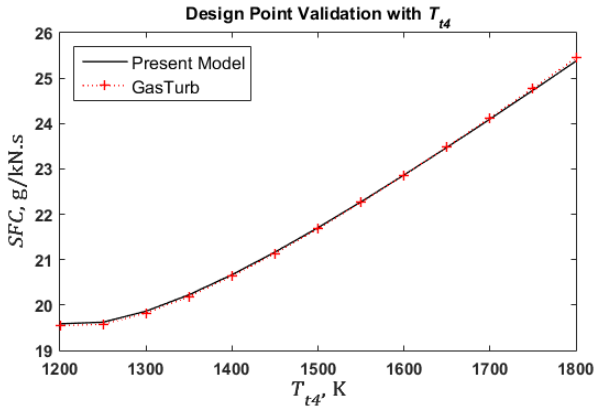

Figure 4.2: Design point validation of specific fuel consumption, SFC with inlet turbine temperature, T_{t4}.

Although not presented here, the specific thrust output results are compared with those obtained with GasTurb 12 [4], recurring to the same parametric analysis described before (for SFC validation). Relative average discrepancies to GasTurb 12 results of 0.077%, 0.036%, 0.020% and 0.024% are obtained, respectively, for M_0, T_{t4}, π_{HPC} and B parametric analyses.

Given the excellent results obtained for the specific fuel consumption and specific thrust, the fuel-air ratio (a relevant parameter in the present study) should present the same level of accuracy. In fact, relative average discrepancies to GasTurb 12 results of 0.076%, 0.183%, 0.083% and 0.080% are obtained, respectively, for M_0, T_{t4}, π_{HPC} and B parametric analyses.

Given the excellent average relative errors verified (always less than 0.2%), the design point is considered validated and therefore eligible for reference calculations for the off-design model, which is validated in the next subsection.

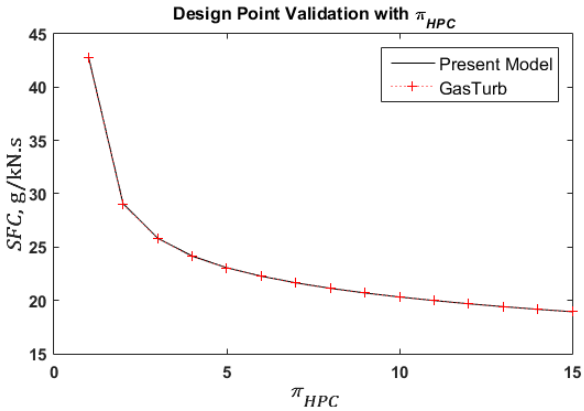

Figure 4.3: Design point validation of specific fuel consumption, SFC, with high-pressure compressor pressure ratio, π_{HPC}.

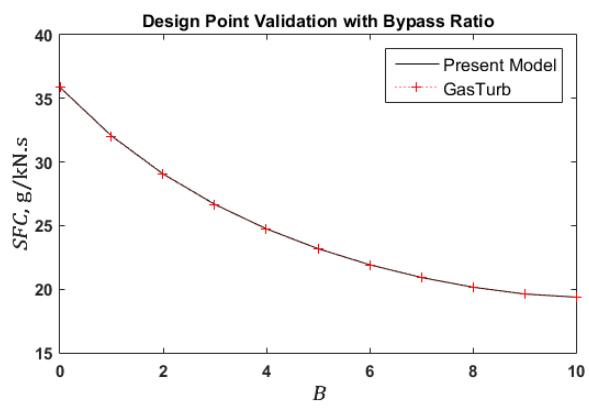

Figure 4.4: Design point validation of specific fuel consumption, SFC, with bypass ratio, B.

4.2.2 Off-Design Model Validation

The off-design model starts with the calculation of the design point. Therefore, high errors on the design calculations could propagate and increase the error of the off-design model. Since that is not the case, the relative errors obtained for the off-design model are negligibly influenced by the design computations.

The validation of the off-design engine model will consist in the following parametric analyses: change Mach number, for two different altitudes (sea level and cruise level) with a relative high-pressure spool speed of $N_H = 0.97$ (assuming a cruise condition with $N_L = 0.95$ [22]); change the high-pressure turbine inlet temperature, T_{t4}, for $M_0 = 0.8$ and $H = 10668$ m; change the relative high-pressure spool speed, N_H, for $M_0 = 0.8$ and $H = 10668$ m.

In a similar manner to the procedure for the design point model validation, the output results parametrically analysed are the specific fuel consumption, SFC, and the specific thrust, Ψ. Being validated for design point calculations and directly related with SFC and Ψ, the validation of fuel-air ratio, f, results is not considered here. Additionally, information about the engine operation performance is also evaluated through the evaluation of the spools relative speeds. For off-design calculations, the variation of the bypass ratio, B, and the high-pressure turbine inlet temperature, T_{t4}, is also analysed.

In the first parametric study analysis, the Mach number is the parameter varied. While maintaining $N_H = 0.97$, M_0 varies from 0 to 1.7 for sea level flight condition and from 0 to 2 for $H = 10668$ m. A shorter range for sea level is defined since for higher flight Mach numbers, SFC becomes unstable and eventually, due to higher flight speed than the exhaust speed (mainly the bypass flow), becomes negative. To showcase this event, exceptionally, at Figure 4.5, the Mach ranges will be the same. Figures 4.5 and 4.6 present calculated and obtained with GasTurb 12 [4] results of specific fuel consumption, SFC, and low-pressure relative spool speed, N_L, respectively, with flight Mach number. Average relative errors, compared to [4] results, for SFC, N_L, Ψ, B and T_{t4} are given in Table 4.3 (Row #1 and #2 for $H = 10668$ m and sea level, respectively). It should be noted that, in Table 4.3, SFC average error is presented for Mach range of 0 to 1.7, for consistency.

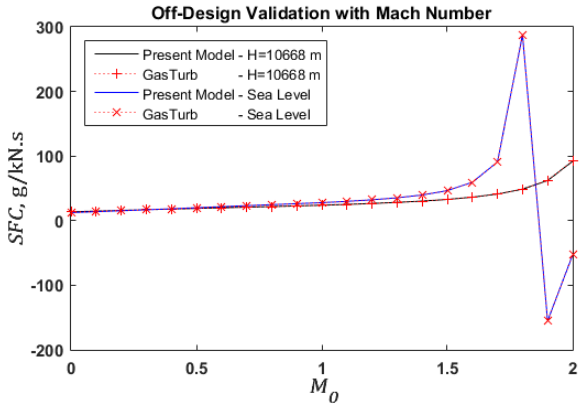

Figure 4.5: Off-design validation of specific fuel consumption, SFC, for given Mach number, M_0.

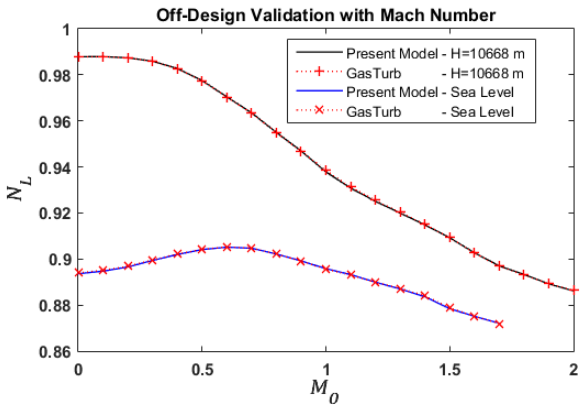

Figure 4.6: Off-design validation of low-pressure relative spool speed, N_L, for given Mach number, M_0.

One of the off-design inputs is the high-pressure turbine inlet temperature, T_{t4}. The same parametric range will be used as for design point validation and the same output results as computed during off-design validation with Mach number (detailed before). Additionally, the high-pressure spool speed, N_H, is also computed. In Figures 4.7 and 4.8, the specific fuel consumption, SFC and the relative spools speeds, respectively, obtained in this off-design model are compared with the results obtained with GasTurb 12 [4]. As previously stated, the calculations are performed for constant $M_0 = 0.8$ and $H = 10668$ m. Average relative errors, compared to [4] results, are given in Table 4.3 (Row #3).

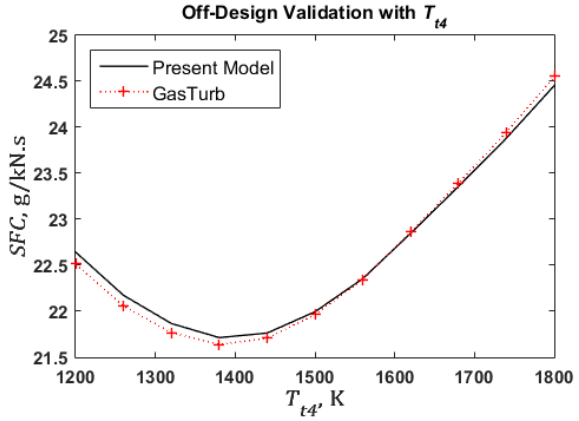

Figure 4.7: Off-design validation of specific fuel consumption, SFC, for given high-pressure turbine inlet total temperature, T_{t4}.

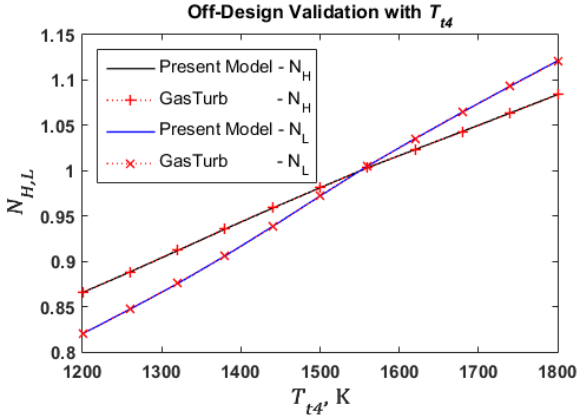

Figure 4.8: Off-design validation of relative spools speeds, N_L and N_H, for given high-pressure turbine inlet total temperature, T_{t4}.

The same procedure, as for the previous parametric analysis, is followed next to validate the model performance with high-pressure relative spool speed, N_H, as off-design input. In Figure 4.9 and Figure 4.10 the same outputs are computed and validated: SFC and N_L (N_H is an input), respectively. N_H is varied from a low value of 0.75 to a high value of 1.1. As with the T_{t4} parametric study, calculations are performed for constant $M_0 = 0.8$ and $H = 10668$ m. Average relative errors, compared to GasTurb 12 [4] results, are given on Table 4.3 (Row #4).

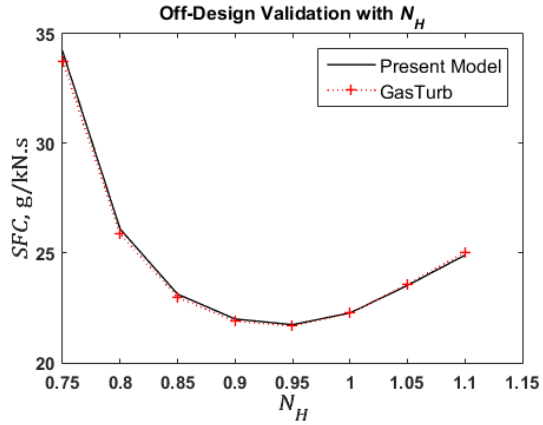

Figure 4.9: Off-design validation of specific fuel consumption, SFC, for given high-pressure relative spool speed, N_H.

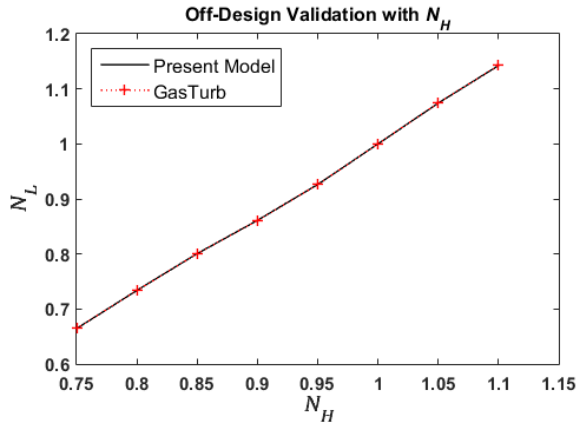

Figure 4.10: Off-design validation of low-pressure relative spool speed, N_L, for given high-pressure relative spool speed, N_H.

Row #	Input Parameters	Average Relative Errors, in %					
		SFC	Ψ	B	T_{t4}	N_L	N_H
1	M_0, at $H = 10668$ m	0.214	0.114	0.015	0.024	0.019	0.000
2	M_0, at sea level	0.101	0.099	0.045	0.028	0.022	0.000
3	T_{t4}	0.236	0.109	0.016	0.000	0.019	0.011
4	N_H	0.559	0.129	0.007	0.054	0.022	0.000

Table 4.3: Off-design average relative errors of results obtained with present model compared to those obtained with a commercial software [4].

4.3 Engine Stationary Performance Results

In this section, performance results will be obtained for design point (Top of Climb), Take-Off, Cruise and for Low Power (60%) operating conditions. In terms of performance parameters, the variation with flight Mach number and during climb at constant speed are also evaluated. All calculations will be based on the design point selection detailed in Table 4.1.

In the present work, it will be considered that 0% and 100% power setting, P, will correspond to low-pressure relative spool speeds, N_L, of 0.5 and 1.05, respectively, assuming direct dependence of power setting on the low-pressure relative spool speed [4].

4.3.1 Top of Climb Flight Condition

For the design point flight condition (Top of Climb), flight takes place at an altitude, H, of 10668 m, a Mach number, M_0, of 0.8 and with a design low-pressure relative spool speed, N_L, of 1 ($P \approx 91\%$). Taking advantage of the present model, validated for the reference fuel (Jet A-1), the specific fuel consumption, SFC, the total thrust F, and the fuel mass flow rate, $\dot{m}_f$, obtained for Top of Climb condition are displayed on Table 4.4, for each of the fuels considered in this study. Additionally, the relative difference of SFC compared with what is obtained with Jet A-1, ΔSFC, in %, is also presented .

Since this corresponds to the design point condition, the bypass ratio, B, high-pressure turbine inlet temperature, T_{t4}, and relative spool speeds, N_L, and N_H, are completely independent of the type of fuel, remaining at the design values of $B = 5.7$, $T_{t4} = 1550$ K and $N_L = N_H = 1$.

Outputs	Jet A-1	GTL	CTL	HEFA R-8	HEFA C.	ATJ-SPK	ATJ-SKA	SIP	CH	HDO-SK	Green Diesel
F, kN	19.76	19.80	19.79	19.80	19.79	19.78	19.75	19.79	19.75	19.80	19.79
$\dot{m}_f$, kg/s	0.440	0.428	0.432	0.432	0.429	0.432	0.437	0.435	0.439	0.442	0.441
SFC, g/kN.s	22.27	21.64	21.82	21.84	21.65	21.82	22.12	21.99	22.21	22.34	22.26
ΔSFC, %		-2.85	-2.03	-1.96	-2.80	-2.03	-0.70	-1.26	-0.30	0.30	-0.05

Table 4.4: Off-design performance results. Top of Climb, TOC (design point).

In the following figure, Figure 4.11, a different analysis is performed, where for the Top of Climb altitude ($H = 10668$ m), the influence of Mach number is analysed. Figure 4.11 presents the increase in specific fuel consumption, SFC (a), and the relative difference of SFC for a given fuel compared to

Jet A-1, ΔSFC (b), with Mach number for all fuels of interest.

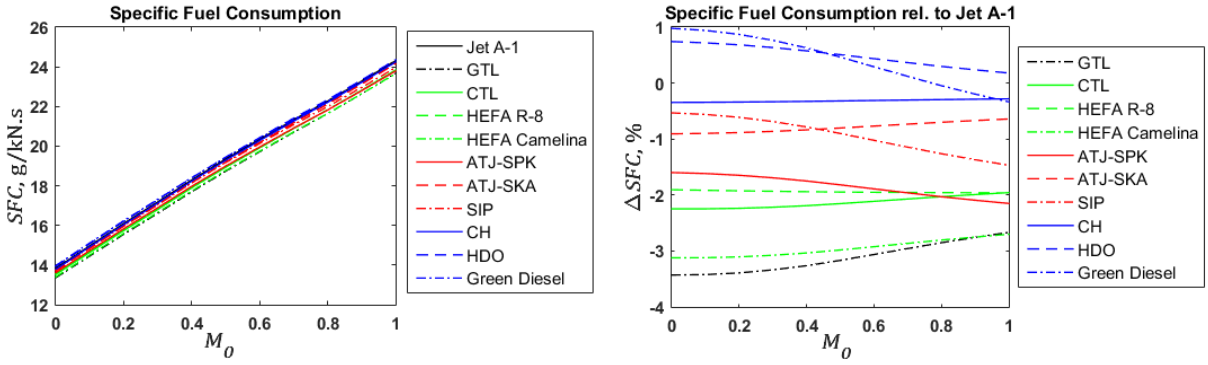

(a) SFC, g/kN.s (b) ΔSFC, %

Figure 4.11: Specific fuel consumption, SFC (a), and relative difference to Jet A-1, ΔSFC (b), with Mach number, at 10668 m of altitude and $N_L = 1$.

4.3.2 Take-Off Condition

An important stage of any aircraft is the Take-Off condition. At this stage, maximum thrust is required and therefore it is important to ensure that any alternative fuel enables the same amount of thrust for a given engine condition (which can be defined by the spools relative speeds). For maximum low-pressure relative spool speed, $N_L = 1.05$ ($P = 100\%$), and considering the worst case scenario with a Take-Off at sea level ($H = 0$ m and $M_0 = 0$), the specific fuel consumption, SFC, the total thrust F, and the fuel mass flow rate, $\dot{m}_f$, computed results for Take-Off condition are displayed on Table 4.5 for each of the fuels considered in this study. Additionally, the relative difference of SFC compared with Jet A-1 is also presented, ΔSFC, in %.

The calculation of the bypass ratio, B, high-pressure turbine inlet temperature, T_{t4}, and relative spool speed, N_H, showcased negligible differences for alternative fuels compared to Jet A-1 (around 0.02% relative errors). At this condition, for all fuels, $T_{t4} = 1702$ K, $N_H = 1.072$ and $B = 5.603$, approximately.

Outputs	Jet A-1	GTL	CTL	HEFA R-8	HEFA C.	ATJ-SPK	ATJ-SKA	SIP	CH	HDO-SK	Green Diesel
F, kN	86.76	86.90	86.86	86.88	86.87	86.83	86.73	86.84	86.74	86.89	86.85
$\dot{m}_f$, kg/s	1.200	1.175	1.181	1.179	1.173	1.173	1.193	1.180	1.197	1.203	1.192
SFC, g/kN.s	13.84	13.53	13.59	13.57	13.50	13.51	13.76	13.58	13.80	13.84	13.72
ΔSFC, %		-2.24	-1.77	-1.91	-2.45	-2.36	-0.55	-1.83	-0.27	0.04	-0.84

Table 4.5: Off-design performance results. Take-Off.

4.3.3 Cruise Flight Condition

For consistency, Cruise flight condition will take place at the Top of Climb altitude and Mach number ($H = 10668$ m and $M_0 = 0.8$) but with a lower low-pressure relative spool speed, based on [22]: $N_L = 0.95$ ($P \approx 82\%$). Taking advantage of the present model, validated for the reference fuel (Jet

A-1), the specific fuel consumption, SFC, the total thrust F, and the fuel mass flow rate, $\dot{m}_f$, obtained for Cruise condition are displayed on Table 4.6 for each of the fuels considered in this study. Additionally, the relative difference of SFC compared with Jet A-1 is also presented, ΔSFC, in %.

For the defined Cruise condition, the bypass ratio, B, high-pressure turbine inlet temperature, T_{t4}, and relative spools speeds, N_L and N_H, are also, approximately, independent of the type of fuel, with values of $B = 5.932$, $T_{t4} = 1462$ K and $N_H = 0.967$ for all fuels.

Outputs	Jet A-1	GTL	CTL	HEFA R-8	HEFA C.	ATJ-SPK	ATJ-SKA	SIP	CH	HDO-SK	Green Diesel
F, kN	17.47	17.51	17.50	17.51	17.50	17.49	17.46	17.50	17.47	17.51	17.50
$\dot{m}_f$, kg/s	0.381	0.370	0.373	0.374	0.370	0.374	0.378	0.378	0.380	0.383	0.383
SFC, g/kN.s	21.80	21.13	21.33	21.37	21.16	21.38	21.63	21.57	21.73	21.89	21.86
ΔSFC, %		-3.07	-2.12	-1.96	-2.93	-1.89	-0.76	-1.03	-0.31	0.42	0.28

Table 4.6: Off-design performance results. Cruise.

4.3.4 Low Power Flight Condition

When analysing the influence of the fuel on the performance of an aero-engine, lower power settings are also relevant. Ground idle and approach conditions, with respective typical thrust setting of 7% and 30% [17], are not analysed with the off-design model. These operating conditions are not analysed with the off-design model due to convergence problems, associated with the high number of iteration variables and iterative guessing of relative spool speeds, with component map reading. A ground idle operating condition will be, however, simulated taking advantage of the transient model, as explained in the next chapter (chapter 5).

In an off-design perspective, to evaluate low power setting influence on the results obtained for each type of fuel, it will be considered a flight condition at $H = 10668$ m and $M_0 = 0.8$ with a power setting of 60%, corresponding to $N_L = 0.83$, referred to as the Low Power condition. This flight condition can be approximated as a flight idle condition. The specific fuel consumption, SFC, the total thrust F, and the fuel mass flow rate, $\dot{m}_f$, obtained for Low Power setting condition are displayed on Table 4.7 for each of the fuels considered in this study. Additionally, the relative difference of SFC compared with Jet A-1 result, ΔSFC, in %, is also presented .

In a similar way to what happened in previous flight conditions (TOC, TO and Cruise), the bypass ratio, B, high-pressure turbine inlet temperature, T_{t4}, and relative spools speeds, N_L and N_H, are also, approximately, independent of the type of fuel, but with values of $B = 6.861$, $T_{t4} = 1222$ K and $N_H = 0.874$ for all fuels.

4.3.5 Climb at Constant Flight Speed

For the range of power setting considered in the present study, relevant flight conditions at steady-state were already analysed: Take-Off, Top of Climb, Cruise (the major portion of an aircraft mission) and Low

Outputs	Jet A-1	GTL	CTL	HEFA R-8	HEFA C.	ATJ-SPK	ATJ-SKA	SIP	CH	HDO-SK	Green Diesel
F, kN	10.50	10.53	10.53	10.53	10.53	10.52	10.50	10.53	10.50	10.54	10.53
$\dot{m}_f$, kg/s	0.236	0.226	0.230	0.232	0.228	0.234	0.233	0.237	0.235	0.239	0.242
SFC, g/kN.s	22.45	21.46	21.85	22.00	21.62	22.20	22.19	22.50	22.36	22.70	22.95
ΔSFC, %		-4.39	-2.67	-2.01	-3.70	-1.10	-1.14	0.25	-0.39	1.12	2.23

Table 4.7: Off-design performance results. Low Power condition ($P = 60\%$).

Power flight. It was, then, considered that, an analysis during the climb portion (from Take-Off to Top of Climb conditions) should be done to verify the influence of altitude. The climb portion will be considered at constant speed, $V = 237.18$ m/s (Top of Climb speed). The engine will operate during climb with a constant low-pressure relative speed of $N_L = 1$.

In Figure 4.12, the specific fuel consumption, SFC (a), and the relative difference of SFC for a given fuel compared to Jet A-1, ΔSFC (b), are presented for a given flight altitude, H. The fact that the flight speed remains constant and altitude is changed implies that the results will differ not only in altitude but in flight Mach number as well.

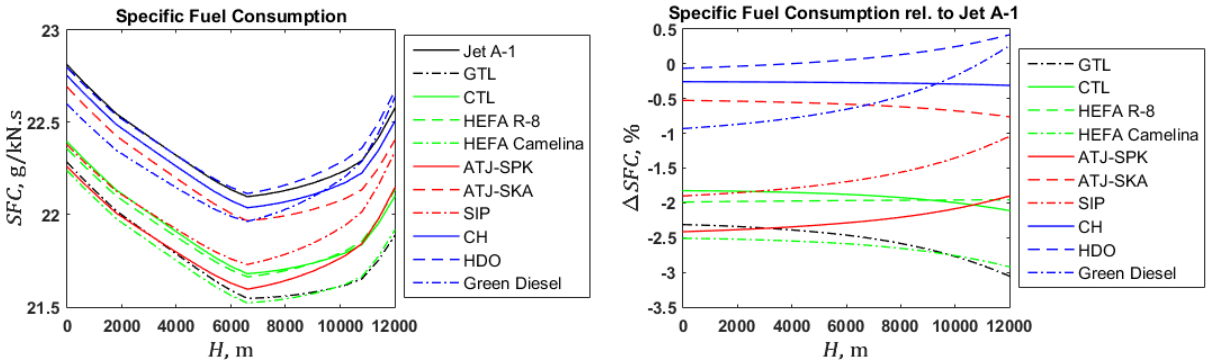

(a) SFC, g/kN.s

(b) ΔSFC, %

Figure 4.12: Specific fuel consumption, SFC (a), and relative difference to Jet A-1, ΔSFC (b), with altitude, during climb (constant speed).

4.3.6 Performance Results for Fuel Blending with Jet A-1

Since most alternative fuels are not eligible to be used as a neat product, it should also be analysed the engine performance results for different than 100% blends (in volume), with Jet A-1. It will be assumed volume blending ratios of 50% for GTL and CTL and HEFA R-8 and Camelina (maximum certified), 30% for ATJ-SPK (maximum certified), 10% for SIP (maximum certified) and Green Diesel (assumed based on high low-temperature viscosity constraint) and 50% for HDO-SK (maximum blend expected). ATJ-SKA and CH, although assumed as possible neat drop-in jet fuels, will also be analysed as 50% blends (the maximum percentage so far approved by the ASTM) with Jet A-1.

The result of this analysis can be observed in Table 4.8, where relative differences of specific fuel consumptions compared with Jet A-1 are presented for the flight conditions analysed in subsections 4.3.1, 4.3.2, 4.3.3 and 4.3.4.

	GTL	CTL	HEFA R-8	HEFA C.	ATJ-SPK	ATJ-SKA	SIP	CH	HDO-SK	Green Diesel
Blend Ratios, Volume %	**50%**	**50%**	**50%**	**50%**	**30%**	**50%**	**10%**	**50%**	**50%**	**10%**
Take-Off	-1.09	-0.87	-0.94	-1.20	-0.71	-0.27	-0.19	-0.14	0.02	-0.09
Top of Climb	-1.43	-1.01	-0.97	-1.39	-0.63	-0.35	-0.15	-0.15	0.13	-0.05
Cruise	-1.56	-1.05	-0.98	-1.45	-0.60	-0.39	-0.13	-0.16	0.19	-0.03
Low Power	-2.30	-1.34	-1.01	-1.86	-0.41	-0.58	-0.04	-0.19	0.51	0.09

Table 4.8: Summary of specific fuel consumption relative differences to Jet A-1, ΔSFC, in %, for off-design calculations with blending of alternative fuels with Jet A-1.

4.3.7 Discussion

In terms of performance, for the flight conditions considered (Take-Off, Top of Climb, Cruise and Low Power flight), in general, all alternative fuels considered showcased similar performance results compared to Jet A-1, with relative variations of specific fuel consumption varying between a minimum of -4.39% and a maximum of 2.23%, occurring at Low Power condition for GTL and Green Diesel burning, respectively. The results presented prove that a turbofan performance may be enhanced with alternative fuels with lower specific fuel consumptions, mostly influenced by higher net heat of combustion values (up to 2.5% increase). The only cases where an alternative fuel (from the ones studied) presents a worse performance than Jet A-1 is for HDO-SK (for all flight conditions), SIP (for Low Power condition) and Green Diesel (for Cruise and Low Power conditions).

In Figure 4.13, one can analyse the influence of power setting on the engine performance for the burning of different fuels (Tables 4.4 to 4.7). It becomes quite clear that fuels such as GTL, CTL, HEFA Camelina and ATJ-SKA, present better performance results for low power conditions (compared to Jet A-1). On the other hand, fuels such as ATJ-SPK, SIP, HDO-SK and Green Diesel, with decrease in power setting, tend to deteriorate the engine performance, when compared with Jet A-1. CH, ATJ-SKA and HEFA R-8 present similar behaviour, compared to Jet A-1, with power setting variation.

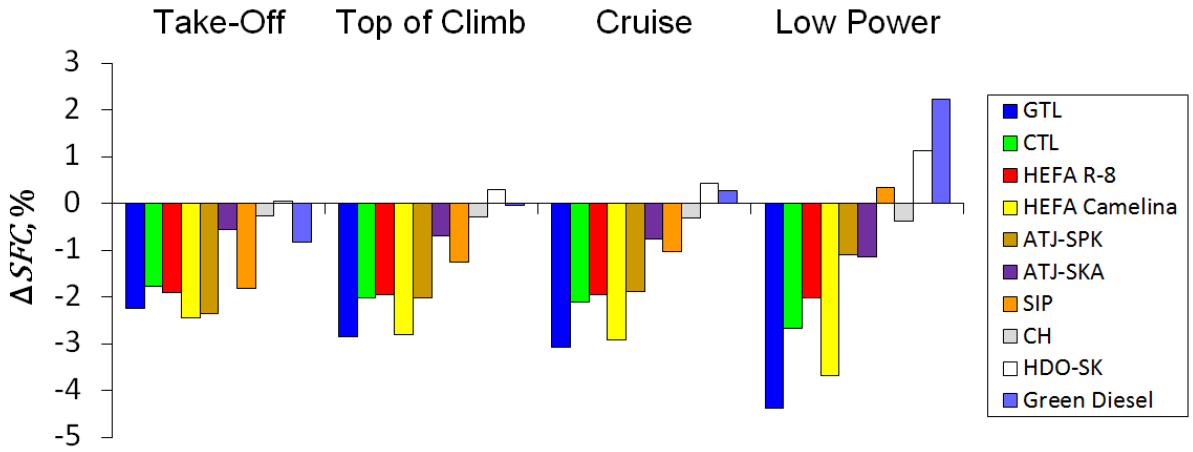

Figure 4.13: Summary of specific fuel consumption relative differences to Jet A-1, ΔSFC, for off-design calculations.

This change in engine performance, compared to Jet A-1, has to do with the quality of fuel atomiza-

tion and fuel evaporation. In the model, for performance calculations, the influence of fuel atomization is quantified during design combustion efficiency calculations. Since, with increase in combustion chamber loading comes a decrease in combustion efficiency, the burning of fuels with worse atomization and evaporation quality may result in worse engine performances for flight conditions requiring lower power settings such as flight idle or ground idle, for example. This is confirmed through the computation of initial mean droplet diameters, D_0, and evaporation constants, λ, for each fuel. In Figures 4.14 and 4.15, the relative differences (to Jet A-1) in % of D_0 and λ, respectively, are presented. Results of Figure 4.15 are obtained considering $H = 10668$ m and $M_0 = 0.8$, with power setting variation.

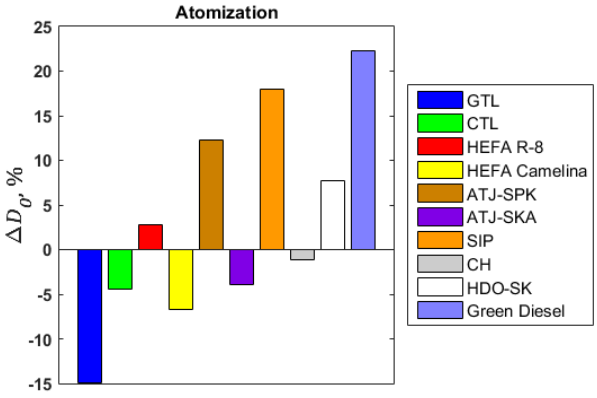

Figure 4.14: Relative difference between mean initial fuel droplet diameters, ΔD_0, of a given fuel compared to Jet A-1.

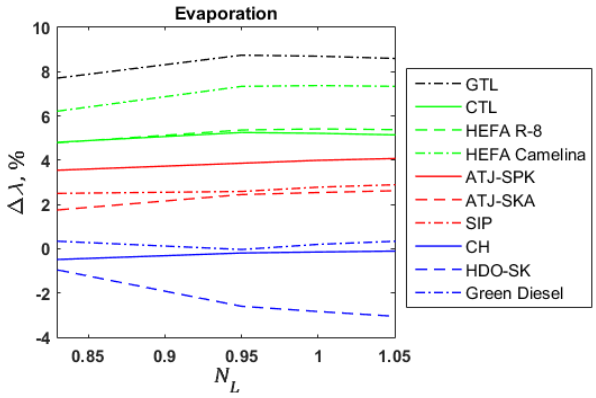

Figure 4.15: Relative difference between fuel evaporation constants, $\Delta\lambda$, of a given fuel compared to Jet A-1.

With computed results of Figures 4.14 and 4.15, it is possible to verify that most alternative fuels present improved evaporation behaviour, mainly a result of typical higher volatility and lower liquid fuel density. The level of atomization differences is highly related with differences in liquid viscosity, where the higher it is its value the worse will be the atomization process. With such results, it becomes clear that atomization shall affect the engine performance in an higher level than the evaporation rate does, even more so, due to the fact that the influence of droplet diameters differences is squared (D^2-Law). This assumption is confirmed through the comparison of design combustion efficiencies, $\eta_{b,R}$, through the design value for Jet A-1 burning, $\eta_{b,R,ref}$, with the calculation of the relative difference $\Delta\eta_{b,R}$, in %, which is presented in Figure 4.16. There, it becomes evident that fuels with worse atomization will induce a worse combustion efficiency.

Recurring to off-design results, for Top of Climb flight level and engine operating condition (Figure 4.11), this assumption is further verified with decrease of specific fuel consumption (compared to Jet A-1) for HDO-SK, Green Diesel, SIP and ATJ-SPK (along with a small decrease for HEFA R-8) with increase in flight Mach number. This was expected since with increase of Mach number, the loading of the combustion chamber decreases.

The climb, at constant speed and TOC engine operating condition, enables one to conclude that all alternative fuels (except for HDO-SK) would enhance the engine performance with decreases in specific fuel consumption up to 2.8 % in the range of altitudes from sea level to cruise level.

The analysis of the engine performance at all flight conditions considered for different blending ratios,

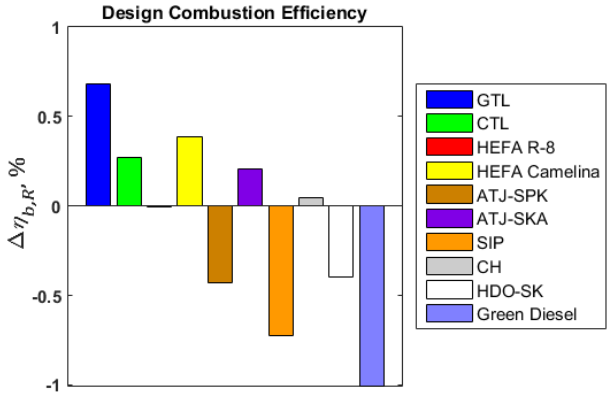

Figure 4.16: Relative difference between design combustion efficiencies of a given fuel compared to Jet A-1, $\Delta\eta_{b,R}$, in %.

as summarized in Table 4.8, shows reduced deviations in performance results, as expected, maintaining an overall improvement of the specific fuel consumption, ΔSFC, in up to 2.30 %.

Comparing present model performance results with results obtained in reference [51], it is possible to compare the burning of HEFA Camelina. For 100% power condition, according to [51], a decrease of 5.26% in fuel mass flow rate compared with Jet A-1 is verified. In the present work, for Take-Off, a lower decrease of 2.25% is verified. For another alternative fuel, CH, performance results may be obtained in reference [52]. Where, for Take-Off condition, a decrease in specific fuel consumption of 0.20% is verified, in the present model, a decrease of 0.29% is verified. Taking into account that, for the comparisons referenced, the fuels considered present slight differences in fuel properties and the engines present different efficiencies and pressure ratios, it is considered that the performance results are satisfactory, confirming an accurate estimation of fuel impacts on the performance of a turbofan.

It should also be highlighted that, parameters such as the high-pressure turbine inlet temperature, the bypass ratio or the high-pressure spool relative speed, for each steady-state condition analysed, presented similar values, with relative differences below 0.1% (somehow independent of the type of fuel). This result is justified, mainly, due to the fact that by designating the engine operating condition through the input of a low-pressure spool speed, N_L, the main differences for each fuel will be the amount of fuel required to be burnt to allow reaching the designated engine operating condition.

As previously discussed, in the present work, a typical low overall pressure ratio commercial turbofan is analysed, so that the evaporation model implemented remains valid (steady-state). If, in the design point selection, a value of high-pressure compressor pressure ratio, $\pi_{HPC,R}$, was assumed with an higher value of 15 (resulting in an engine with an overall pressure ratio of 30) and the inlet mass flow rate, $\dot{m}_R$, increased to a value of 400 kg/s, relative differences in specific fuel consumption remain almost unchanged. In fact, for this case, relative variations of specific fuel consumption varying between a minimum of -4.90% and a maximum of 2.18%, for Low Power flight would be obtained (highly similar to original respective values of -4.39% and 2.23%). This result proves that with the present model, for a low overall pressure ratio turbofan, performance estimations computed may be considered as reasonable estimations for a wide range of turbofans, for different fuel burning.

Chapter 5

Transient Performance Results

In the present chapter, transient/dynamic results will be presented. The transient engine model, described in chapter 3, is first validated for a conventional fuel employed. As with off-design results validation, the validation process for transient conditions is also based on results obtained with GasTurb 12 [4]. With the modelling properly validated it is possible to compute transient behaviour of the given aero-engine for the burning of different types of fuels.

Since the following transient analyses occur for short periods of simulation time (10 to 20 s), emissions results will not be thoroughly analysed, the focus will be mainly to verify if there is any substantial transient (operational) performance response difference for different fuels. All transient analyses detailed in the present chapter were performed for time steps, Δt, of 0.1 s.

For dynamic/transient analyses, which depends on the design point calculations and initial flight condition ($t = 0$ s) defined with an off-design calculation, 2 engine parameters are additionally required, i.e. the low-pressure and high-pressure spools polar moments of inertia, I_L and I_H, respectively. Based on the development presented on reference [50], these parameters were selected as reasonable values of 2 kg.m^2 and 3 kg.m^2, respectively (as in Table 5.1).

Transient Parameters
$I_L = 2$ kg.m^2
$I_H = 3$ kg.m^2

Table 5.1: Spools polar moments of inertia selection.

As previously stated, taking advantage of the transient model, a ground idle steady-state operating condition will be analysed (subsection 5.2.4).

5.1 Engine Transient Model Validation

The present transient model, enables the user to define 3 different time-dependent inputs: power setting, P_{demand}, in % (directly related with $N_{L,demand}$), fuel mass flow rate, $\dot{m}_{f,demand}$ or total thrust, F_{demand}. For fuel mass flow demand validation, low demand (deceleration) and high demand (acceleration) are

analysed. For the power setting input with elapsed time, a deceleration transient response will be verified for the Proportional (P), the Proportional-Integral (PI) and the Proportional-Derivative (PD) controllers. The total thrust demand is validated by comparison between steady-state off-design model results with the transient model outputs when a steady-state condition is reached.

The first transient condition to be validated represents a low fuel mass flow demand (a deceleration). For a Top of Climb (TOC) initial flight condition and a step decrease of fuel mass flow input to a value of 0.2 kg/s, results of specific fuel consumption, SFC, specific thrust, Ψ, low-pressure and high-pressure relative spool speeds, N_L and N_H respectively, bypass ratio, B, and high-pressure turbine inlet temperature, T_{t4}, are computed with elapsed time and compared to the results obtained with GasTurb 12 [4]. The comparison of SFC and N_L results are presented in Figures 5.1 and 5.2, respectively. Additional results are presented in Appendix B (Figure B.8).

Excellent results compared to those obtained with GasTurb 12 [4] are verified, with maximum relative errors ranging from 1.098% to 9.118%, typically near the simulation time when the given demand is changed, and mean relative errors ranging from 0.201% to 0.960%, for all outputs considered in the validation process.

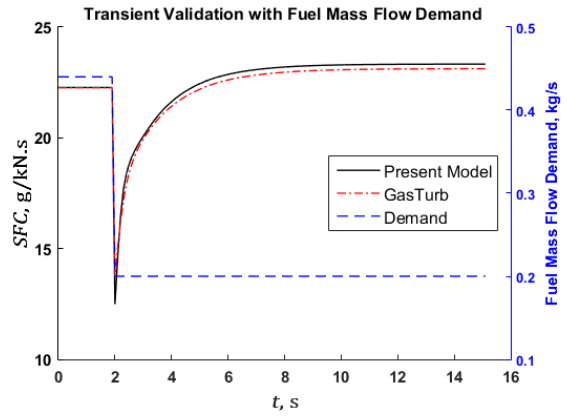

Figure 5.1: Transient validation of specific fuel consumption, SFC, with time, t, for $\dot{m}_{f,demand}(t)$ input (deceleration).

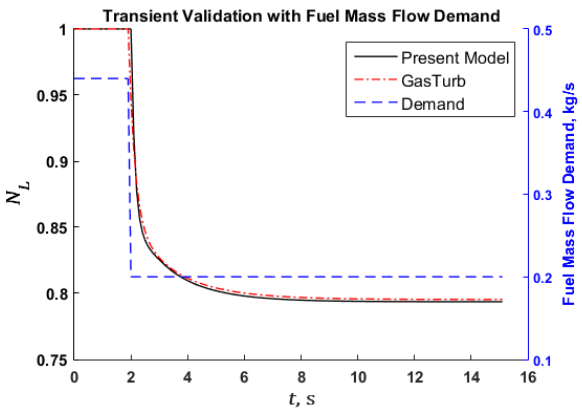

Figure 5.2: Transient validation of low-pressure relative spool speed, N_L, with time, t, for $\dot{m}_{f,demand}(t)$ input (deceleration).

As easily depicted from figures analyses, the transient response for fuel mass flow deceleration is validated for the present case and it is assumed that therefore for other initial conditions, the same type of results is obtained. To verify if the same type of results is obtained for an acceleration, the same procedure was followed for initial altitude of $H = 5000$ m, flight Mach number of $M_0 = 0.6$, high-pressure relative spool speed of $N_H = 0.95$ and transient step fuel mass flow input to a value of 0.7 kg/s. Similar results are obtained through comparison with GasTurb 12 [4] results, with maximum relative errors ranging from 0.810% to 8.338% and mean relative errors ranging from 0.036% to 0.137%, for all outputs considered in the validation process.

Considering the aircraft flying at Top of Climb condition, the transient response based on a change in power setting, defined as P, and directly related with the low-pressure relative spool speed, N_L, will be evaluated. In this validation process, from a power setting of approximately 91%, corresponding to

$N_L = 1$, a step decrease in power to 75% ($N_L = 0.9125$) is demanded and the same output results as before computed. Considering a Proportional controller (with $C_P = 0.1$), specific fuel consumption, SFC, specific thrust, Ψ, low-pressure and high-pressure relative spool speeds, N_L and N_H respectively, bypass ratio, B, and high-pressure turbine inlet temperature, T_{t4}, results are computed with elapsed time and compared with results obtained with GasTurb 12 [4]. The comparison of SFC and N_L results is presented in Figures 5.3 and 5.4, respectively. Additional results are presented in Appendix B (Figure B.9).

The comparison of results obtained with present model with those obtained with GasTurb 12 [4] showcase good agreement with maximum relative errors ranging from 0.234% to 0.734% and mean relative errors ranging from 0.078% to 0.328%, for all outputs considered.

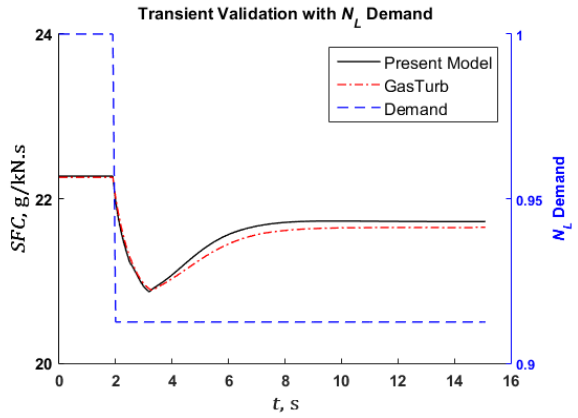

Figure 5.3: Transient validation of specific fuel consumption, SFC, with time, t, for $N_{L,demand}(t)$ input (deceleration with proportional control).

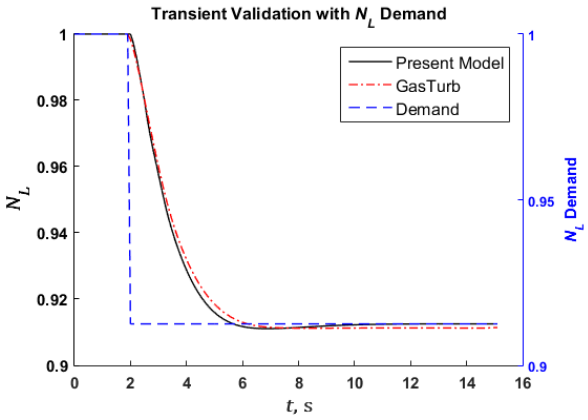

Figure 5.4: Transient validation of low-pressure relative spool speed, N_L, with time, t, for $N_{L,demand}$ input (deceleration with proportional control).

Although, for simplicity and concision, transient results will only be obtained for Proportional controller employment, Integral and Derivative controllers should also be validated. To do so, the same initial conditions are considered (TOC) and P demand (from about 91% to 75%), a Proportional-Integral controller is analysed with gains of $C_P = 0.1$ and $C_I = 0.05$ and a Proportional-Derivative controller is analysed with gains of $C_P = 0.1$ and $C_D = 0.05$. The present model results and comparison with GasTurb 12 [4] results are presented in Appendix B (Figures B.10 and B.11, respectively).

The total thrust demand, $F_{demand}(t)$, transient simulation is validated based on the fact that, for a given step demand in total thrust, a steady-state condition is eventually reached. In fact, for a Low Power initial condition, with a step demand of thrust to 15 kN, after 20 s (simulation time), a stabilized low-pressure relative spool speed of 0.9051 is obtained (for combustion of Jet A-1). For an off-design calculation with the same value of steady-state low-pressure relative spool speed, a total thrust of 15.0005 kN is computed, which validates the transient modelling for thrust demand.

5.2 Transient Model Results

Transient performance analyses of an aero-engine fuelled with different types of fuels are important in order to verify if for a given rapid change of engine demand, either a steep deceleration or acceleration, the performance of the engine and flight safety is not compromised. To evaluate this situation the 3 types of time-dependent inputs of the present model will be considered. Given the types of inputs available, two types of decelerations are considered (fuel mass flow and power setting decrease) and a type of acceleration is considered (thrust demand increase).

5.2.1 Fuel Mass Flow Rate Demand

For user-defined fuel mass flow rate demand, a deceleration engine response is to be considered. It follows that for an initial time interval (between 0 and 5 s), an initial fuel mass flow rate is demanded (close to the initial conditions for all fuels). Then, for the last 10 seconds of the simulation, a step decrease of fuel mass flow rate demand is defined and the results processed.

The initial flight condition will be the Top of Climb condition, with $H = 10668$ m, $M_0 = 0.8$ and $N_L = 1$. For the first 5 seconds of the simulation, a fuel mass flow of 0.43 kg/s is demanded. Then a steep step decrease in fuel mass flow will be prompted to a value of 0.3 kg/s, as depicted in Figure 5.5.

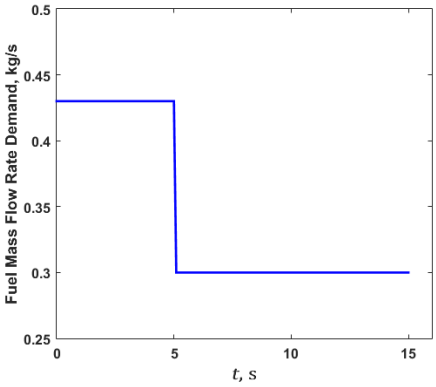

Figure 5.5: Fuel mass flow demand, $\dot{m}_{f,demand}(t)$, with elapsed time, t (deceleration).

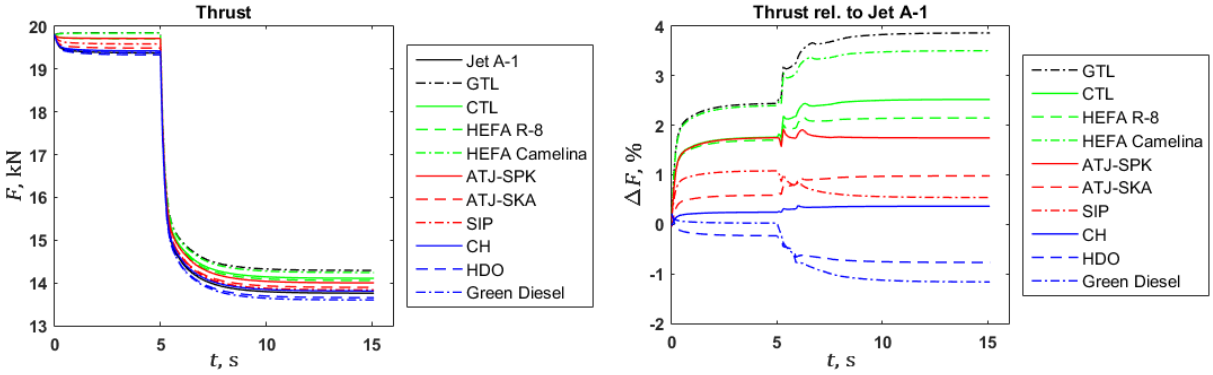

(a) F, kN (b) ΔF, %

Figure 5.6: Total thrust, F (a), and relative difference, ΔF (b), with time, t, for $\dot{m}_{f,demand}(t)$ input (deceleration).

Through transient simulation, results of specific fuel consumption, SFC, low and high-pressure relative spool speeds, N_L and N_H, bypass ratio, B, high-pressure turbine inlet temperature, T_{t4} and total thrust, F, with time, t, are readily computed. In Figure 5.6 (a), thrust results, F, are plotted for each fuel burning. The relative difference between computed F for a given fuel compared to what would be obtained with Jet A-1 fuelling, ΔF in %, is also presented in Figure 5.6 (b). Since fuel mass flow rate is being demanded, the impact of the burning of different fuels on performance may be verified with the computation of thrust. Additional results are presented in Appendix B (Figures B.12 and B.13).

5.2.2 Power Setting Demand

In the present model, transient deceleration may also be simulated taking into account the direct relation of power setting, P, in %, with the low-pressure relative spool speed, N_L. With an initial Top of Climb flight condition, with H = 10668 m, M_0 = 0.8 and N_L = 1, after 2 seconds, a step decrease of N_L is performed, demanding a value of 0.9125 (P =75%), as presented in Figure 5.7. A Proportional controller with gain of C_P = 0.1 is used in this transient analysis.

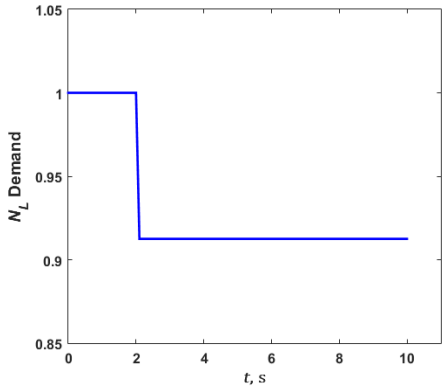

Figure 5.7: Power setting demand through low-pressure relative spool speed, $N_{L,demand}(t)$, with elapsed time, t (deceleration).

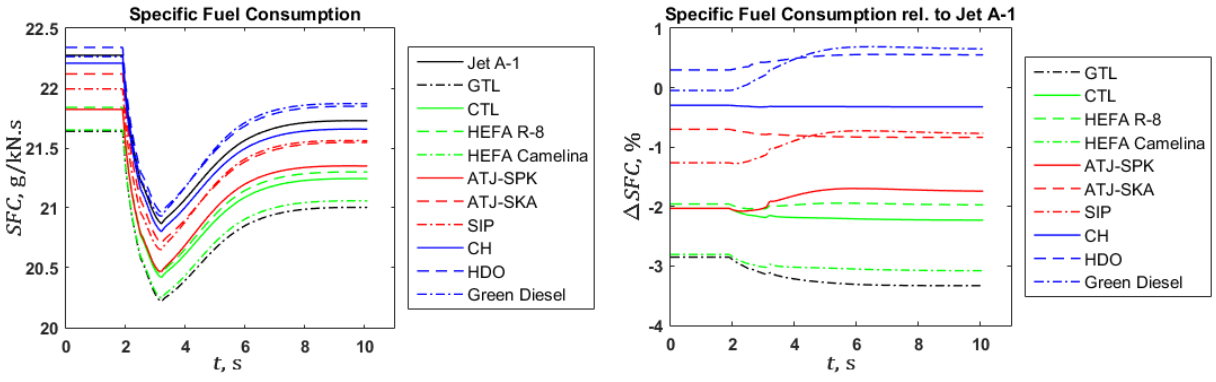

(a) SFC, g/kN.s (b) ΔSFC, %

Figure 5.8: Specific fuel consumption, SFC (a), and relative difference, ΔSFC (b), with time, t, for $N_{L,demand}$ deceleration (C_P = 0.1).

In Figure 5.8 (a), specific fuel consumption results, SFC, are plotted for each fuel burning. The relative difference between computed SFC for a given fuel compared to what would be obtained with

Jet A-1 fuelling, ΔSFC, in %, is also presented in Figure 5.8 (b). For parameters such as the total thrust, F, low and high-pressure relative spool speeds, N_L and N_H, bypass ratio, B and the high-pressure turbine inlet temperature, T_{t4}, differences are negligible and therefore not presented. In fact, the maximum relative deviation to results with Jet A-1 occurred for thrust calculation, with a minimum of -0.247% and maximum of 0.253%. Due to negligible total thrust variations, it follows that fuel mass flow rate results with time are similar to those presented for SFC (Figure 5.8).

5.2.3 Total Thrust Demand

As analysed in chapter 4, at steady-state flight conditions, for several types of power settings, the difference of total thrust for any given alternative fuel (from the ones studied) compared to what is obtained with Jet A-1 is typically negligible. In fact for all off-design calculations performed, maximum absolute (in N) and relative thrust deviations (in %) of 140 N and 0.32%, respectively, were obtained. Nevertheless, with the total thrust demand input of the present model, it will be considered the case where for an initial time interval it is demanded a certain total thrust (in the vicinity of the initial condition for most fuels) followed by a steep step increase in total thrust demanded.

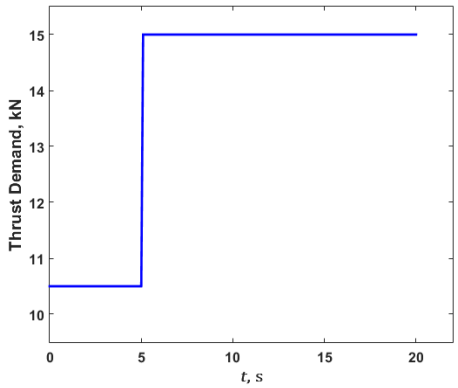

Figure 5.9: Thrust demand, $F_{demand}(t)$, with elapsed time, t (acceleration).

In order to achieve so, during the first 5 seconds of the simulation, a total thrust demand of 10.5 kN is applied. Then, for the remaining 15 seconds, 15 kN are demanded, as presented in Figure 5.9. As with the power setting input, a Proportional controller is considered, but with a gain of $C_P = 0.02$. The initial flight condition is the same as for Low Power steady-state condition (see subsection 4.3.4), with $H = 10668$ m, $M_0 = 0.8$ and a power setting of 60%, corresponding to $N_L = 0.83$.

Given the fact that a total thrust input is demanded, only fuel mass flow rates, $\dot{m}_f$ (a), and respective relative differences to Jet A-1, $\Delta\dot{m}_f$ (b), are presented in Figure 5.10. For parameters such as the total thrust, F, low and high-pressure relative spool speeds, N_L and N_H, bypass ratio, B and the high-pressure turbine inlet temperature, T_{t4}, differences are negligible and therefore not presented. In fact, the maximum relative deviation to results with Jet A-1 occurred for high-pressure turbine inlet temperature with a maximum of 0.45% and for thrust calculation with a minimum of -0.12%. Due to negligible total thrust variations, it follows that results of ΔSFC with time are similar to those presented for $\Delta\dot{m}_f$ (Figure 5.10).

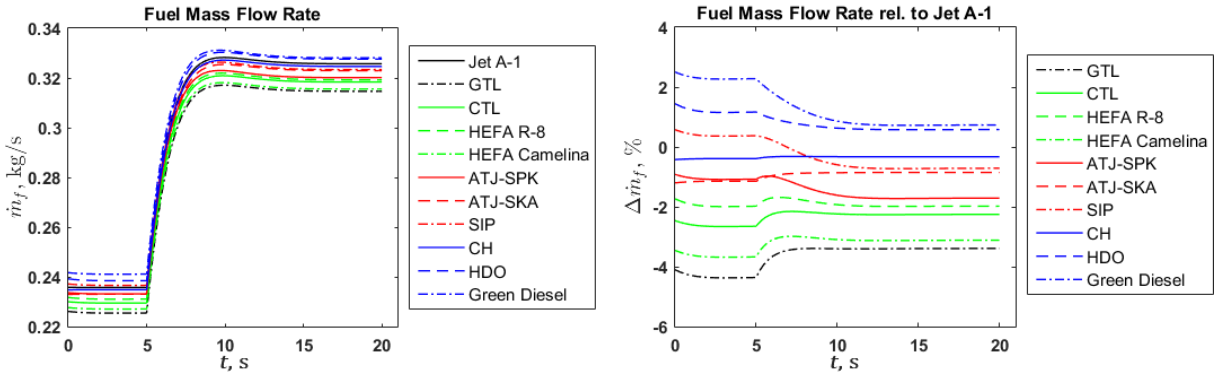

(a) $\dot{m}_f$, kg/s (b) $\Delta\dot{m}_f$, %

Figure 5.10: Fuel mass flow rate, $\dot{m}_f$ (a), and relative difference, $\Delta\dot{m}_f$ (b), with time, t, for $F_{demand}(t)$ acceleration ($C_P = 0.02$).

5.2.4 Ground Idle Operating Condition

As previously stated, the off-design model implemented in the present work presents convergence errors near surge conditions, mainly due to the highly iterative nature of the process, with 7 iteration variables, and required guessing of relative spool speeds. With the implemented transient model, the user may "slowly" demand a low value of N_L until a steady-state condition is reached. Through transient analyses with each time step a new set of initial iteration variables is defined. The biggest drawback is the computation time required.

For sea level and $M_0 = 0$, and a power setting of 10% considered ($N_L = 0.555$), a reasonable Ground Idle condition is simulated. In Table 5.2, specific fuel consumption results, relative to Jet A-1, are presented. These results follow the pattern of performance changes with power setting discussed in subsection 4.3.7. It should be highlighted that comparing off-design calculations for Jet A-1 with GasTurb 12 [4], and results of T_{t4} and $\dot{m}_f$ obtained with this transient simulation, relative errors of 0.03% and 0.57%, respectively are obtained, which validates the reached steady-state condition assumption.

Outputs	GTL	CTL	HEFA R-8	HEFA C.	ATJ-SPK	ATJ-SKA	SIP	CH	HDO-SK	Green Diesel
ΔSFC, %	-4.73	-2.81	-2.02	-3.89	-0.87	-1.23	0.73	-0.40	1.31	2.80

Table 5.2: Specific fuel consumption relative differences to Jet A-1, ΔSFC, for a Ground Idle operating condition, at sea level, $M_0 = 0$ and for $P = 10\%$.

5.2.5 Discussion

The main objective of the simplified aero-engine turbofan transient/dynamic performance implementation was to analyse if, through the burning of different fuels, flight safety might be jeopardised. This analysis was performed taking advantage of the different types of transient-specific types of input modelled, with change in fuel mass flow rate, change in low-pressure relative spool speed and different total thrust demands. These conditions were simulated in the present work since an aircraft must be capable, in adverse situations, of performing steep accelerations or decelerations.

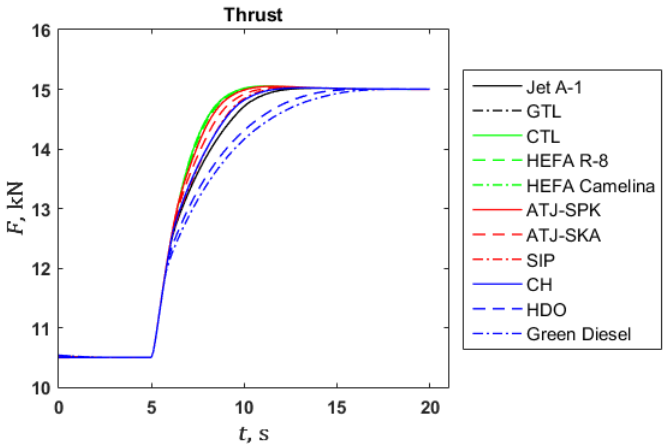

Figure 5.11: Thrust, F, with elapsed time, t, ($F_{demand}(t)$ acceleration), with fuel mass flow rate control.

Taking into account all transient results presented, it becomes clear that for the flight manoeuvres considered and modelling of the engine, the burning of any of the alternative fuels considered in this study present qualitatively the same type of transient performance. In fact, for all conditions analysed, if the time required for achieving a difference of 0.5% compared with the final result (steady-state result) is calculated, only differences in the order of accuracy of the time step utilised (0.1 s) are verified. Meaning that only advances and delays of 0.1 s are typically verified, to achieve a certain steady-state condition.

Although all transient results presented lead to an overall assumption that the different types of fuels studied would perform equally in transient operations, when compared with Jet A-1, it should be highlighted that due to the simplified modelling and taking into account the high similarities in fuel heating values, these results were expected. Given the model implemented, one could additionally verify if, for a given acceleration operation, and fuel mass flow rate limited (based on Jet A-1 results), any fuel could present itself as a dangerous option.

Through a simplified analysis, and defining a fuel mass flow corrected, $\dot{m}_f/p_{t3}$, of 0.93 kg/s.MPa, for the thrust demand acceleration of subsection 5.2.3, additional results are obtained. The limit value for fuel mass flow corrected of 0.93 kg/s.MPa is based on the achieved fuel mass flow corrected for Jet A-1 of approximately 0.92 kg/s.MPa. In Figure 5.11, the transient thrust response is presented.

With this analysis, where fuel mass flow rate is controlled, real engine behaviour may be greatly approximated. It follows that, from Figure 5.11 analysis, through burning of fuels such as HDO-SK and Green Diesel, significant delays in transient response may be verified. When computed the required time for reaching a total thrust below a 2% difference from the desired output, it is possible to conclude that an increase in required time of 1.8 s and 2.7 s is verified, for HDO-SK and Green Diesel, respectively, when compared with Jet A-1. Since between total thrust demand of 10.5 kN to 15 kN, 15 simulation seconds are elapsed, HDO-SK and Green Diesel delays would represent 12% and 18% delays, respectively, of the total transient response. On the other hand, the remaining alternative fuels present better results with improvements in up to 1.6 s. In conclusion, given the results verified and presented in Figure 5.11, experimental transient simulations must be performed for different types of power settings in order to assess the effect a given fuel may have on transient responses.

Chapter 6

Pollutant Emissions Results

In this chapter, pollutant emissions (NO_x, CO, UHC and soot) results will focus on most of the flight conditions considered in chapter 4, such as, Top of Climb, Take-Off and Cruise, as well as a relevant steady-state operating condition considered in chapter 5, that is, the Ground Idle operating condition.

Typically, with increase in power setting, pollutant emissions of NO_x and soot increase, while of CO and UHC decrease. In fact, for a given flight altitude and Mach number ($H = 0$ m and $M_0 = 0$), and varying the low-pressure relative spool speed, N_L, from 0.83 to 1.05, NO_x, CO and UHC emission indexes are computed and this assumption is confirmed, as presented in Figure B.14 (Appendix B). Although not clear in Figure B.14, UHC emissions decrease from 1.43 g/kg to 0.56 g/kg. The presented results are average values for a residence time of 4 ms (which will be assumed for Jet A-1 NO_x, CO and UHC emissions calculations). It should also be noted that for such conditions, soot concentration, S, also increases with increase in power, as expected (from a value of 0.0006 to 0.1098 mg/kg).

It should be pointed out that results concerning pollutant emissions of NO_x, CO and UHC are presented as average results with maximum and minimum values (error bars) defined, ranging from infinitely fast evaporation to evaporation requiring the combustion residence time (of one of the fuels). To distinguish different evaporation behaviours, different markers will be plotted. In cases where the difference of pollutant emitted for burning of a given fuel relative to Jet A-1 increases with increase in evaporation time, an "x" marker is presented. Otherwise, a circle, "o", is considered. It follows that, the infinitely fast evaporation ($\tau_e = 0$ s) condition corresponds to a minimum computed difference in pollutant emissions, ΔEI_i, when a marker "x" is plotted and to a maximum computed difference for a "o" marker.

6.1 NO_x Pollutant Emissions

As detailed in section 3.10, NO_x emissions will be quantified through the computation of respective emission indexes (equation 3.89), based on reference values estimated for Jet A-1 and time of evaporation variation considered. Then, relative differences of NO_x emissions, ΔEI_{NO_x}, in %, for the burning of a certain fuel compared with Jet A-1, may be computed. Results of this procedure are presented in Figure 6.1, for steady-state flight conditions: Take-Off (a), Top of Climb (b), Cruise (c) and Idle (d) conditions.

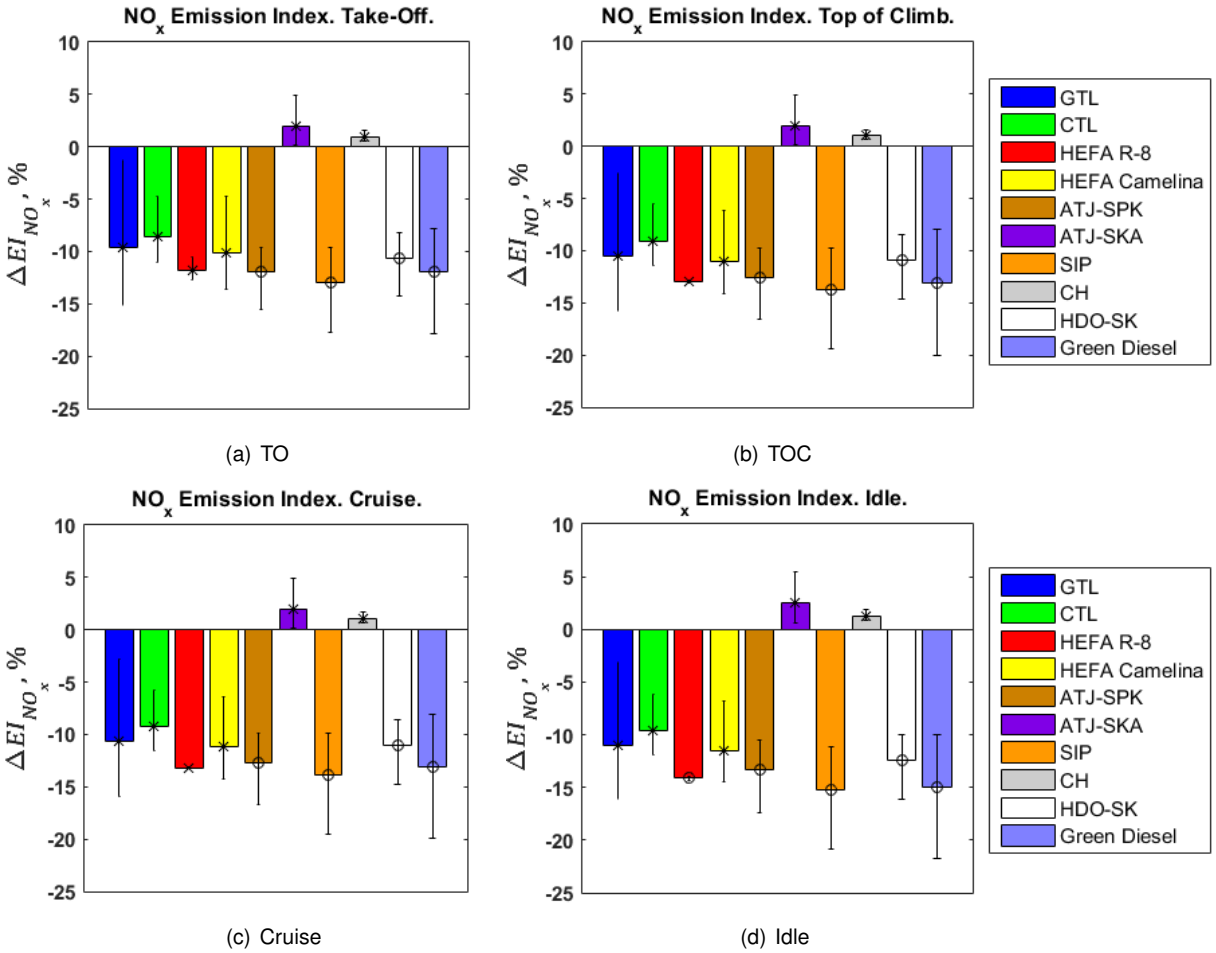

(a) TO (b) TOC

(c) Cruise (d) Idle

Figure 6.1: ΔEI_{NO_x} for Take-Off (a), Top of Climb (b), Cruise (c) and Idle (d) conditions.

6.2 CO Pollutant Emissions

As detailed in section 3.10, CO emissions will be quantified through the computation of respective emission indexes (equation 3.90), based on reference values estimated for Jet A-1 and time of evaporation variation considered. Then, relative differences of CO emissions, ΔEI_{CO}, in %, for the burning of a certain fuel compared with Jet A-1, may be computed. Results of this procedure are presented in Figure 6.2, for steady-state flight conditions: Take-Off (a), Top of Climb (b), Cruise (c) and Idle (d) conditions.

6.3 UHC Pollutant Emissions

UHC emissions will be quantified through the computation of respective emission indexes (equation 3.91), based on reference values estimated for Jet A-1 and time of evaporation variation considered. Then, relative differences of UHC emissions, ΔEI_{UHC}, in %, for the burning of a certain fuel compared with Jet A-1, may be computed. Results of this procedure are presented in Figure 6.3 (page 74), for steady-state flight conditions: Take-Off (a), Top of Climb (b), Cruise (c) and Idle (d) conditions.

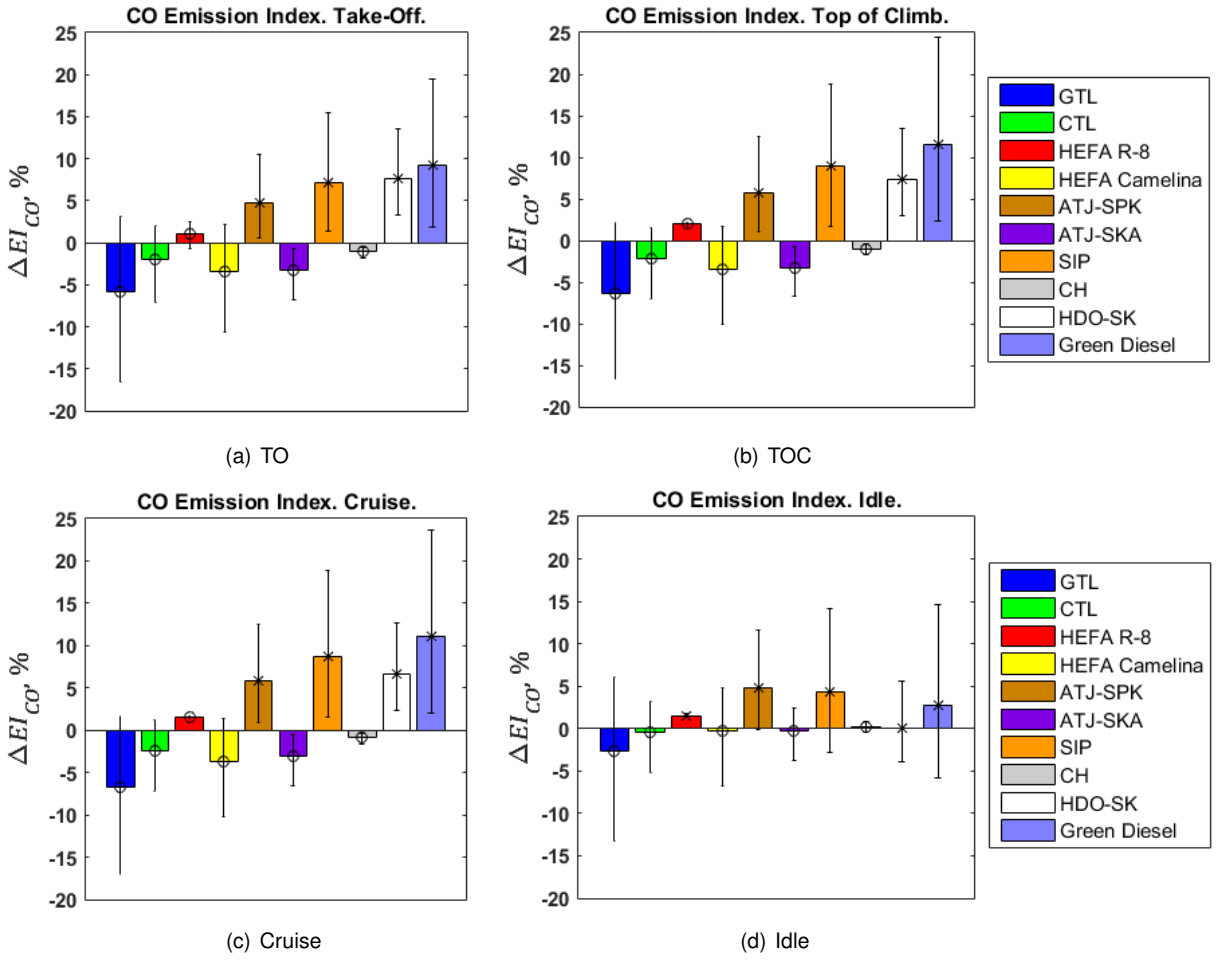

(a) TO (b) TOC

(c) Cruise (d) Idle

Figure 6.2: ΔEI_{CO} for Take-Off (a), Top of Climb (b), Cruise (c) and Idle (d) conditions.

6.4 Soot Pollutant Emissions

Taking into account the model for estimation of soot exhaust gas concentration, S in mg/kg, soot pollutant emissions are directly assessed in this study (equation 3.92). In Figure 6.4 (page 75), soot pollutant emissions of a given fuel relative to those estimated for Jet A-1, ΔS, in %, are given for steady-state flight conditions: Take-Off (a), Top of Climb (b), Cruise (c) and Idle (d) conditions.

6.5 Pollutant Emissions Results for Fuel Blending with Jet A-1

Since most alternative fuels are not eligible to be used as a neat product, it should also be analysed the pollutant emissions results for different than 100% blends, with Jet A-1. The result of this analysis can be observed in Figure 6.5. This analysis is focused only in the Cruise condition due to its bigger influence in the overall mass pollutant emissions compared to other portions of a commercial aircraft's mission. The blending volumes considered are the same as in subsection 4.3.6 (page 76).

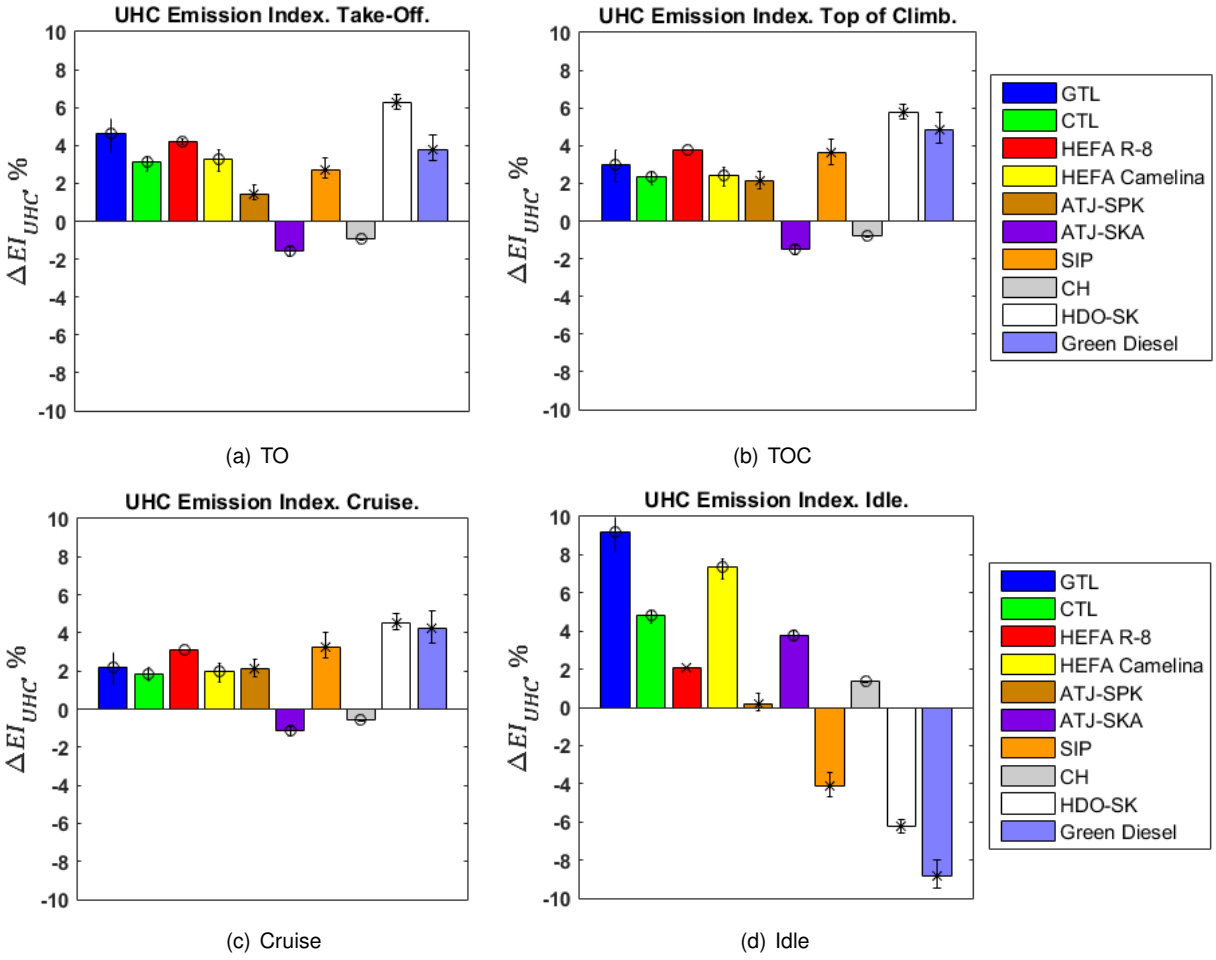

(a) TO (b) TOC

(c) Cruise (d) Idle

Figure 6.3: ΔEI_{UHC} for Take-Off (a), Top of Climb (b), Cruise (c) and Idle (d) conditions.

6.6 Discussion

In this section, the computed relative differences in pollutant emissions for the burning of alternative fuels when compared with Jet A-1 will be analysed. The main objective of the discussion of results obtained will be to verify if emitted oxides of nitrogen, NO_x, carbon monoxides, CO, unburned hydrocarbons, UHC, and soot (smoke), S, present high discrepancies and if the burning of alternative fuels results in better overall environmental performance.

Due to the nature of the present study of pollutant emissions of NO_x, CO and UHC, where a reference residence time is fixed and evaporation times varied, comparison between the different fuels studied shall take into account the influence of the relationship between residence and evaporation times.

Through the analysis of oxides of nitrogen emissions, it is possible to conclude that, although the pollutant emissions estimations are only based on empirical correlations, the results obtained give sufficient margins to readily assume that alternative fuels burning may reduce, considerably, NO_x pollutant emissions. With minimum average ΔEI_{NO_x} ranging from approximately -8% to -14%, most of the fuels studied are eligible candidates for a decrease in NO_x emissions. Exception being ATJ-SKA and CH, which are the fuels with similar composition compared with Jet A-1. The fact that the increase in NO_x emissions occurs only in a range of 1% to 2%, for ATJ-SKA and CH, and taking into account the mini-

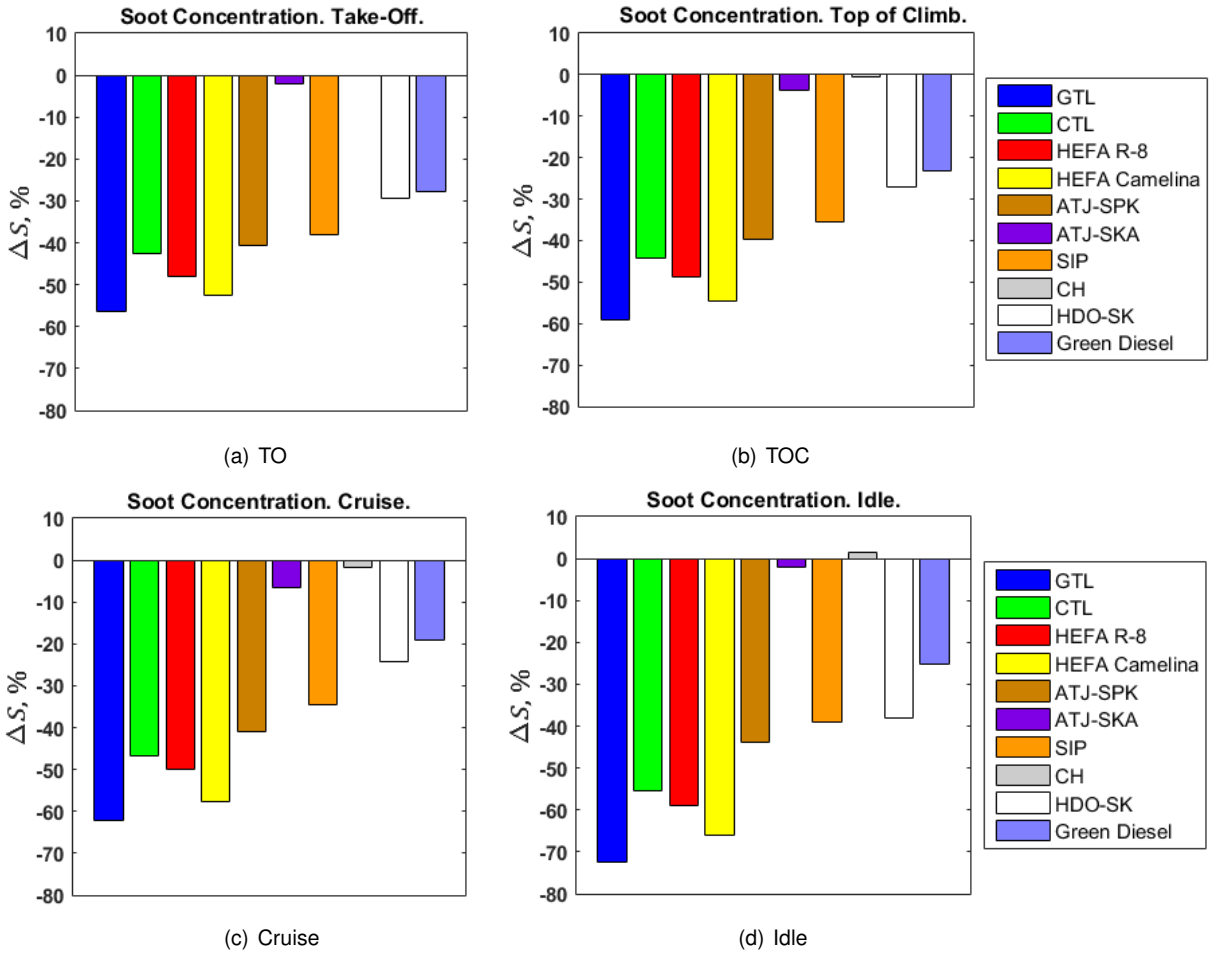

(a) TO (b) TOC

(c) Cruise (d) Idle

Figure 6.4: ΔS for Take-Off (a), Top of Climb (b), Cruise (c) and Idle (d) conditions.

mum values (infinitely fast evaporation, for such fuels), one can assume that the burning of this types of fuel will have negligible effects compared to what would be obtained with Jet A-1. The actual differences of NO_x pollutant emissions, with change in fuel, is mostly based on stoichiometric flame temperature differences, where lower temperatures are preferred. This fact justifies the low dependence on power setting verified.

For the case of carbon monoxide pollutant emissions, in general, for the flight conditions considered, fuels such as GTL, CTL, HEFA Camelina, ATJ-SKA and CH present negative average ΔEI_{CO} values, in up to 6.8% (for GTL during cruise). The remaining fuels studied, HEFA R-8, ATJ-SPK, SIP, HDO-SK and Green Diesel present worse results, with up to 11.5% increase in CO pollutant emissions (maximum average value for Green Diesel, for Top of Climb).

Additionally, one can conclude that typically, and inversely to what happens for pollutant NO_x emissions, GTL, CTL, Camelina, ATJ-SKA and CH fuels, with decrease of overall residence time (for example, for primary zones with lower volumes), tend to present better CO results compared with Jet A-1. Fuels like ATJ-SPK, SIP, HDO-SK and Green Diesel have an opposite impact. For the case of HEFA R-8, residence and evaporation dependence is lower and, for most flight conditions, an increase in CO may be assumed.

In fact, the analysis of the results concerning CO pollutant emissions clearly indicates that the latter

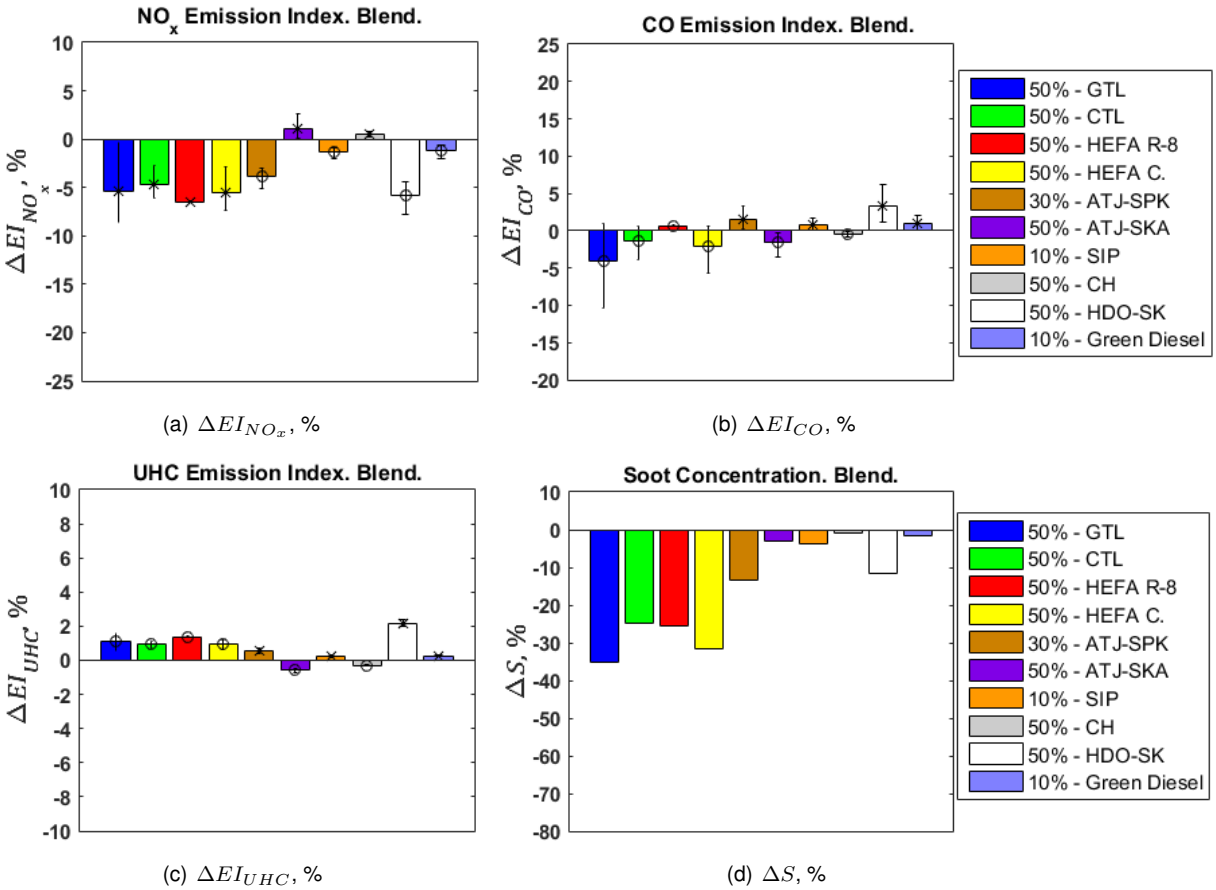

(a) ΔEI_{NO_x}, %

(b) ΔEI_{CO}, %

(c) ΔEI_{UHC}, %

(d) ΔS, %

Figure 6.5: ΔEI_{NO_x} (a), ΔEI_{CO} (b), ΔEI_{UHC} (c) and ΔS (d) for Cruise condition and fuel mixtures.

fuels referenced will most likely induce higher pollutant emissions of CO, since even minimum values are still positive increments on pollutant emissions (only exception for SIP, HDO-SK and Green Diesel, for Idle operating condition and HEFA R-8 for Take-Off condition).

During the analysis of unburned hydrocarbons, UHC, pollutant emissions, it should not be forgotten the fact that the complexity of the inherent estimation brings additional inaccuracies to the results obtained. For all flight conditions, the majority of fuels showcase an increase in UHC pollutant emissions, when compared to Jet A-1. The only exceptions occurring for ATJ-SKA and CH for Cruise, Top of Climb and Take-Off conditions and SIP, HDO-SK and Green Diesel for Idle operating condition. Taking into account the error bars plotted (accounting for evaporation influence), and comparing to NO_x and CO estimations, it is possible to verify that with the present estimation the influence of residence and evaporation times is somewhat negligible.

In the steady-state calculations performed, with low-pressure spool speed as input (defining power setting), the mixing pollutant term presents negligible differences between different fuels. In fact, for Take-Off (for example), a maximum relative deviation in combustor pressure loss of 0.02% (corresponding to 16.48 Pa absolute difference) is verified. Therefore, main differences in pollutant emissions are due to reaction and evaporation (and atomization).

With that in mind, the results obtained for CO are justified since, with lower difference between residence and evaporation times, fuels with better atomization will tend to present improved pollutant

emissions results. The opposite occurring for NO_x emissions, where a lower residence time is preferred. In the case of UHC estimations, the same applies as for CO, but, due to the lesser influence of residence and evaporation times in the comparison of different fuels results, the main differences verified have to do with the reaction term (accounted for flame temperatures in correlations).

In Figure 6.6, the adiabatic flame temperature (here generically referenced to as T_{flame}) is presented for each fuel (a) as well as the relative difference of each alternative fuel flame temperature compared with Jet A-1 (b), for an inlet temperature of 750 K, inlet pressure of 1 MPa and equivalence ratio, Φ (Appendix C, equation C.13), ranging from 0.8 to 1.2.

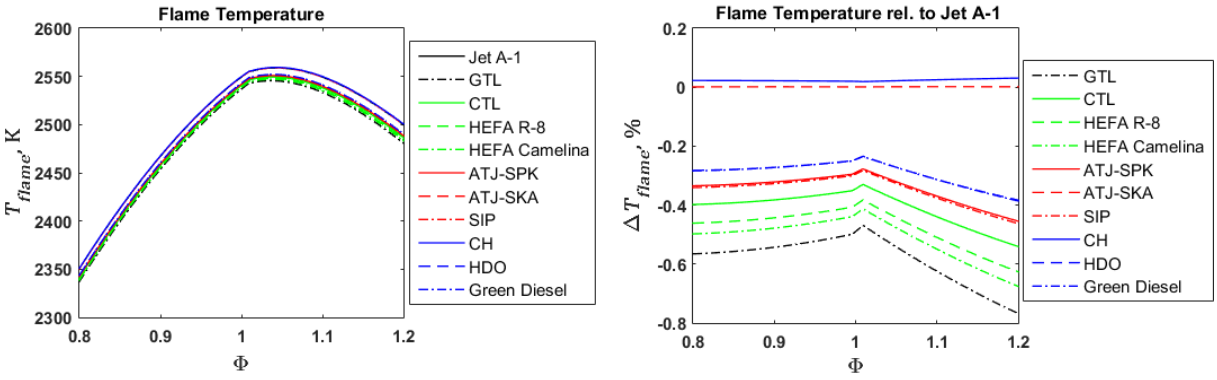

(a) T_{flame}, K (b) ΔT_{flame}, %

Figure 6.6: Flame temperature, T_{flame} (a), and relative difference to Jet A-1, ΔT_{flame} (b), with equivalence ratio, Φ.

From the analysis of Figure 6.6, one can conclude that for the same inlet conditions (temperature and pressure) and same equivalence ratios (dependent on stoichiometric conditions of each fuel), all fuels considered present lower temperatures ranging from -0.24% to -0.76% (for the equivalence ratio range considered). This fact does not justify the discussed results of CO and UHC emissions, where, for example, Green Diesel at Idle condition decrease unburned hydrocarbons emissions. Basically, remembering the steady-state (operational) performance analysis (Table 5.2), at Idle condition, fuels like Green Diesel present worse specific fuel consumption when compared with remaining fuels. Which for similar thrust deployed (as for Low Power flight condition), results in increased fuel mass flow rate and increased fuel-air ratio (negligible differences in air mass flow rate).

At this stage, it should be noted the fact that, in higher power setting conditions (TO, TOC and Cruise), the fuel-air mixture in the primary zone, for the engine analysed, is rich, $\Phi_{pz} > 1$, whereas for Idle operating condition is lean $\Phi_{pz} < 1$. As presented in Figure 6.6, for lean fuel-air mixtures, with increase in fuel-air ratio, there is, typically, an increase in flame temperature, which is preferred for CO and UHC pollutant emissions. In conclusion, the results discussed for CO and UHC are highly influenced by the effect of the fuel-air ratio which is highly dependent on the operating condition and on the type of engine.

In the present study, soot emissions were also studied. For most fuels and all flight conditions, decreases in soot concentration in up to -72% (GTL for idle operating condition) when compared with Jet A-1 were obtained. Therefore, although the approximations used may not be considered as the most

accurate possible (e.g. the secondary-zone average temperature estimation) and the correlation used regarded only as an approximation of results (soot formation is highly complex), it is safe to assume that most alternative fuels may decrease substantially the concentration of soot (smoke) emitted in the exhaust gas, based on the results of the present work. This assumption is corroborated with the fact that the decrease in aromatic content typically results in lower soot emissions [3].

The emissions calculation for different than neat blends, for Cruise condition, resulted in expected results, where typically all absolute deviations from Jet A-1 decreased. Even for blends of 50% (in volume) with Jet A-1, fuels such as GTL, CTL, HEFA R-8 and HEFA Camelina continue to exhibit good results in respect to NO_x and soot emissions, mainly. With NO_x emissions decrease in the order of 5% and soot in the order of 20%.

The influence of the type of engine on pollutant emissions may be evaluated as in subsection 4.3.7. With this type of analysis, where results accuracy may be reduced due to non-steady-state evaporation, it is possible to conclude that although quantitative differences may arise in pollutant emissions results, the general trend is similar to what was obtained for the type of engine considered in this study (see Figure B.15, presented in Appendix B).

To verify the validity of pollutant emissions results, obtained in the present work, comparison with different results available in the literature should be performed. For HEFA Camelina, for example, in reference [51], for a take-off condition, a decrease in NO_x emissions of 9.4% is verified. In the present work, HEFA Camelina presented an average decrease of 10.1%. For a different HEFA Camelina [53] and for cruise conditions, a decrease of 14.3% of NO_x and increase of 0.4% of CO pollutant emissions are verified. In the present work, similar results would be obtained considering conditions where evaporation is neglected, with a decrease of 14.3% of NO_x and an increase of 1.3% of CO computed. According to reference [54], for a cruise condition, 6% decrease in NO_x and 58% decrease in S would be verified for a given GTL compared with JP-8 (identical to Jet A-1); CO and UHC were not reported due to impossibility of detection (low concentrations). In the present work, a 62% decrease in soot concentration and an average NO_x decrease of 10.7 % is verified. In [55], an HEFA-SPK type of fuel (from Neste Oil) was burned an results of UHC, CO, NO_x and smoke pollutant emissions plotted for a given thrust ratio, where it becomes evident that, with increase in thrust, UHC emissions range from approximately 4% increase to negligible differences at 100% of thrust. Additionally, in the same study, one can confirm that at take-off (assuming 100% thrust) an approximate decrease of 10% in NO_x emissions is verified.

Since engines, flight conditions considered and fuel properties vary in the literature, the comparison of present model results with selected results obtained in the literature (experimental and analytical), indicates that the present model showcases overall reasonable and satisfactory results.

In conclusion, for the fuels of interest considered, taking into account NO_x pollutant emissions differences computed, computed differences in CO emissions with increase in evaporation time required (or decrease in residence time), differences in soot emissions obtained and decrease in CO_2 and H_2O with decrease in fuel consumption, fuels such as GTL, CTL and HEFA Camelina may induce a generalized improvement on the environmental performance of the engine, neglecting the impact of UHC emissions, and even considering the maximum certified blending ratios.

Chapter 7

Conclusions

7.1 Achievements

In order to evaluate the operational performance and environmental impact of alternative jet fuel burning, a simple aero-engine turbofan 0-D model was implemented. Enabling the study of different operating conditions, a design and off-design model was developed, along with a transient model. All models were validated with excellent agreement, through comparison of performance results for burning of Jet A-1 obtained with present models and with GasTurb 12. Then, modelling approaches such as fuel properties estimations, evaporation and flame temperature models, as well as performance and pollutant emissions results with different fuels, obtained in the present work, were compared with selected results from the literature. This validation process showed an overall good agreement, confirming the present model validity for performance and pollutant emissions calculations for a typical two-spool turbofan and combustion of different fuels.

From the analysis of the performance results obtained in the present work, it is possible to conclude that most of the alternative fuels considered may not only satisfy typical flight performance demands but improve them as well, when compared with conventional jet fuel burning. In this regard, the net heat of combustion of the fuel plays a major part, along with the atomization and evaporation quality, with influence mainly visible with variation of power setting. In an overall perspective, fuels that may be viewed as better options compared with the conventional jet fuel are FT-SPK, HEFA-SPK, ATJ-SPK, ATJ-SKA and CH fuels. Additionally, a decrease in fuel consumption results in a satisfactory decrease in greenhouse gases emissions such as CO_2 and H_2O (products of complete combustion).

Although small discrepancies were verified in all transient simulations performed, fuel impact on transient response was evidenced when considering fuel mass flow rate control. In fact, through a simplified analysis of fuel mass flow rate maximum injection control, it was possible to verify that for a certain steep acceleration demand, fuels, such as HDO-SK or Green Diesel, may required a significant additional time to achieve demanded operating conditions, which may compromise flight safety.

In an environmental analysis, through NO_x, CO, UHC and soot pollutant emissions estimations, from empirical correlations, despite its high complexity, it was possible to conclude that alternative fuels

properties will mostly influence soot emissions. In fact, for all flight conditions, typically, the burning of alternative fuels will result in a considerable decrease in soot emissions. This is mostly associated with the lower aromatic content of the alternative fuels considered.

For the case of NO_x pollutant emissions, excluding fuels such as ATJ-SKA and CH, overall good results, with decrease in pollutant emissions, are verified. These results are mostly a function of the differences in stoichiometric flame temperature. For CO pollutant emissions, on the other hand, typically a result of incomplete combustion, an higher atomization and evaporation dependence is verified. It follows that, with a decrease in combustion residence time (ideal for NO_x emissions), fuels, such as GTL, CTL, HEFA Camelina, ATJ-SKA and CH, may reduce considerably CO pollutant emissions in a wide range of flight conditions due to associated lower evaporation time required. With UHC pollutant emissions calculations it is possible to conclude that they are mostly influenced by the fuel-air ratio employed, affecting the flame temperature calculation (with lower temperatures preferred).

Finally, taking into account all results computed, in terms of performance and pollutant emissions, it is possible to conclude that there is already a wide range of alternative jet fuel possibilities that can improve the results currently obtained with a conventional jet. In fact, taking into account fuel properties specification limits, it is possible to conclude that the blending of fuels will still, mostly, be associated with an improvement in performance and pollutant emissions. Fuels such as ATJ-SKA and CH, studied in the present work, showcase similar results and in some situations improved results in comparison with Jet A-1, which is regarded as a significant step towards neat alternative fuel implementation.

With overall improvements in performance and pollutant emissions results, and better life cycle CO_2 emissions, it is confirmed that a worldwide use of sustainable alternative fuels will ultimately be dependent on an economical perspective. With five types of alternative fuels production pathways approved for use in commercial flights, as a blend, and proven technical feasibility of a wide range of alternative fuels, as in the present work, the sustainable future of the aviation industry is considered as secured and shall be only dependent on the costs of fuels and support given by the policymakers towards the sustainable alternative fuels pathway growth.

7.2 Future Work

For a further development of the present work, the author considers that the technical departments where improvements can be performed would mostly be relative to fuel properties, the evaporation model and transient combustion.

The accuracy of results could be significantly enhanced if all fuel relevant properties were experimentally analysed for a given fuel sample, including pressure and temperature dependence. Given inherent limitations of the steady-state evaporation model, incorporation of a more robust evaporation model, considering transient behaviour, would increase the range of overall pressure ratios valid for accurate results. Finally, the author considers that, a transient combustion model accounting for fuel effects could enhance the quality of transient response comparison.

Bibliography

[1] International Civil Aviation Organization, *ICAO Environmental Report 2013, Aviation and Climate Change*, 2013.

[2] International Air Transport Association, *IATA Sustainable Aviation Fuel Roadmap*, 1st Edition, 2015.

[3] Lefebvre, A., and Ballal, D., *Gas Turbine Combustion: Alternative Fuels and Emissions*, 3rd Edition, CRC Press, 2010.

[4] Kurzke, J., *GasTurb 12: Design and Off-Design Performance of Gas Turbines*, GasTurb GmbH, 2015.

[5] Air Transport Action Group, "Reducing Emissions from Aviation Through Carbon Neutral Growth from 2020", Working Paper developed for the 38th ICAO Assembly, 2013.

[6] International Air Transport Association, *Fact Sheet - Alternative Fuels*, 2015.

[7] Radich, T., "The Flight Paths for Biojet Fuel", EIA Working Paper Series, 2015.

[8] International Air Transport Association, *IATA 2014 Report on Alternative Fuels*, 9th Edition, 2014.

[9] Brown, N., "FAA Alternative Jet Fuels R&D Update", CLEEN Consortium Meeting, 19 November 2014.

[10] Coordinating Research and Council, "Handbook of Aviation Fuel Properties", 3rd Edition, CRC Report No. 635, 2004.

[11] Lefebvre, A., "Fuel Effects on Gas Turbine Combustion", Report AFWAL-TR-83-2004, 1983.

[12] Odgers, J., and Kretschmer, D., *Gas turbine fuels and their influence on combustion*, ABACUS PRESS, 1986.

[13] Sousa, J. M. M., "Aircraft Emissions - MEAer 2013/2014", Emissions Lectures, Aerospace Engineering, Instituto Superior Técnico, 2013.

[14] Walsh, P., and Fletcher, P., *Gas Turbine Performance*, 2nd Edition, Blackwell Science, 2004.

[15] Bräunling, W., *Flugzeugtriebwerke - Grundlagen, Aero-Thermodynamik, Ideale und reale Kreisprozesse, Thermische Turbomaschinen, Komponenten, Emissionen und Systeme*, 4th Edition, Springer-Verlag, 2015.

[16] Chin, J., and Lefebvre, A., "Steady-State Evaporation Characteristics of Hydrocarbon Fuel Drops", *AIAA Journal*, 21(10), 1437-1443, 1983.

[17] International Civil Aviation Organization, *Environmental Protection - Annex 16, Volume II to the Convention of International Civil Aviation: Aircraft Engine Emissions - Amendment 7*, 3rd Edition, 17 November 2011.

[18] Rizk, N., and Mongia, H., "Emissions Predictions of Different Gas Turbine Combustors", AIAA Paper 94-0118, 1994.

[19] Cohen, H., Rogers, G., and Saravanamuttoo, H., *Gas Turbine Theory*, 4th Edition, Longman Group Limited, 1996.

[20] NATO, *Performance Prediction and Simulation of Gas Turbine Engine Operation for Aircraft, Marine, Vehicular, and Power Generation*, Report RTO-TR-AVT-036, 2007.

[21] The MathWorks®, Inc., *MATLAB® Primer R2015a*, 2015.

[22] Stevenson, J., and Saravanamuttoo, H., "Simulating Indirect Thrust Measurement Methods for High-Bypass Turbofans", *Journal of Engineering for Gas Turbines and Power*, 117(1), 38-46, 1995.

[23] Mattingly, J., *Elements of propulsion: Gas Turbines and Rockets*, 2nd Edition, AIAA Education Series, American Institute of Aeronautics and Astronautic, 2006.

[24] Gaudet, S., *Development of a Dynamic Modeling and Control System Design Methodology for Gas Turbines*, Master Thesis, Carleton University, 2007.

[25] Rahman, N., and Whidborne, J., "Real-Time Transient Three Spool Turbofan Engine Simulation: A Hybrid Approach", *Journal of Engineering for Gas Turbines and Power*, 131(5), 051602-1:8 (8 pages), 2009.

[26] Zilhão, L., *Early-Stage Design Optimization of a Low NO_x Emissions Turbofan at Off-Design Operating Conditions*, Master Thesis, Instituto Superior Técnico, 2014.

[27] Chandrasekaran, N., and Guha, A., "Study of Prediction Methods for NO_x Emission from Turbofan Engines", *Journal of Propulsion and Power*, 28(1), 170-180, 2012.

[28] Zschocke, A., Scheuermann, S., and Ortner, J., "High Biofuel Blends in Aviation (HBBA)", Lufthansa and WIWeB Interim Report ENER/C2/2012/420-1, 2015.

[29] Lew, L., and Biddle, T., "Evaluation of Amyris Direct Sugar to Hydrocarbon (DSHC) Fuel", CLEEN Program, Pratt & Whitney, Report DOT/FAA/AEE/2014-07, 2014.

[30] SkyNRG, "Technology Section", Accessed at 25 February 2016, <www.skynrg.com/technology-section/>, 2013.

[31] Torres, J., "Impact of Alternative Fuels Present in Airports on Aircraft Rescue and Firefighting Response", Federal Aviation Administration Report DOT/FAA/TC-14/22, 2014.

[32] Csonka, S., "Alternative Aviation Fuels - Status in the US", CAAFI - CORE-JetFuel Cooperation Workshop, Alexandria, Virginia, 28 April 2016.

[33] Faaij, A., and Dijk, M., "White Paper on Sustainable Jet Fuel: Rationale for sustainable aviation fuel", Utrecht University and SkyNRG, 2012.

[34] Güell, B., Bugge, M., Kempegowda, R., George, A., and Paap, S., "Benchmark of conversion and production technologies for synthetic biofuels for aviation", SINTEF Report Version 2, 2012.

[35] Wang, W., and Tao, L., "Bio-jet fuel conversion technologies", *Renewable and Sustainable Energy Reviews*, 53, 801-822, 2016.

[36] Mawhood, R., Cobas, A., and Slade, R., "Establishing a European renewable jet fuel supply chain: the technoeconomic potential of biomass conversion technologies", Imperial College London Report, RenJet Project, 2014.

[37] GEVO, "ASTM Completes Revision of Standard Specification", Accessed at 5 May 2016, <http://ir.gevo.com/phoenix.zhtml?c=238618&p=irol-newsArticle&ID=2156242>, 2016.

[38] Cortright, R., Dally, B., Kenney, K., Thompson, D., and Ginestra, C., "Virent is Replacing Crude Oil.", CAAFI SOAP-Jet Webinar, 21 March 2014.

[39] Holladay, J., "Jet fuel advances in bio-oil and alcohol upgrading", CORE-JetFuel: Sustainable alternative aviation fuels workshop, 1 June 2015.

[40] Rumizen, M., "Certification-Qualification Breakout Session", FAA/CAAFI, 28 January 2014.

[41] U.S. Energy Information Administration, "Petroleum & other Liquids. Data: Prices", Accessed at 15 June 2016, <https://www.eia.gov/petroleum/data.cfm#prices/>, 2016.

[42] Wauquier, J., *Petroleum Refining. Volume 1. Crude Oil. Petroleum Products. Process Flowsheets*, Editions Technip, 1995.

[43] Riazi, M., *Characterization and Properties of Petroleum Fractions*, 1st Edition, American Society for Testing and Materials (ASTM), 2005.

[44] Gülder, Ö. L., "Flame Temperature Estimation of Conventional and Future Jet Fuels", *Journal of Engineering for Gas Turbines and Power*, 108, 376-380, 1986.

[45] Law, C. K., "Recent advances in droplet vaporization and combustion", *Progress in Energy and Combustion Science*, 8, 171-201, 1982.

[46] Kadoya, K., Matsunaga, N., and Nagashima, A., "Viscosity and Thermal Conductivity of Dry Air in the Gaseous Phase", *Journal of Physical and Chemical Reference Data*, 14(4), 947-970, 1985.

[47] Givler, S., and Abraham, J., "Supercritical Droplet Vaporization and Combustion Studies", *Progress in Energy and Combustion Science*, 22(1), 1-28, 1996.

[48] Ghassemi, H., Baek, S., and Khan, Q., "Experimental Study on Evaporation of Kerosene Droplets at Elevated Pressures and Temperatures", *Combustion Science and Technology*, 178(9), 1669-1684, 2006.

[49] Meier, N., "Civil Turbojet/Turbofan Specifications", Accessed at 22 February 2016, <http://www.jet-engine.net/civtfspec.html>, 2005.

[50] Soon, L., "Two Combustor Engine for Military Applications", PhD Thesis, Cranfield University, Department of Power and Propulsion, 2009.

[51] Lokesh, K., Sethi, V., Nikolaidis, T., Goodger, E., and Nalianda, D., "Life cycle greenhouse gas analysis of biojet fuels with a technical investigation into their impact on jet engine performance", *Biomass and Bioenergy*, 77, 26-44, 2015.

[52] Lew, L., and Biddle, T., "Evaluation of ARA Catalytic Hydrothermolysis (CH) Fuel", CLEEN Program, Pratt & Whitney, Report DOT/FAA/AEE/2014-08, 2014.

[53] Mazlan, N., Savill, M., and Kipouros, T., "Evaluating NO_x and CO emissions of bio-SPK fuel using a simplified engine combustion model: A preliminary study towards sustainable environment", *Proceedings of the Institution of Mechanical Engineers Part G: Journal of Aerospace Engineering*, 1-7, 2016.

[54] Timko, M., Yu, Z., Onasch, T., and Wong, H., et al., "Particulate Emissions of Gas Turbine Engine Combustion of a Fischer-Tropsch Synthetic Fuel", *Energy and Fuels*, 24(11), 5883-5896, 2010.

[55] International Coordinating Council of Aerospace Industries Associations, ”Impact of alternative fuels on aircraft engine emissions”, Conference on Aviation and Alternative Fuels, Rio de Janeiro, November 2009.

[56] Gleason, C., Oller, T., Shayeson, M., and Bahr, D., ”Evaluation of Fuel Character Effects on J79 Engine Combustion System”, DTIC Report AFAPL-TR-79-2015, 1979.

[57] Grout, M., and Salaün, P., *Instrumentation Industrielle. Spécification et installation des capteurs et vannes de régulation*, 4th Edition, Dunod, 2015.

[58] Bessee, G., Hutzler, S., and Wilson, G., ”Propulsion and power rapid response Research and Development (R&D) support. Delivery order 0011: Analysis of synthetic aviation fuels”, DTIC Report AFRL-RZ-WP-TR-2011-2084, 2011.

[59] Brankovic, A., Ryder, R., Hendricks, R., and Huber, M., ”A Step Towards CO_2-Neutral Aviation”, Report NASA/TM-2008-214998, National Aeronautics and Space Administration, 2008.

[60] Zhang, C., Hui, X., Lin, Y., and Sung, C., ”Recent development in studies of alternative jet fuel combustion: Progress, challenges, and opportunities”, *Renewable and Sustainable Energy Reviews*, 54, 120-138, 2016.

[61] Hui, X., Kumar, C., Sung, C., Edwards, T., and Gardner, D., ”Experimental studies on the combustion characteristics of alternative jet fuels”, *Fuel*, 98, 176-182, 2012.

[62] Parkash, S., *Refining Processes Handbook*, Elsevier, 2003.

[63] Weisser, K., and Turgeon, R., ”90/10 JP5/Synthesized iso-paraffin specification and fit-for-purpose test results”, NAVAIR SYSCOM Report 441/14-010, 2014.

[64] Shukla, R., Naveen, A., Singh, G., and Kirti, S., ”Surface Tension of Binary Liquid Mixtures at 298.15, 303.15 and 313.15 K”, *Research Journal of Recent Sciences*, 1, 224-231, 2012.

[65] Prak, D., Jones, M., Trulove, P., et al., ”Physical and Chemical Analysis of Alcohol-to-Jet (ATJ) Fuel and Development of Surrogate Fuel Mixtures”, *Energy and Fuels*, 29, 3760-3769, 2015.

[66] Corporan, E., Edwards, T., Shafer, L., DeWitt, M. J., et al., ”Chemical, thermal stability, seal swell, and emissions studies of alternative jet fuels”, *Energy and Fuels*, 25(3), 955-966, 2011.

[67] Weisser, K., and Turgeon, R., ”50/50 JP5/ATJ5 specification and fit-for-purpose test results”, NAVAIR SYSCOM Report 441/14-011, 2014.

[68] McAfee, E., ”The Aemetis Biorefinery: 100% Replacement, Renewable Jet and Diesel Fuels by Conversion of Existing Biofuels Refinery Facilities”, Advanced Biofuels Marketing Conference, San Francisco, 29 October 2012.

[69] Held, A., ”Virent is replacing crude oil.”, Virent Inc., Louisiana Biofuels and Bioprocessing Summit, Baton Rouge, Louisiana, 11-12 September 2012.

[70] Malinowski, A., Czarnocka, J., and Biernat, K., ”An Analysis of Physico-Chemical Properties of the Next Generation Biofuels and Their Correlation with the Requirements of Diesel Engine”, In: *Biodiesel - Feedstocks, Production and Applications*, Editor Fang, Z., InTech, 2012.

[71] Lapuerta, M., Villajos, M., Agudelo, J., and Boehman, A., ”Key properties and blending strategies of hydrotreated vegetable oil as biofuel for diesel engines”, *Fuel Processing Technology*, 92(12), 2406-2411, 2011.

Appendix A

Fuel Properties Summary

In the present Appendix, fuel properties are summarized in Table A.1. Additionally, most relevant fuel properties are detailed and the assumptions followed to estimate required and unknown fuel properties (with variation in temperature, for example), for the present model implementation, are presented and validated. Finally, the fuel blending model implementation is also presented and validated.

A.1 Boiling Point

Since jet fuels are typically a mixture os different substances, there is not a single boiling temperature for a given pressure, as there is for pure substances. The temperature at which vaporization occurs varies from the boiling point of the most volatile component to the boiling point of the least volatile component [43]. For such cases, typically a distillation curve is plotted (ASTM D86), and the volume percentage of fuel recovered is plotted against the ambient temperature (Figure A.1).

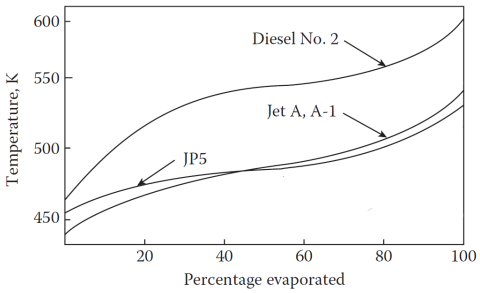

Figure A.1: ASTM D86 distillation curves for various fuels ([3], adapted).

In estimation of fuel properties, the fuel boiling point, T_b, is commonly used and very useful. In the present thesis, its value will always be given as a volume mean temperature [42], based on the 10%, 50% and 90% volume % recovered temperatures, T_{10}, T_{50} and T_{90}, respectively:

$$T_b = \frac{T_{10} + 2.T_{50} + T_{90}}{4}. \tag{A.1}$$

It should noted that, in the present work, all references to the fuel boiling point are, in fact, references

to the normal boiling point (sea level atmospheric pressure), typically referred to, in the literature, as T_{bn}.

A.2 Hydrogen Content

For the liquid fuels that are to be studied in the present thesis, it will be assumed that each fuel, with good approximation, is mainly composed by carbon and hydrogen. Following this assumption, if the hydrogen mass content percentage, $H\%$, is known for a given fuel, its hydrogen-to-carbon molar ratio, ψ , may be estimated by [56]

$$\psi = \frac{12,011 * (H\%/100)}{1,0079 * (1 - H\%/100)}. \tag{A.2}$$

The estimation of ψ will be particularly important for the stoichiometric fuel-to-air ratio, adiabatic flame temperature and combustion gases specific heat computations. Its value is close to 2, for most jet fuels.

A.3 Liquid Fuel Density

For all cases studied, the knowledge of the fuel density at 15 ^{o}C, ρ_{15}, was obtained in the literature. However, the liquid fuel density must be estimated for different temperatures, such as, at initial fuel temperature in the combustion chamber, 25 ^{o}C, at normal boiling temperature, T_b, or at near critical temperature, T_{cr}, in evaporation calculations.

For density calculations such as at 25 ^{o}C or for 60 ^{o}F (or approximately 15.5 ^{o}C [43]), ASTM D1250 standard for petroleum is followed to calculate the fuel density at temperature T in K, ρ_F, with

$$\alpha_{15} = \frac{K_0}{\rho_{15}^2} + \frac{K_1}{\rho_{15}}, \tag{A.3}$$

$$VCF = e^{-\alpha_{15}(T-273.15-15).[1+0.8\alpha_{15}(T-273.15-15)]}, \tag{A.4}$$

$$\rho_F = \rho_{15}.VCF, \tag{A.5}$$

where α_{15} is the thermal expansion coefficient at the base temperature 15 ^{o}C, VCF the volume correction factor and $K_0 = 594.5418$ and $K_1 = 0$ for the "jet fuel" group [57]. It should be pointed out that, although values of parameters K_0 and K_1 are valid in a range of ρ_{15} between 779 and 838.5 kg/m^3, for alternative fuels this range will be neglected, since they are not petroleum fractions and results are satisfactory regardless. In Figure A.2, for a range of temperatures from 0 ^{o}C to 60 ^{o}C, this assumption is validated with good results (maximum relative error of 0.61% and mean relative error of 0.23%) for different fuel densities obtained in the literature [10, 58].

For higher temperatures, near boiling states, where pressure effects may be significant, a different method is assumed, based on [16] and validated there for different fuels: AvGas, n-Heptane, JP-4, JP-5 and DF-2 (diesel). In this method, first the density of the fuel at 288.6 K, $\rho_{288.6}$, is calculated with equation A.5; then the thermal expansion coefficient, C_{ex}, is interpolated from Figure A.3 and finally, the

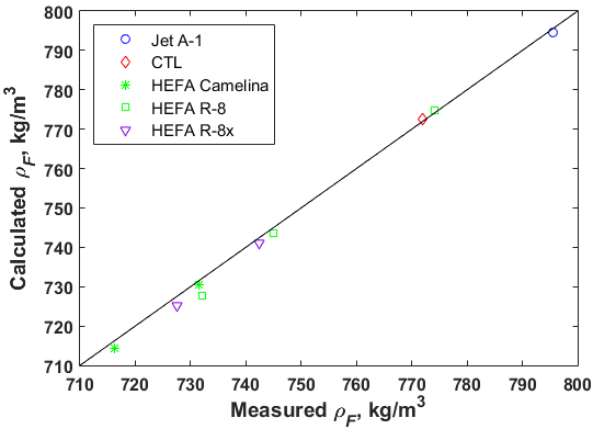

Figure A.2: Comparison between calculated fuel densities (equation A.5) with respective measured values [10, 58].

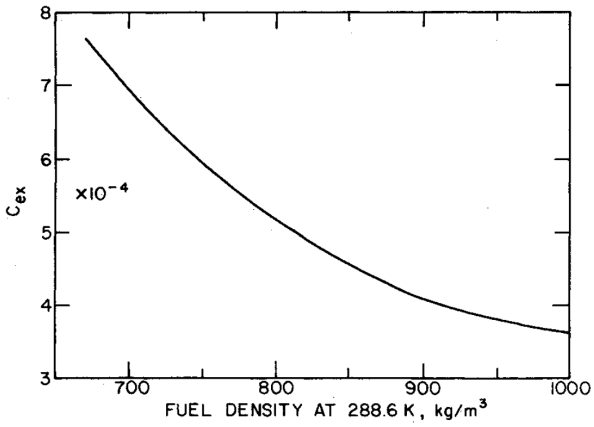

Figure A.3: Effect of fuel density on coefficient of thermal expansion [16].

density of the fuel may be calculated at a given temperature T, in K, by

$$\rho_F = \rho_{288.6}\left[1 - 1.8C_{ex}(T - 288.6) - 0.09\left(\frac{T - 288.6}{T_{cr} - 288.6}\right)^2\right]. \tag{A.6}$$

For JP-8, based on properties present in [59] and critical temperature, T_{cr}, estimation as it is explained next (section A.4), if the density at its normal boiling temperature (681.7 kg/m^3 [59]) was calculated with equation A.5 instead of equation A.6, respective results of 695.93 kg/m^3 (2.09% error) and 685.67 kg/m^3 (0.58% error) would be obtained, confirming the increased accuracy of equation A.6 for higher temperatures density estimations.

For liquid fuels, the specific gravity (SG) is defined as the ratio of density of a liquid to that of water. For liquid petroleum fractions and crude oils, densities of both the oil and water at same temperature are usually expressed at 15.5 ^{o}C and 1 atm [43]. In the present work, this approach will be followed.

A.4 Critical Properties and Molecular Weight

In the previous equation (equation A.6), the knowledge of critical temperature, T_{cr}, is required. Unfortunately, for all alternative fuels researched, neither critical temperatures, T_{cr}, nor critical pressures, p_{cr}, were obtained. Therefore, from [43], their estimation will be based on the *Riazi-Daubert Method*, based on T_b, in K, and specific gravity, SG, with T_{cr}, in K, and p_{cr}, in Pa, given by

$$T_{cr} = 9.5233[\exp(-9.314 \times 10^{-4}T_b - 0.544442SG + 6.4791 \times 10^{-4}T_b.SG)].T_b^{0.81067}.SG^{0.53691}, \tag{A.7}$$

$$p_{cr} = 3.1958 \times 10^5[\exp(-8.505 \times 10^{-3}T_b - 4.8014SG + 5.749 \times 10^{-3}T_b.SG)].T_b^{-0.4844}.SG^{4.0846}. \tag{A.8}$$

Based on the same method, the molecular weight of a given fuel (if unknown), MW_F in kg/kmol, may

be estimated by

$$MW_F = 42.965[\exp(2.097 \times 10^{-4} T_b - 7.78712SG + 2.08476 \times 10^{-3} T_b.SG)].T_b^{1.26007}.SG^{4.98308}. \quad \text{(A.9)}$$

Equations A.7, A.8 and A.9 can be applied to hydrocarbons with molecular weight ranging from 70 to 700 kg/kmol, which covers all possible molecular weights for the fuels studied. This method was selected since it is considered an highly accurate one, recognized as the standard method of estimating molecular weight of petroleum fractions in the industry [43]. As presented in Figures A.5 and A.4, excellent results are obtained for estimations of T_{cr} and MW_F, with maximum relative errors of 1.67% and 3.93%, respectively.

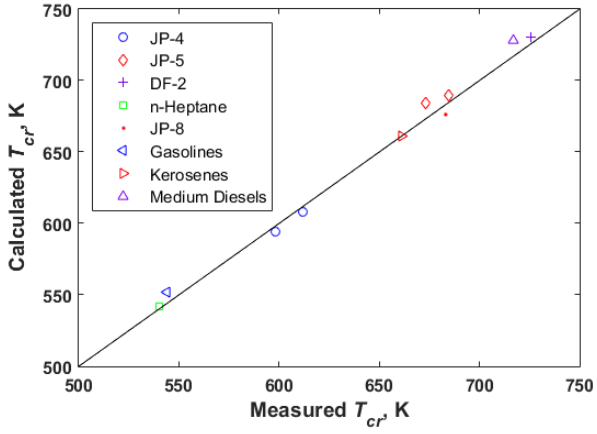

Figure A.4: Comparison between calculated fuel critical temperatures (equation A.7) with respective measured values [3, 12, 16].

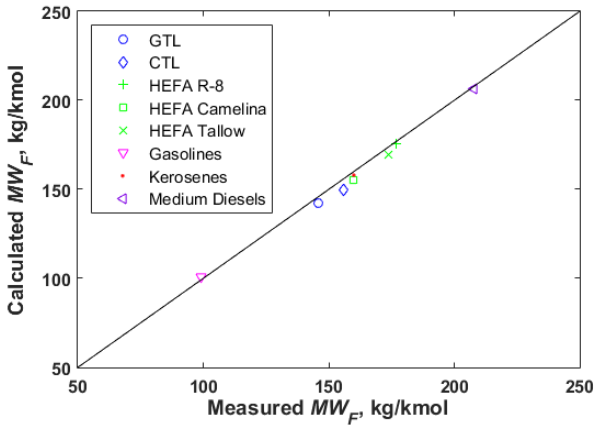

Figure A.5: Comparison between calculated fuel molecular weight (equation A.9) with respective measured values [12, 60, 61].

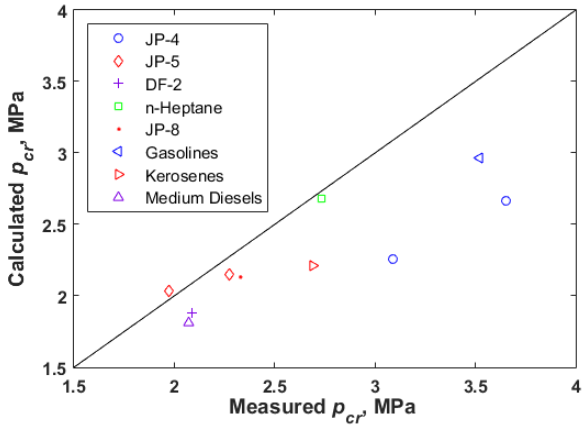

Figure A.6: Comparison between calculated fuel critical pressures (equation A.8) with respective measured values [3, 12, 16].

For p_{cr} estimation, higher deviations from experimental values (see Figure A.6) are observed with a maximum error of 27.10% and mean average error of 12.93%. This was expected since for pure hydrocarbons estimations in [43] an average absolute error of 5.8% was obtained compared to 0.4% for T_{cr} estimation. The influence of p_{cr} value estimation will only be present in the calculation of evaporation rates of fuels and, as concluded in the evaporation model validation (section 3.3 and Appendix B with

Figure B.2), its influence on evaporation constant calculations may be considered as negligible.

In the validation of critical properties and molecular weight estimations, the sources of fuel properties were [3, 12, 16] and [12, 60, 61], respectively.

A.5 Liquid Viscosity

The viscosity of a liquid fuel is a measure of its resistance to flow [12]. In the atomization of a fuel, viscosity has an important role, with high fuel viscosities resulting in large fuel droplets injected for combustion. Therefore, in this study, its knowledge is considered as mandatory. The fuel viscosity may be defined as dynamic viscosity, μ_F, in N.s/m^2, or as kinematic viscosity, $\nu_F = \frac{\mu_F}{\rho_F}$, in m^2/s.

Knowing the kinematic viscosity at temperatures T_1 and T_2, in K, respectively ν_1 and ν_2, according to ASTM D341 standard, the kinematic viscosity, in mm^2/s, at a different temperature, T, may be estimated [43] by

$$\log\log(\nu_F + 0.7 + c_T) = A_1 + B_1 \log T, \tag{A.10}$$

with

$$B_1 = \frac{\log\log(\nu_2 + 0.7 + c_{T_2}) - \log\log(\nu_1 + 0.7 + c_{T_1})}{\log\frac{T_2}{T_1}}, \tag{A.11}$$

$$A_1 = \log\log(\nu_1 + 0.7 + c_{T_1}) - B_1 \log T_1. \tag{A.12}$$

In the previous relations $c_T = 0$ for $\nu_F \geq 1.5$ mm^2/s and $c_T = 0.085(\nu_F - 1.5)^2$ mm^2/s otherwise. Then, to estimate the kinematic viscosity of the fuel at its initial temperature, 25 ^{o}C, for combustion, parameters A_1 and B_1 are calculated first and, with equation A.10 and definition of c_T, its value is properly computed. In Figure A.7, for a range of temperatures between -40 ^{o}C and 25 ^{o}C, kinematic viscosities of certain fuels are calculated and compared with correspondent measured values [12, 58]. For the fuels considered, a maximum relative error of 11.34% and a mean relative error of 5.07% were obtained, which, although high in comparison with other properties estimations, are considered as reasonable, mainly due to the wide range of temperatures considered.

If, for a given fuel, only one value of viscosity measurement for a given temperature is available in the literature, another value will be estimated for 38^{o}C according to [43]:

$$\begin{aligned}\log\nu_{38} = {} & 4.39371 - 1.94733K_W + 0.12769K_W^2 + 3.2629\times10^{-4}API^2 - 1.18246\times10^{-2}K_W.API \\ & + \frac{0.171617K_W^2 + 10.9943API + 9.50663\times10^{-2}API^2 - 0.860218K_W.API}{API + 50.3642 - 4.78231K_W},\end{aligned} \tag{A.13}$$

with

$$K_W = \frac{(1.8T_b)^{1/3}}{SG}, \tag{A.14}$$

$$API = \frac{141.5}{SG} - 131.5. \tag{A.15}$$

Due to the nature of the estimation, with average error in the range of 15-20% for petroleum fractions [43], fuels requiring this approximation are expected to have worse viscosity estimations than otherwise.

This estimation must only be used for $10 < K_W < 12.5$ (Watson factor) and $0 < API < 80$. Comparing kinematic viscosities at 40^oC, for HEFA R-8 and Camelina (fuels of interest, presented in Table A.1), respective relative errors of 10.07% and 9.18% would be obtained for computed values at a similar temperature (38^oC), with equation A.13, thus confirming the expected accuracy of such estimations.

A.6 Surface Tension

For fuel atomization, another relevant property of a fuel is its surface tension, σ_F, which defines the force required for unit increase in length of that liquid [43]. If, for a certain fuel, no information on surface tension can be acquired in the literature, a value for a certain temperature can be estimated [43] by

$$\sigma_F = \frac{0.6737\left(1 - \frac{T}{T_{cr}}\right)}{K_W}, \tag{A.16}$$

where σ_F comes in N/m and temperatures T and T_{cr} in K. In Figure A.8, the accuracy of this estimation is evaluated by comparing measured values of surface tension at a certain temperature, ranging from -10 ^{o}C to 100 ^{o}C [12, 58], with values calculated with equation A.16. Doing so, for the fuels and range of temperatures considered, a maximum relative error of 19.26% and a mean relative error of 5.73% is obtained, which is considered as reasonable for the present study.

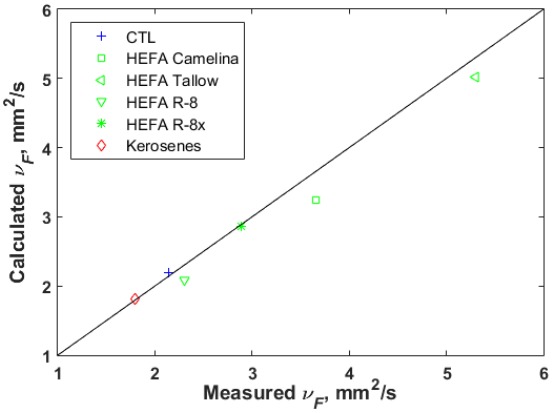

Figure A.7: Comparison between calculated fuel kinematic viscosities (equation A.10) with respective measured values [12, 58].

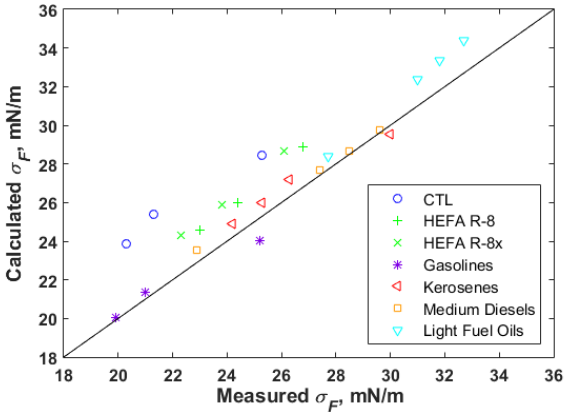

Figure A.8: Comparison between calculated fuel surface tension (equation A.16) with respective measured values [12, 58].

Although for some fuels a value of surface tension was obtained from the literature, for a given temperature, in this work, all surface tension values will be estimated with the previous equation (equation A.16). Given the fact that, for most types of alternative fuels here considered, values of surface tension were not found in the literature, this was decided so that comparisons between surface tensions are consistent.

A.7 Fuel Blending

In the present model, the user may define the volume blending ratio of a certain alternative fuel with the reference fuel (Jet A-1). Its modelling is briefly explained next. Is should be pointed out that all fuel mixtures/blends are defined by the alternative fuel to be blended with Jet A-1 and its respective volume ratio.

For a given fuel, designated here by subscript i, and the reference fuel, designated by subscript ref, the mixture/blending of the two fuels is completely defined by their volume ratio, $x_{v,i}$:

$$x_{v,i} = \frac{\text{Volume of Fuel } i}{\text{Volume of Mixture}}. \tag{A.17}$$

It then follows, with known fuel densities (for a certain temperature) and molecular weights, the calculation [43] of the mass/weight ratio, $x_{w,i}$, and the molar ratio, $x_{n,i}$, with

$$x_{w,i} = \frac{\rho_i.x_{v,i}}{\rho_i.x_{v,i} + \rho_{ref}.(1 - x_{v,i})}, \tag{A.18}$$

$$x_{n,i} = \frac{x_{w,i}}{x_{w,i} + \frac{MW_i}{MW_{ref}}.(1 - x_{w,i})}. \tag{A.19}$$

A.7.1 Distillation Range of the Mixture

To obtain the average boiling temperature of a certain fuel mixture, $T_{b,mix}$, differences in distillation range temperatures must be computed. With this goal, a graphical summation method, according to reference [62], is followed to calculate the temperatures for 10%, 50% and 90% of fuel volume recovered ($T_{10,mix}$, $T_{50,mix}$ and $T_{90,mix}$, respectively). With this method, good results are obtained as easily depicted from the analysis of Figure A.9, which is based on [28, 63]. For all cases, and considering several volume ratios (10%, 25%, 50%, 60%, 70%, 80% and 90%, depending on the source), relative mean errors of 0.38%, 0.47% and 0.63% were obtained for calculation of $T_{10,mix}$, $T_{50,mix}$ and $T_{90,mix}$, respectively.

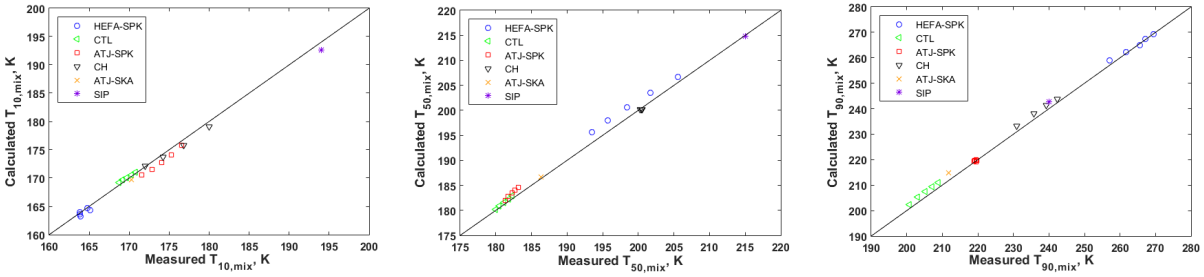

(a) $T_{10,mix}$ (b) $T_{50,mix}$ (c) $T_{90,mix}$

Figure A.9: Comparison between calculated 10% (a), 50% (b) and 90% (c) volume recovered temperatures of a certain mixture (referred fuel with conventional kerosene) with respective measured values [28, 63].

A.7.2 Density, Viscosity and Surface Tension of the Mixture

The calculation of the fuel mixture density, ρ_{mix}, will be based on the definition of weight ratio [43], and simply given by

$$\frac{1}{\rho_{mix}} = \frac{x_{w,i}}{\rho_i} + \frac{1 - x_{w,i}}{\rho_{ref}}. \tag{A.20}$$

Taking into account fuel properties in references [28, 63], with this method, excellent results are obtained for several volume ratios (10%, 25%, 50%, 60%, 70%, 80% and 90%, depending on the source) with mean and maximum relative errors of 0.01% and 0.09%, respectively. Results are presented in Figure A.10.

The kinematic viscosity of the fuel mixture, ν_{mix}, follows the approach given in reference [42]. For known fuel weight ratios, it follows:

$$\log\log(\nu_{mix} + 0.7 + c_{T,mix}) = x_{w,i}.\log\log(\nu_i + 0.7 + c_{T,i}) + (1 - x_{w,i}).\log\log(\nu_{ref} + 0.7 + c_{T,ref}). \tag{A.21}$$

Taking into account fuel properties in references [28, 63], good results are obtained with this method for several volume ratios (10%, 25%, 50%, 60%, 70%, 80% and 90%, depending on the source) with mean and maximum relative errors of 1.15% and 3.51%, respectively. Results are presented in Figure A.11.

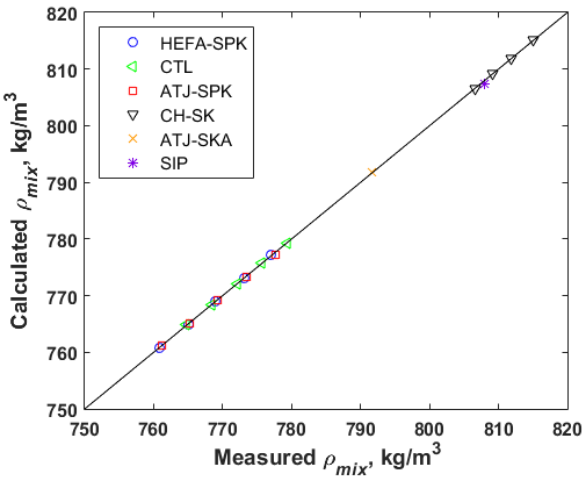

Figure A.10: Comparison between calculated liquid density of a certain mixture (referred fuel with conventional kerosene) with respective measured values [28, 63].

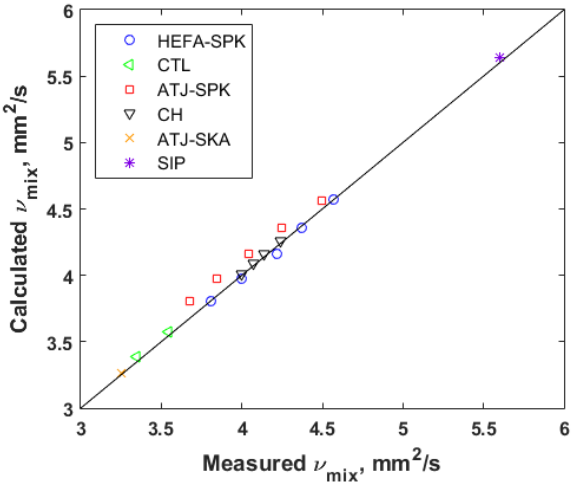

Figure A.11: Comparison between calculated liquid kinematic viscosity of a certain mixture (referred fuel with conventional kerosene) with respective measured values [28, 63].

The surface tension of the fuel mixture, σ_{mix}, follows the approach given in reference [64]. With this approach, assuming additivity:

$$\sigma_{mix} = \frac{\sigma_i.\sigma_{ref}}{\sigma_i.(1 - x_{v,i}) + \sigma_{ref}.x_{v,i}}. \tag{A.22}$$

For the case of blending an ATJ-SPK with JP-5 [65], with a 30% volume ratio, a relative error of 1.27% would be obtained comparing the measured surface tension for the referred mixture and the result obtained with equation A.22.

A.7.3 Net Heat of Combustion of the Mixture

The net heat of combustion of the fuel mixture, ΔH_{mix}, follows the approach given in reference [42]. Doing so, a simple calculation is required:

$$\Delta H_{mix} = x_{w,i}.\Delta H_i + (1 - x_{w,i}).\Delta H_{ref}. \tag{A.23}$$

Taking into account fuel properties in references [28, 63], with this method, excellent results are obtained for several volume ratios (10%, 25%, 50%, 60% and 70%, depending on the source) with mean and maximum relative errors of 0.06% and 0.22%, respectively. Results are presented in Figure A.12.

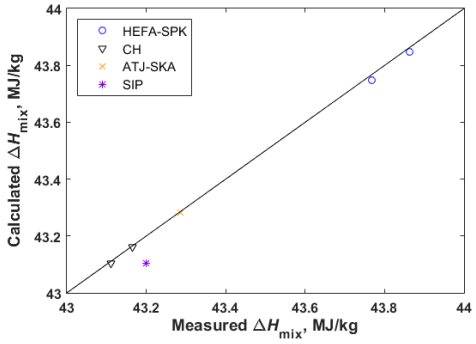

Figure A.12: Comparison between calculated net heat of combustion of a certain mixture (referred fuel with conventional kerosene) with respective measured values [28, 63].

A.7.4 Molecular Weight and Hydrogen-to-Carbon Ratio of the Mixture

The estimation of the molecular weight, MW_{mix}, and the hydrogen-to-carbon molar ratio, ψ_{mix}, of the fuel mixture will follow the same simple assumption of mass additivity of the mixture. Then

$$\psi_{mix} = x_{n,i}.\psi_i + (1 - x_{n,i}).\psi_{ref}, \tag{A.24}$$

$$MW_{mix} = x_{n,i}.MW_i + (1 - x_{n,i}).MW_{ref}. \tag{A.25}$$

The validity of the assumptions presented above is verified based on a 50% volume ratio blending of FT-SPK with JP-8 as in references [54] . Relative errors of 1.33% and 0.02% were obtained for the calculation of molecular weight and hydrogen-to-carbon ratio of the mixture, respectively, when compared with [54] results.

It should be highlighted the fact that, in the present model, the calculation of mixture critical properties will be performed with equations A.7 and A.8 (critical temperature and pressure, respectively) for calculated mixture density, ρ_{mix}, at 15.5 ^{o}C and mixture average boiling point, $T_{b,mix}$. For the case of fuel blending, with hydrogen-to-carbon molar ratio, ψ_{mix}, and with an algebraic rearrangement, hydrogen content (in weight), $H\%_{mix}$, is obtained with equation A.2.

Properties	ASTM D1655	Jet A-1	GTL	CTL	HEFA R-8	HEFA C.	ATJ-SPK	ATJ-SKA	SIP	CH	HDO-SK	Green Diesel
Net Heat of Combustion, MJ/kg	min. 42.8	43.2	44.2	44.0	44.1	44.3	44.3	43.4	44.1	43.3	43.3	43.7
Density at 15^{o}C, kg/m^3	775-840	802	737	762	763	751	774	786	774	804	812	777
Viscosity at -20^{o}C, mm^2/s	max. 8	3.92	2.60	3.60	5.50	3.30	8.40	3.42	14.10	3.50	6.10	14.77
Viscosity at 25^{o}C[a], mm^2/s	-	1.52	0.99[b]	1.45	1.89	1.36	2.61	1.37[b]	3.14	1.44	1.97[b]	3.56[c]
Surface Tension at 25^{o}C[d], mN/m	-	27.4	23.8	25.2	25.8	24.8	26.2	26.4	26.7	27.5	28.0	27.0
Initial Boiling Point, ^{o}C	-	151	146	149	156	151	179	165	237	150	159	190
10% Recovered, ^{o}C	max. 205	169	162	166	178	161	188	175	244	165	178	243
50% Recovered, ^{o}C	-	199	169	180	218	182	206	187	245	200	213	275
90% Recovered, ^{o}C	-	243	184	208	263	237	249	206	245	249	260	288
Final Boiling Point, ^{o}C	max. 300	262	198	228	274	259	273	250	258	268	280	306
Hydrogen Content, weight %	-	13.87	15.60	15.10	15.30	15.40	14.90	13.80[e]	14.90	13.80	14.90[f]	14.70
H/C (ψ)[g], molar ratio	-	1.919	2.203	2.119	2.153	2.169	2.087	1.908	2.087	1.908	2.087	2.054
Molecular Weight, kg/kmol	-	160.5[h]	146.0	156.0	177.0	160	169.9[h]	151.9[h]	195.6[h]	161.0[h]	169.5[h]	217.5[h]
Critical Temperature[i], ^{o}C	-	392.3	346.5	364.5	394.2	367.1	392.2	375.6	418.3	393.7	406.8	438.8
Critical Pressure[j], bar	-	21.88	20.95	21.27	17.80	19.79	19.09	22.34	16.21	21.91	21.12	14.42
Aromatic Content, volume %	max. 25	18.1	0[k]	0[k]	0[k]	0[k]	0[k]	15.2	1.5	17	0.8	0[k]
Smoke Point, mm	min. 25[l]	23	40	40	40	50	33	23	42	24	27	27
Flash Point, ^{o}C	min. 38	42.2	44.0	44.0	48.0	43.0	60.0	48.5	105	46	50	71
Freezing Point, ^{o}C	max. -47	-52	-54	$<$-78	-49	$<$-77	$<$-82	$<$-80	$<$-83	-57	$<$-80	-21[m]
Lubricity, mm	max. 0.85	-	0.75	0.87	0.92	0.76	0.84	0.61	0.56	0.57	-	0.73
Sources:	[3, 10]	[10, 29]	[60, 66]	[58, 60, 66]	[58, 61, 66]	[58, 60, 66]	[28, 67]	[28]	[28, 63]	[52, 68]	[38, 69]	[70, 71]

a: Liquid kinematic viscosity at 25^{o}C estimated with equation A.10 based on viscosity at two different temperatures. b: Only a value of viscosity at -20^{o}C obtained in the literature, with required additional estimation with equation A.13. c: Green Diesel viscosity temperature dependence based on values at 40 and 50^{o}C. d: Surface tension values estimated with equation A.16. e: ATJ-SKA hydrogen-to-carbon ratio approximated as equal to CH's. f: HDO-SK hydrogen-to-carbon ratio estimated based on [43] and on the negligible aromatic content. g: Hydrogen-to-carbon ratio, ψ, based on hydrogen content, $H\%$, computed with equation A.2. h: Molecular weight estimated with equation A.9. i: Fuel critical temperature estimated with equation A.7. j: Fuel critical pressure estimated with equation A.8. k: Negligible aromatic content. l: Or minimum smoke point of 18 mm and maximum content of naphthalenes of 3% (in volume). m: Pour point presented, instead of freezing point.

Table A.1: Fuels of interest specifications.

Appendix B

Supplementary Data

In the present Appendix, flame temperature model validation is presented in section B.1, the evaporation model is validated in section B.2, unscaled engine component maps (diffuser and rotating components) are displayed in section B.3, additional transient validation results are displayed in section B.4 and additional performance and pollutant emissions results are presented in section B.5 .

B.1 Flame Temperature Validation

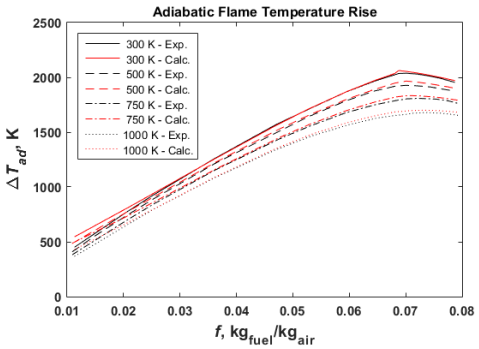

Figure B.1: Present model adiabatic flame temperature rise, ΔT_{ad}, for JP-5 calculation compared with results from [3].

B.2 Evaporation Model Validation

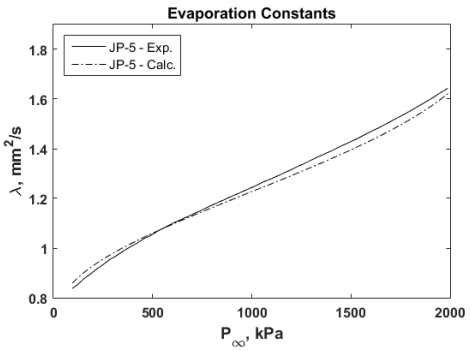

(a) JP-5

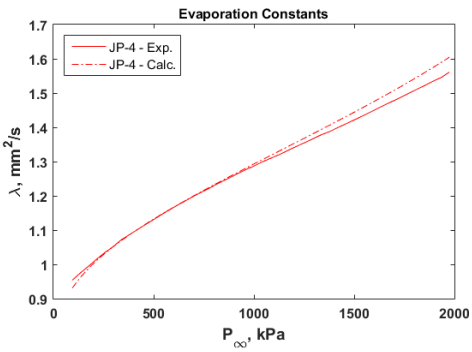

(b) JP-4

Figure B.2: Evaporation constants of JP-5 (a) and JP-4 (b) with ambient pressure for ambient temperature of 2000 K. Calculated values compared with results presented in [16].

B.3 Engine Component Maps

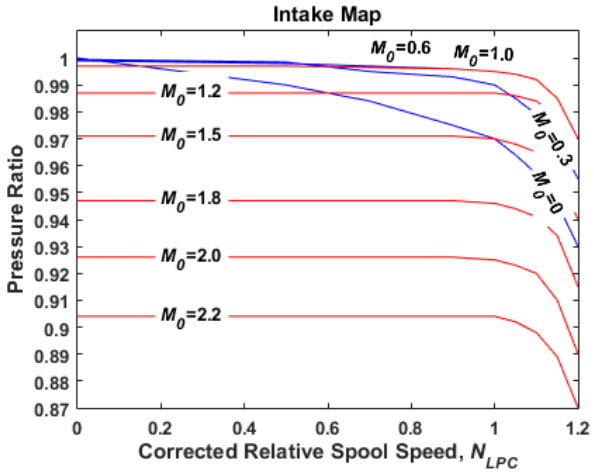

Figure B.3: Diffuser pressure ratio, π_d, as a function of the relative corrected spool speed of LPC, N_{LPC}, and flight Mach number, M_0 [4].

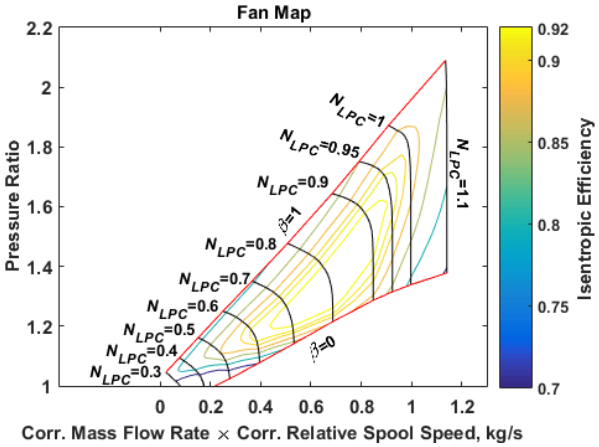

Figure B.4: Fan unscaled map. Based on data from [4].

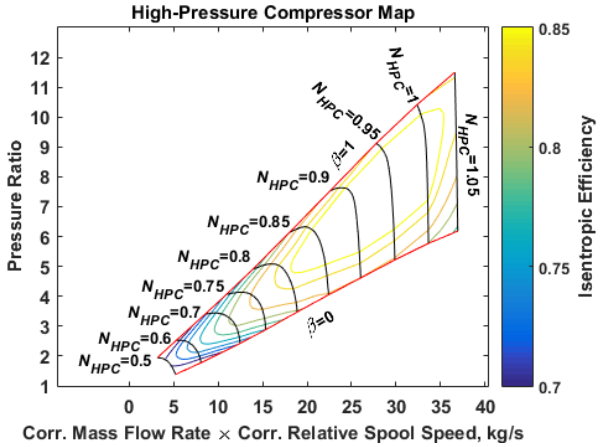

Figure B.5: High-pressure compressor unscaled map. Based on data from [4].

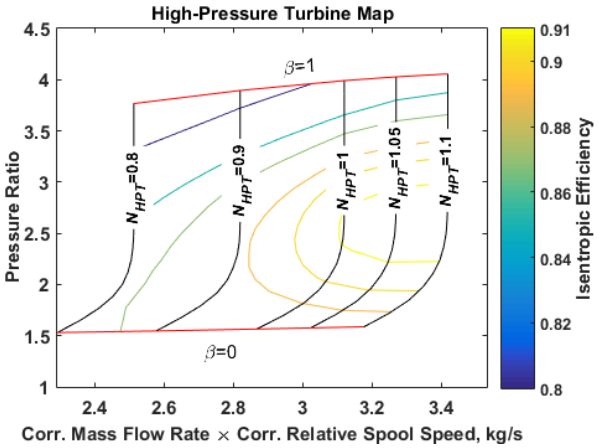

Figure B.6: High-pressure turbine unscaled map. Based on data from [4].

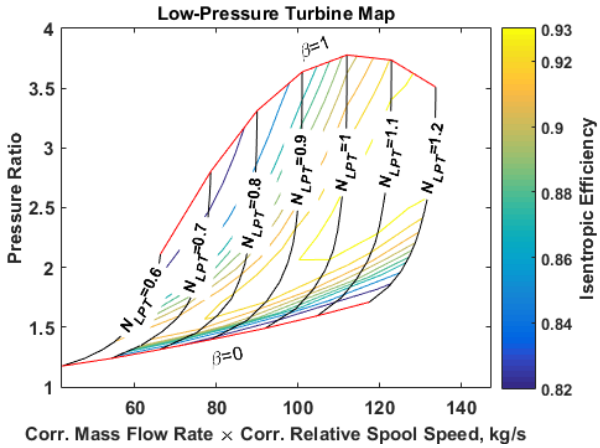

Figure B.7: Low-pressure turbine unscaled map. Based on data from [4].

B.4 Additional Transient Validation Results

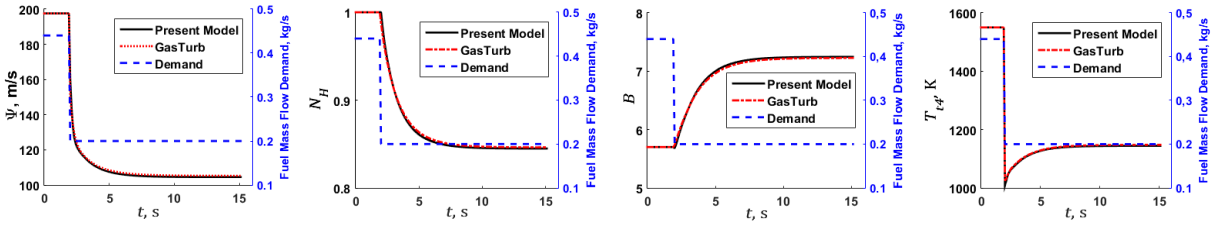

(a) Specific thrust (b) High-pressure relative spool speed (c) Bypass ratio (d) High-pressure turbine inlet temperature

Figure B.8: Ψ (a), N_H (b), B (c) and T_{t4} (d) with time, t, for $\dot{m}_{f,deman}(t)$ input (deceleration).

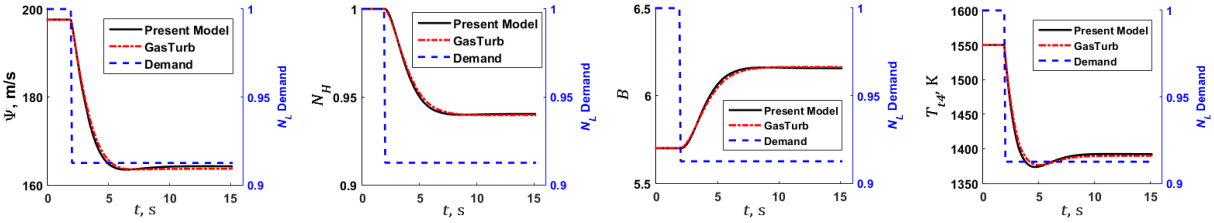

(a) Specific thrust (b) High-pressure relative spool speed (c) Bypass ratio (d) High-pressure turbine inlet temperature

Figure B.9: Ψ (a), N_H (b), B (c) and T_{t4} (d) with time, t, for $N_{L,demand}(t)$ input (deceleration, with Proportional control).

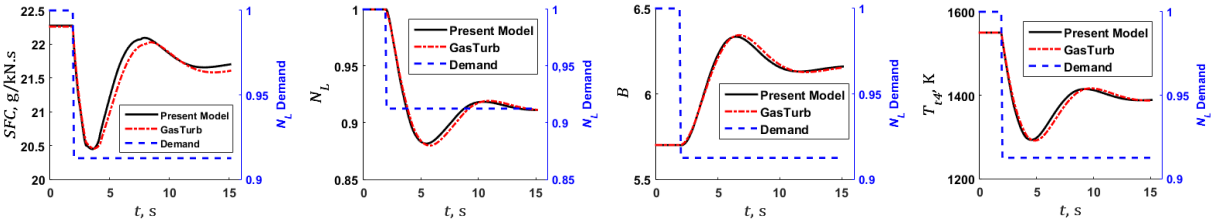

(a) Specific fuel consumption (b) Low-pressure relative spool speed (c) Bypass ratio (d) High-pressure turbine inlet temperature

Figure B.10: SFC (a), N_L (b), B (c) and T_{t4} (d) with time, t, for $N_{L,demand}(t)$ input (deceleration with PI control).

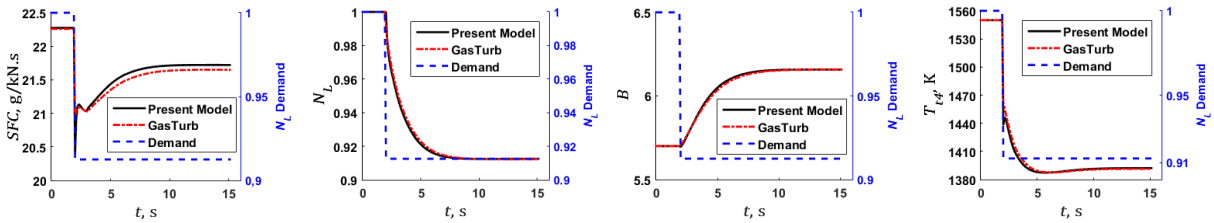

(a) Specific fuel consumption (b) Low-pressure relative spool speed (c) Bypass ratio (d) High-pressure turbine inlet temperature

Figure B.11: SFC (a), N_L (b), B (c) and T_{t4} (d) with time, t, for $N_{L,demand}(t)$ input (deceleration with PD control).

B.5 Additional Performance and Pollutant Emissions Results

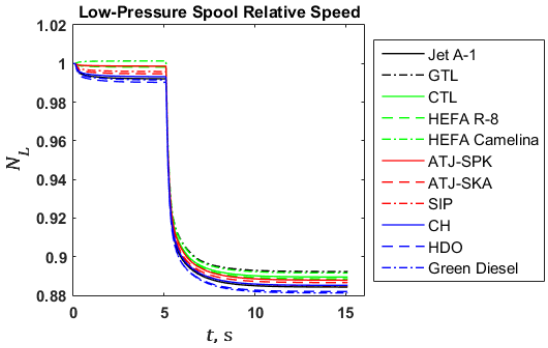

Figure B.12: Low-pressure relative spool speed, N_L, with time, t, for $\dot{m}_{f,demand}(t)$ input (deceleration).

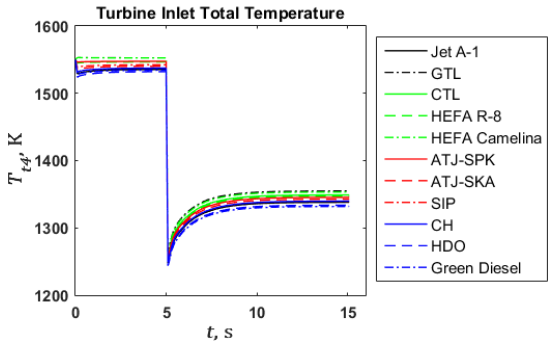

Figure B.13: High-pressure turbine inlet temperature, T_{t4}, with time, t, for $\dot{m}_{f,demand}(t)$ input (deceleration).

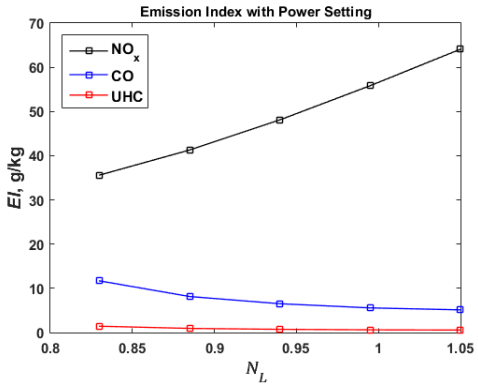

Figure B.14: EI_{NO_x}, EI_{CO} and EI_{UHC} with N_L for same altitude ($H = 0$ m) and Mach number ($M_0 = 0$).

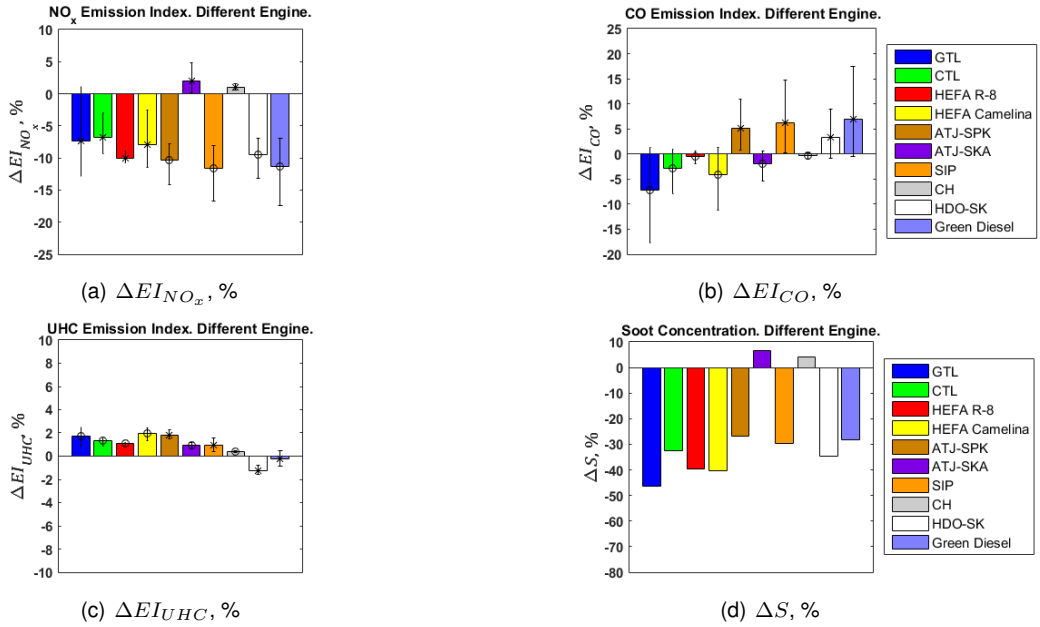

(a) ΔEI_{NO_x}, %

(b) ΔEI_{CO}, %

(c) ΔEI_{UHC}, %

(d) ΔS, %

Figure B.15: ΔEI_{NO_x} (a), ΔEI_{CO} (b), ΔEI_{UHC} (c) and ΔS (d) for higher overall pressure ratio engine and Cruise flight condition.

Appendix C

Gas Model Summary

To obtain the coefficients presented on equation 3.6 (A, B, C, D and E), the coefficients of the individual gas components (subscript i) must be defined. Typically, the chemical reaction representative of the combustion of a hydrocarbon fuel is given by

$$\mathsf{C}_n\mathsf{H}_m + a \times \mathsf{O}_2 = b \times \mathsf{CO}_2 + c \times \mathsf{H}_2\mathsf{O}. \tag{C.1}$$

The previous equation (C.1), with unknowns a, b and c, only includes carbon dioxide and water as combustion products due to their higher proportions compared to other products. Defining hydrogen-to-carbon molar ratio as $\psi = \frac{m}{n}$, the chemical combustion balance can be further simplified to the form:

$$\mathsf{CH}_\psi + \left(1 + \frac{\psi}{4}\right) \times \mathsf{O}_2 = \mathsf{CO}_2 + \frac{\psi}{2} \times \mathsf{H}_2\mathsf{O}. \tag{C.2}$$

For a given fuel-air ratio, f, defined as the ratio between the mass of fuel over the mass of air employed (equation 3.19), considering the carbon, oxygen and hydrogen molecular weights, $MW_C =$ 12.011 kg/kmol, $MW_O =$ 15.994 kg/kmol and $MW_H =$ 1.00791 kg/kmol, respectively, and knowing the common air mass composition: 75.52 % of N_2, 23.142% of O_2, 1.288% of Ar and approximately 0.05% of CO_2 (neglecting Ne); for a given gas, one can relate the proportions of the individual components (subscript i) in relation to air, f'_i, based on f and ψ:

$$f'_{N_2} = 0.7552, \tag{C.3}$$

$$f'_{Ar} = 0.01288, \tag{C.4}$$

$$f'_{O_2} = 0.23142 - \frac{31.9988 + 7.9997 \times \psi}{12.011 + 1.00791 \times \psi} \times f, \tag{C.5}$$

$$f'_{CO_2} = 0.0005 + \frac{44.0098}{12.011 + 1.00791 \times \psi} \times f, \tag{C.6}$$

$$f'_{H_2O} = \frac{9.00761 \times \psi}{12.011 + 1.00791 \times \psi} \times f. \tag{C.7}$$

Finally, considering the influence of all individual components, the combustion gas specific heat polynomial (equation 3.6) is defined as

$$C_p = \frac{\sum(C_{p_i} \times \dot{m}_i)}{\dot{m}_f + \dot{m}_a} = \frac{\sum(C_{p_i} \times f'_i)}{1+f}. \tag{C.8}$$

Individual specific heats, C_{p_i}, are quartic polynomials as well, function of temperature, with coefficients A_i, B_i, C_i, D_i and E_i presented in table form [15] for two temperature intervals: 300 K $< T <$ 1000 K and 1000 K $< T <$ 2500 K. Then, coefficients A, B, C, D and E of equation 3.6 may be obtained for a given fuel-air ratio, f, hydrogen to carbon ratio, ψ, and temperature interval, in K. Throughout the present thesis, the specific heat of dry air will be calculated for $f = 0$.

For engine inlet calculations, dry air static temperatures are lower than 300 K. However, with the calculation of dry air specific heat for 216.65 K, 240 K, 260 K, 280 K and 300 K, an average absolute difference of 2.06 J/kg.K and relative difference of 0.21% would be verified, comparing with dry air specific heat given in [14], which is considered a good approximation.

Based on mass flow rates of air, $\dot{m}_a$, fuel, $\dot{m}_F$, and of individual components i, $\dot{m}_i$, and individual components molecular weights, MW_i, the gas molecular weight, MW_g, may be computed by

$$MW_g = \frac{\dot{m}_a + \dot{m}_F}{\sum \frac{\dot{m}_i}{MW_i}} = \frac{1+f}{\sum \frac{f'_i}{MW_i}}. \tag{C.9}$$

Taking into account equation 3.10, the difference between enthalpies (Δh) corresponding to temperatures T_2 and T_1 will be given by

$$\Delta h = \int_{T_1}^{T_2} c_p(T, f, \psi).dT = A(T_2 - T_1) + \frac{B}{2}(T_2^2 - T_1^2) + \frac{C}{3}(T_2^3 - T_1^3) + \frac{D}{4}(T_2^4 - T_1^4) + \frac{E}{5}(T_2^5 - T_1^5). \tag{C.10}$$

For entropy calculations (isentropic and polytropic, for example), with equation 3.12, the entropy difference between a state 2 and 1 is given by

$$\Delta s = A.\ln(T_2/T_1) + B(T_2 - T_1) + \frac{C}{2}(T_2^2 - T_1^2) + \frac{D}{3}(T_2^3 - T_1^3) + \frac{E}{4}(T_2^4 - T_1^4) - R.\ln\frac{p_2}{p_1}. \tag{C.11}$$

During the present work, the definition of the stoichiometric fuel-air ratio, f_{st}, which defines the fuel-air mixture required for complete combustion, based on the hydrogen-to-carbon ratio, ψ, is given by

$$f_{st} = \frac{12.011 + 1.00791\psi}{2 \times (1 + 0.25\psi).(15.9994 + 3.762 \times 14.0067)}. \tag{C.12}$$

If the fuel-air mixture for combustion is not stoichiometric, lean, if higher ($\Phi < 1$), or rich, if lower ($\Phi > 1$), fuel-air mixtures are considered. Where, Φ, is the equivalence ratio:

$$\Phi = \frac{f}{f_{st}}. \tag{C.13}$$

It should also be highlighted that, given the gas model considered with the specific heat dependent on temperature, f and ψ, whenever it is possible to obtain a certain station result (temperature or pressure) through polynomial root solving, that will be the standard procedure. Otherwise, through algebraic manipulation and with a simple Newton-Raphson method, results are readily computed.